THE UNIVERSITY
of EDINBURGH

Systematic approximation methods for stochastic biochemical kinetics

Philipp Thomas

Doctor of Philosophy
University of Edinburgh
2015

I would like to express my gratitude to...

...my parents, Petra and Dr Holger Thomas, for their continuous and unconditional support, as well as my friends in Edinburgh, especially Andrea, Ricardo, Sebastian and Alejandro. I am indebted to my supervisors, Dr Ramon Grima and Dr Nikola Popović for their extensive support, guidance and dedication to my project. I am grateful to Dr Arthur V. Straube and Dr Christian Fleck for their support during the earlier stages of my PhD. I thank the members of our group, David Schnoerr, Harriet Jones, David K Toner, Dr Claudia Cianci, and Stephen Smith, for sharing their time and knowledge with me over the last few years. I have enjoyed many stimulating discussions with the people of SynthSys and, in particular, Prof Vincent Danos and Prof Peter Swain. I am indebted to David Schnoerr and Dr Claudia Cianci for many corrections on this manuscript. Finally, I like to thank my examiners Prof Jacques Vanneste and Prof Peter Sollich for showing me a simple derivation of the path-integral.

Declaration

I declare that this thesis was composed by myself and that the work contained therein is my own, except where work has been included which has formed part of jointly-authored publications stated below, or explicitly stated otherwise in the text. Further, I declare that the work has not been submitted for any other degree or professional qualification except as specified.

Material in this work also appears in the following jointly authored papers:

- [1] R. Grima, P. Thomas, and A. V. Straube. How accurate are the nonlinear chemical Fokker-Planck and chemical Langevin equations? *J Chem Phys*, **135**, 084103 (2011). *Lays out leading order results on which Chapter 3 is based on.*
- [2] P. Thomas, H. Matuschek, and R. Grima. Computation of biochemical pathway fluctuations beyond the linear noise approximation using iNA. In *Bioinformatics and Biomed (BIBM), 2012 IEEE Int Conf on*, pages 1–5. IEEE (2012). *Parts of which have been included in Section 3.3.*
- [3] P. Thomas and R. Grima. Approximate probability distributions of the master equation. *Phys Rev E*, **92**, 012120 (2015). *Parts of which have been included in Chapter 4.*
- [4] P. Thomas, et al. System size expansion of the master equation using Feynman rules and diagrams. *J Phys A: Math Theor*, **47**, 455007 (2014). *Parts of which have been included in Chapter 5.*
- [5] P. Thomas, et al. Signatures of nonlinearity in single cell noise-induced oscillations. *J Theor Biol*, **335**, 222 (2013). *Parts of which have been included in Section 5.5.*

Edinburgh, July 2015

Philipp Thomas

Lay Summary

Intracellular biochemistry is stochastic because of the random timing of the reactions by which biomolecules are synthesised in living cells. These intrinsic fluctuations roughly scale as the inverse square root of the number of molecules. Since intracellular abundances range from a few tens to thousands of molecules, it is anticipated that molecular fluctuations affect many intracellular processes. Mathematical models that describe these stochastic processes are however often analytically intractable. This thesis therefore develops approximation methods that allow to study stochasticity in biochemical networks systematically. Based on the system size expansion of the Chemical Master Equation we obtain explicit expressions for moments, correlation functions, and probability distributions as an expansion in a small parameter that corresponds to the inverse square root of the number of molecules. The theory is hence expected to resemble closely the outcomes of single cell experiments.

Abstract

Experimental studies have shown that the protein abundance in living cells varies from few tens to several thousands molecules per species. Molecular fluctuations roughly scale as the inverse square root of the number of molecules due to the random timing of reactions. It is hence expected that intrinsic noise plays an important role in the dynamics of biochemical networks.

The Chemical Master Equation is the accepted description of these systems under well-mixed conditions. Because analytical solutions to this equation are available only for simple systems, one often has to resort to approximation methods. A popular technique is an expansion in the inverse volume to which the reactants are confined, called van Kampen's system size expansion. Its leading order terms are given by the phenomenological rate equations and the linear noise approximation that quantify the mean concentrations and the Gaussian fluctuations about them, respectively. While these approximations are valid in the limit of large molecule numbers, it is known that physiological conditions often imply low molecule numbers.

We here develop systematic approximation methods based on higher terms in the system size expansion for general biochemical networks. We present an asymptotic series for the moments of the Chemical Master Equation that can be computed to arbitrary precision in the system size expansion. We then derive an analytical approximation of the corresponding time-dependent probability distribution. Finally, we devise a diagrammatic technique based on the path-integral method that allows to compute time-correlation functions. We show through the use of biological examples that the first few terms of the expansion yield accurate approximations even for low number of molecules. The theory is hence expected to closely resemble the outcomes of single cell experiments.

Contents

1 Introduction

Recent experiments reveal that molecular fluctuations inside living cells scale roughly as the inverse square root of the number of molecules [6, 7]. The sources of these intrinsic fluctuations are the random timings of the reactions by which molecules are synthesized in the cell and interact in complex biochemical networks [8–10]. Since the abundance of proteins varies from few tens to several thousands of molecules per cell [11, 12], it is expected that intrinsic fluctuations play an important role in the dynamics of biochemical networks. Deterministic models based on rate equations (REs), which have been used traditionally for *in vitro* kinetics, cannot account for these effects and are hence insufficient to infer biological parameters from experimental single cell data. Characterization of *in vivo* kinetics therefore requires stochastic models that predict statistics – such as moments, time-correlation functions and probability distributions – that quantify the cell-to-cell variability that is observed experimentally.

The conventional means of probing stochasticity in biochemical systems is a Monte-Carlo technique that has been popularised by Gillespie [13, 14, 1976]. The stochastic simulation algorithm (SSA) allows to obtain exact sample paths of the biochemical dynamics under well-mixed conditions from which, at least in principle, every statistic of interest can be obtained. The method, however, necessarily simulates every reaction event and can therefore become computationally expensive for networks with a large number of reactions. Moreover, the considerable amount of ensemble averaging typically prevents one from obtaining accurate statistics, specifically, when one studies the dynamics of biochemical systems over wide ranges of the parameter space. Accelerated simulation methods are therefore widely studied [15].

An equivalent approach dating back to Delbrück [16, 1940] is given by the Chemical Master Equation (CME). This approach has been reviewed early by McQuarrie [17–19, 1963] and has later been supported by physical arguments of Gillespie [14, 20]. The equation is the differential form of the Chapman-Kolmogorov identity for the Markov process described by the SSA [21]. The CME represents a countable set of homogeneous linear first-order ordinary differential equations (ODEs) for the probabilities of observing the system in any combination of molecule numbers of the chemical species.

Numerical solution of these equations is commonly based on state space truncation [22, 23]. However, it turns out to be computationally demanding because of combinatorial explosion, especially, when some species are present in large numbers of molecules. Techniques addressing this issue are subject to ongoing research [24–26].

Analytical solution of the CME seems accessible only for simple systems. A direct

solution, for instance, has been obtained for certain networks of unimolecular reactions [27], for one-step processes with a single species [28], or for networks that are reducible to these cases [29]. More commonly, the generating function approach is employed [19, 30–34]. Yet, these theoretical approaches seem to be mostly limited to networks with a single species because they generally rely on the solution of nonlinear partial differential equations (PDEs). Equivalent techniques are given by the Poisson representation [31, 35, 36], the spectral method [37], and the path-integral approach [38–42]. Stationary solutions for reaction networks composed of bimolecular reactions and a large number of species are known in detailed balance conditions [43, 44], in conditions satisfied by the deficiency zero theorem [45], or for examples defying combinatorial explosion [33, 46, 47]. The CME is therefore generally considered analytically intractable because the dynamics arising from the law of mass action is close to the complexity of Turing machines [48, 49].

Putatively simpler questions arise when one is interested in the first few moments only. While the equations for the moments are straight-forwardly derived from the CME [50], they can be solved exactly only for reaction networks comprising up to unimolecular reactions [19]. In this case the equations for the first few moments are closed due to the linearity in the law of mass action; similar arguments hold for the correlation functions of these networks [51]. When bimolecular reactions are present, as we will assume from now on, the law of mass action is nonlinear and hence these equations constitute an infinite hierarchy of coupled ODEs which, albeit being linear, cannot be solved.

Approximation methods often represent more efficient means for obtaining the desired statistics from the CME. Since the importance of noise in biological systems was recognised in the past decades, recent years have seen an increasing search for approximation methods that appreciate the low molecule number conditions found in the intracellular environment [49]. Two main techniques are dominating the literature: moment closure approximations and the linear noise approximation (LNA).

The first approach aims at solving the moment equations by expressing higher order moments in terms of lower order moments [52–56]. The merit of the method is that an infinite systems of linear ODEs is replaced by an approximate but closed system of nonlinear ODEs which allow for efficient numerical solution [57]. The disadvantage of the method is that its accuracy generally depends on prior assumptions about the underlying distribution functions [58]. Recent studies have employed this approach to reconstruct probability distributions through the maximum entropy approach [55, 59, 60].

The second method, given by the LNA, represents the main analytical tool to characterize biochemical reactions in living cells to date [61–70], and is also widely applied to parameter inference [71–75]. The LNA is derived from the system size expansion (SSE) of the CME [76], sometimes called the Ω-expansion, which has been proposed by van Kampen [77, 1961] for the master equation and has later been applied in the context

of chemical systems [44, 1976]. The method relies on the existence of a large parameter called the system size Ω, which for chemical systems coincides with the volume to which the reactants are confined, that allows to systematically expand the CME about its deterministic limit. The implicit reasoning is that large volumes imply high number of molecules as the expansion is carried out at constant concentration. The method leads to an effective PDE approximation of the discrete CME for which only the first few terms are dominant in the large system size limit. The first term in the expansion describes the deterministic limit and is given by the REs. The latter equations coincide precisely with the equations that have been formulated phenomenologically based on the law of mass action for *in vitro* kinetics. The second term is given by a Fokker-Planck equation with linear coefficients and is called the LNA. Its predictions are that the average concentrations follow the REs and the fluctuations about these averages are described by a Gaussian process in the limit of large system size. It is this property which allows one to obtain moments, correlation functions, as well as the probability density in closed form.

Van Kampen's studies have been paralleled by the seminal work of Kurtz [78, 79, 1970/71] on limit theorems for the random time change representation of the SSA [80]. Specifically, for finite times, Kurtz rigorously showed that under certain assumptions the stochastic process converges in probability to the solution of the REs. This result also holds in the strong sense and can be generalized to the LNA [81, 1978]. However, the employed assumptions are typically restrictive in applications, especially when one is interested in the stationary statistics to which the LNA is routinely applied [61, 67, 70, 82].

It is well known that the LNA prediction of the first two moments agrees exactly with the first two moments of the CME for networks composed of unimolecular reactions [83]. It is however the case that the solution of the CME can in some instances be in severe disagreement with the solution of the LNA. This is typically the case when bimolecular reactions involve molecular species that are present in low molecule numbers. Terms in the SSE that go beyond the LNA have been discussed by van Kampen for the first two moments of a semiconductor system [44]. However, such approximations have long been dismissed because the SSE is obtained from solving an effective PDE approximation to the CME for which positive definiteness cannot be guaranteed and its solutions cannot be regarded as probabilities [84]. Recent work has challenged this view by computing the leading order corrections to the REs using higher order terms in the SSE [85]. These correction terms are not genuine statistical moments but are instead interpreted as the leading term in the asymptotic expansion of the true moment [1]. By comparison with exact simulations using the SSA, it has been shown that these can provide accurate approximations of the true mean concentrations of the CME [85]. This work has been extended to reaction networks with arbitrary number of species and is called effective mesoscopic rate equations (EMREs) [86]. Thereupon these equations have been studied for enzyme reaction networks of moderate [87] and

large size [88]. Similarly, non-Gaussian corrections to the skewness have been obtained for autocatalytic reactions [89]. These studies have shown that the higher terms in the SSE can provide good approximations to moments of the CME in moderate to low molecule number conditions which are important in applications. Despite these developments, the SSE (beyond the LNA terms) remains poorly understood, to date, and many aspects that are relevant in recent applications are to be explored.

We here develop the SSE as an analysis tool for the CME. Thereby we formulate novel approximation methods for the estimation of moments, correlation functions and probability distributions that are valid in conditions involving moderately large molecule numbers. These are given in terms of asymptotic series in a small parameter – the inverse system size. The methods are hence systematic in the sense that they can be truncated to a certain order, or their approximation accuracy may be refined by taking into account higher order terms. Throughout, the main findings of this thesis are highlighted as *Results* including a concise derivation. We do not claim mathematical rigour but we demonstrate the validity of the asymptotic expansions in specific applications and show that these provide reasonable approximations also for low molecule numbers. The outline of this thesis is as follows.

In Chapter 2, the formalisms of the SSA and the CME are reviewed. We then, in Section 2.4, develop the SSE of the CME in detail and obtain explicit expressions for the corresponding PDE approximation. In Chapter 3, we give a solution to its moments as an asymptotic series in the inverse system size. An explicit system of ODEs for the expansion coefficients is obtained in Section 3.1. It is shown that these equations are closed and hence the expansion of the moments can be systematically truncated to any desired order. These results enable us to investigate the convergence properties of the series in Section 3.2, a question which, even in simple cases, has still not been addressed. A method for optimal truncation is proposed. We then apply this methodology to a model of gene expression in Section 3.3, and demonstrate that the proposed approximations taking into account higher order terms in the SSE perform significantly better than the Gaussian approximation provided by the LNA.

In Chapter 4, we investigate the question what are the distributions underlying the asymptotic expansion of the moments. The PDE approximation of the CME is solved perturbatively using the technique of orthogonal polynomials. It is shown in Section 4.1 how to obtain an asymptotic expansion of the continuous probability density of molecular concentrations. Again, the series be truncated systematically to any desired order in the inverse system size. In Section 4.2 we give a novel formulation of the SSE in terms of an asymptotic expansion of the discrete probability distribution. A renormalisation procedure that allows to achieve rapid convergence for processes with nonlinear propensities is derived in Section 4.3. The efficacy of the new method to predict transients of the molecule number distribution for a gene expression network is demonstrated in Section 4.4.

In Chapter 5 an alternative derivation of the SSE from the the path-integral ap-

proach is given. This enables us to investigate higher order terms in the expansions of correlation functions and power spectra. To that end, the derivation of the characteristic functional of the CME, an exact statistic that contains all information about the stochastic process at all times, is outlined in Section 5.1. The LNA is obtained as the saddle point approximation thereof. In order to cope with the large number of higher-order terms in the expansion, a novel diagrammatic technique is proposed in Section 5.2 from which the SSE can be constructed systematically using a set of *Feynman rules*. In Section 5.3 these rules are employed to approximate the power spectrum for the CME of general multi-species networks to leading order beyond the LNA. These are of particular interest because power spectra are commonly used to quantify biological rhythms, both experimentally [90–93] and theoretically [94–97]. In Section 5.4, it is shown that the theory captures oscillations in a simple reaction network that are not described by RE and LNA terms. In particular, we demonstrate that the present theory allows us to predict these dynamics over large ranges of parameters and molecule numbers. In Section 5.5 we derive a an effective theory for the power spectra of stochastic biochemical systems whose corresponding deterministic counterpart is close to a Hopf bifurcation. We demonstrate that the method is particularly valuable for the interpretation of recently acquired single cell data. We conclude with a discussion in Chapter 6 where we elaborate on the significance of our results. A list of abbreviations is provided at the end of this thesis.

2 Stochastic modelling of biochemical reaction networks

2.1 Stochastic formulation of biochemical reaction kinetics

The general formulation of biochemical reaction kinetics considers a set of N_S distinct chemical species confined to a volume Ω. The species $(X_1(t), .., X_{N_S})$ react via R chemical reactions of the type

$$s_{1j}X_1 + ... + s_{N_Sj}X_{N_S} \xrightarrow{k_j} r_{1j}X_1 + ... + r_{N_Sj}X_{N_S}, \tag{2.1}$$

where j is the reaction index running from 1 to R, k_j is the reaction rate of the j^{th} reaction, and s_{ij} and r_{ij} are the stoichiometric coefficients.

The microscopic kinetics of such a chemical mixture is described by collision theory. Within this framework two types of collisions are considered: (i) elastic non-reactive collisions that lead to thermal randomization of molecular velocities, and (ii) reactive collisions affecting only the population numbers of molecular species via one of the reactions in (2.1). If the overwhelming majority of collisions are non-reactive, one can assume that the conditions under which reactive collisions occur are *well-mixed*. On a mesoscopic scale such a mixture is homogeneously distributed throughout the volume Ω but not in chemical equilibrium. As a consequence, the state of the system may be described by the state vector $\boldsymbol{X}(t) \equiv (X_1(t), ..., X_{N_S}(t))$ of molecular populations only, independent of molecular positions and velocities. Strictly speaking, this description does take into account solvation effects. An extension of these arguments to well-mixed solutions that are dilute in the reactant molecules has been given by Gillespie [98]. Such a description better accounts for the conditions of the intracellular environment where reactants diffuse in aqueous solution.

These arguments lead to a formulation of stochastic biochemical kinetics which states that, given $\boldsymbol{X}(t) = \boldsymbol{n}$, the probability for one of the R reactions to occur within the next infinitesimal time interval $[t, t + \mathrm{d}t)$ equals $w_r(\boldsymbol{n}, \Omega)\mathrm{d}t$ [15]. The function $w_r(\boldsymbol{n}, \Omega)$ is called the propensity function and is given by

$$w_r(\boldsymbol{n}, \Omega) = \Omega k_r \prod_{i=1}^{N_S} \Omega^{-s_{ir}} s_{i_r}! \binom{n_i}{s_{ir}}, \tag{2.2}$$

which explicitly depends on the size of the reaction volume Ω. Reactions of this type

are referred to as satisfying mass action kinetics. Though from microscopic considerations only up to unimolecular ($\sum_{i=1}^{N_S} s_{ir} = 1$) and bimolecular ($\sum_{i=1}^{N_S} s_{ir} = 2$) are to be considered. Zero-order reactions ($\sum_{i=1}^{N_S} s_{ir} = 0$) are commonly used to describe open systems [76] such as intracellular compartments. While the latter reactions are often referred as elementary, higher-order reactions are also commonly used to describe effective reactions [31, 99].

2.2 Stochastic Simulation Algorithm

The SSA is a Monte Carlo technique which can be used to simulate exact sample paths of the stochastic reaction dynamics [13, 14]. Over the past two decades, the algorithm was popularized for the study of gene expression in single cells [9, 10]. Specifically, one commonly associates a realization of a stochastic process obtained with the state of a single cell. A simple formulation of the algorithm is given by the *first reaction method*:

> *For each reaction r draw a reaction time τ_r from an exponential distribution with rate w_r. Execute the fastest reaction, advance time and repeat.*

An alternative method, called the *direct method*, uses the fact that the fastest reaction time is also exponentially distributed

$$\Pr\left(\min\{\tau_1, \ldots, \tau_R\} > t\right) = \exp\left(-t \sum_{r=1}^{R} w_r\right), \tag{2.3}$$

and the index j of the fastest reaction has probability

$$\Pr\left(\tau_j = \min\{\tau_1, \ldots, \tau_R\}\right) = \frac{w_j}{\sum_{r=1}^{R} w_r}. \tag{2.4}$$

Several other variants of these algorithms exist in the literature [15, 100]. However in many situations of practical interest, the application of the SSA is computationally expensive mainly due to the two reasons: (i) whenever the fluctuations are large, e.g., the case when one of the species occurs in low molecule numbers, a considerably large amount of ensemble averaging of the stochastic trajectories is needed to obtain statistically accurate results. (ii) the SSA simulates each reaction event explicitly which becomes computationally expensive whenever at least one of the propensities is very large or, equivalently, at least one molecular species is present in large molecule numbers.

2.3 The Chemical Master Equation

An alternative description that is exactly equivalent to the SSA is the CME. Specifically, the CME is the time-evolution equation for the probability $P(\boldsymbol{X} = \boldsymbol{n}, t|\boldsymbol{X} = \boldsymbol{n}_0, t_0)$ that the molecular species are found in a particular mesoscopic state $\boldsymbol{n} = (n_1, ..., n_{N_S})^T$

at time t, where n_i is the number of molecules of the i^{th} species, given that the state was $\boldsymbol{X}(t_0) = \boldsymbol{n}_0$ at some initial time t_0. Henceforth we will use the shorthand notation $P(\boldsymbol{n}, t) \equiv P(\boldsymbol{X} = \boldsymbol{n}, t|\boldsymbol{X} = \boldsymbol{n}_0, t_0)$ and the explicit dependence on the initial condition is understood. The change in probability is either one of the R reactions occurring, i.e. $w_r(\boldsymbol{n})\mathrm{d}t$, or no reaction occurring during an infinitesimal interval $\mathrm{d}t$, i.e. Eq. (2.3), times the probability of that previous state. The result is:

$$\begin{aligned} P(\boldsymbol{n}, t+\mathrm{d}t) =& P(\boldsymbol{n}, t) \underbrace{\left(1 - \sum_{r=1}^{R} w_r(\boldsymbol{n}, \Omega)\mathrm{d}t + O(\mathrm{d}t^2)\right)}_{\text{no reaction in } [t, t+\mathrm{d}t)} \\ &+ \sum_{r=1}^{R} P(\boldsymbol{n} - \boldsymbol{S}_r, t) \underbrace{w_r(\boldsymbol{n} - \boldsymbol{S}_r, \Omega)\mathrm{d}t}_{\text{prob. of } r^{th} \text{ reaction in } [t, t+\mathrm{d}t)} + O(\mathrm{d}t^2), \end{aligned} \tag{2.5}$$

where $\boldsymbol{S}_r$ is the vector formed by the columns of the stoichiometric matrix $S_{ir} = r_{ir} - s_{ir}$. Note that the probability of two reactions occurring is $O(\mathrm{d}t^2)$. Hence the equation for the probability $P(\boldsymbol{n}, t)$ is given by

$$\frac{\mathrm{d}P(\boldsymbol{n}, t)}{\mathrm{d}t} = \sum_{r=1}^{R} \left(\prod_{i=1}^{N_S} E_i^{-S_{ir}} - 1 \right) w_r\left(\boldsymbol{n}, \Omega\right) P(\boldsymbol{n}, t), \tag{2.6}$$

Here, the step operator E_i is formally defined by its action on a function of the molecule numbers as

$$E_i^{-S_{ir}} g(n_1, ..., n_i, ..., n_{N_S}) = g(n_1, ..., n_i - S_{ir}, ..., n_{N_S}), \tag{2.7}$$

to ease the notation.

2.4 The expansion of the Chemical Master Equation

The CME is typically intractable for computational purposes because of the inherent large state space. This section lays out the SSE of the CME on which the approximation methods developed in the following chapters are based on. The starting point of the analysis is van Kampen's ansatz

$$\frac{\boldsymbol{n}}{\Omega} = [\boldsymbol{X}] + \Omega^{-1/2}\boldsymbol{\epsilon}, \tag{2.8}$$

which separates the instantaneous concentration into a deterministic part given by the solution $[\boldsymbol{X}]$ of the macroscopic REs for the reaction scheme (2.1) and the fluctuations around it parametrised by the fluctuations $\boldsymbol{\epsilon}$. The expansion of the CME is now carried out using the following steps:

(i) Associating a continuous density: In a first step, we associate the probability of the molecule numbers $P(\boldsymbol{n},t)$ with a continuous probability density $\Pi(\boldsymbol{\epsilon},t)$ for the fluctuations $\boldsymbol{\epsilon}$. Assuming $\boldsymbol{n}$ is a continuous random variable, Eq. (2.8) implies

$$\begin{aligned}\Pi(\boldsymbol{\epsilon},t) =& \left|\frac{\partial \boldsymbol{n}}{\partial \boldsymbol{\epsilon}}\right| P(\boldsymbol{n}=\Omega[\boldsymbol{X}]+\Omega^{1/2}\boldsymbol{\epsilon},t) \\ =& \Omega^{N_S/2} P(\boldsymbol{n}=\Omega[\boldsymbol{X}]+\Omega^{1/2}\boldsymbol{\epsilon},t),\end{aligned} \tag{2.9}$$

according to the change of variables theorem [101]. Note that $\left|\frac{\partial \boldsymbol{n}}{\partial \boldsymbol{\epsilon}}\right| = \Omega^{N_S/2}$ is just the Jacobian determinant of the transformation (2.8). Note also that this step was given in the derivation of van Kampen [76]. A generalization of this result to the discrete probability distributions is given in Chapter 4, Result 4.5.

(ii) Expansion of the step operator: One now expands the step operator using its formal Taylor series

$$\begin{aligned}&E_i^{-S_{ir}} w_r\left(\boldsymbol{n},\Omega\right) P(\boldsymbol{n},t) \\ &\quad = w_r\left(n_1,\ldots,n_i-S_{ir},\ldots,n_{N_S},\Omega\right) P(n_1,\ldots,n_i-S_{ir},\ldots,n_{N_S},t) \\ &\quad = e^{-S_{ir}\frac{\partial}{\partial n_i}} w_r\left(\boldsymbol{n},\Omega\right) P(\boldsymbol{n},t).\end{aligned} \tag{2.10}$$

We express the above equation in terms of the $\boldsymbol{\epsilon}$-variables by virtue of van Kampen's ansatz, Eq. (2.8), and Eq. (2.9)

$$\begin{aligned}&E_i^{-S_{ir}} w_r\left(\boldsymbol{n},\Omega\right) P(\boldsymbol{n},t) \\ &\quad = \left(e^{-\Omega^{-1/2}S_{ir}\partial_{\epsilon_i}}\right) w_r(\Omega[\boldsymbol{X}]+\Omega^{1/2}\boldsymbol{\epsilon},\Omega) P(\boldsymbol{n}=\Omega[\boldsymbol{X}]+\Omega^{1/2}\boldsymbol{\epsilon},t) \\ &\quad = \Omega^{-N_S/2}\left(e^{-\Omega^{-1/2}S_{ir}\partial_{\epsilon_i}}\right) w_r(\Omega[\boldsymbol{X}]+\Omega^{1/2}\boldsymbol{\epsilon},\Omega)\Pi(\boldsymbol{\epsilon},t),\end{aligned} \tag{2.11}$$

where ∂_{ϵ_i} denotes $\frac{\partial}{\partial \epsilon_i}$.

(iii) Expansion of the propensity: It remains to expand the propensity about the deterministic limit

$$\begin{aligned}&w_r(\Omega[\boldsymbol{X}]+\Omega^{1/2}\boldsymbol{\epsilon},\Omega) \\ &\qquad = \sum_{n=0}^{\infty}\frac{\Omega^{-n/2}}{n!}\sum_{i_1=0}^{N_S}\ldots\sum_{i_n=0}^{N_S}\epsilon_{i_1}\ldots\epsilon_{i_n}\partial_{[X_{i_1}]}\ldots\partial_{[X_{i_n}]} w_r(\Omega[\boldsymbol{X}],\Omega),\end{aligned} \tag{2.12}$$

Note that $w_r(\Omega[\boldsymbol{X}],\Omega)$ is just the propensity evaluated at the macroscopic concentrations. Its explicit dependence on Ω is determined as follows.

For each reaction propensity we will assume that it has an expansion in the inverse

system size of the form

$$w_r(\boldsymbol{n},\Omega) = \Omega \sum_{s=0}^{\infty} \Omega^{-s} f_r^{(s)}\left(\frac{\boldsymbol{n}}{\Omega}\right), \tag{2.13}$$

which we require for the CME to have a deterministic limit. In particular,

$$f_r^{(0)}([\boldsymbol{X}]) = \lim_{\Omega\to\infty} \frac{w_r(\Omega[\boldsymbol{X}],\Omega)}{\Omega} \neq 0, \tag{2.14}$$

is the deterministic rate function that depends on the concentration $[X]$ and is independent of Ω. We remark that for reaction networks with mass action propensities, Eq. (2.2), or effective propensities that have been deduced from it, have a finite expansion of the form (2.13).

Before proceeding we illustrate this scaling for mass action kinetics and non-elementary propensities. Following Eq. (2.2), the reaction $s_{1r}X_1 \xrightarrow{k_r} r_{1r}X_1$ has the propensity

$$w_r(n_1,\Omega) = \Omega k_r \Omega^{-s_{1r}} s_{1r}! \binom{n_1}{s_{1r}}. \tag{2.15}$$

Using now the Taylor expansion of the binomial coefficient, we find

$$s_{1r}!\binom{n_1}{s_{1r}} = \Omega^{s_{1r}} \sum_{s=0}^{s_{1r}-1} \Omega^{-s} \left(\frac{n_1}{\Omega}\right)^{s_{1r}-s} \mathfrak{s}(s_{1r}, s_{1r}-s). \tag{2.16}$$

and hence $f_r^{(0)}\left(\frac{n_1}{\Omega}\right) = k_r\left(\frac{n_1}{\Omega}\right)^{s_{1r}}$,

$$f_r^{(s)}\left(\frac{n_1}{\Omega}\right) = k_r \left(\frac{n_1}{\Omega}\right)^{s_{1r}-s} \mathfrak{s}(s_{1r}, s_{1r}-s), \tag{2.17}$$

and $f_r^{(s)} = 0$ for $s \geq s_{1r}$, where $\mathfrak{s}$ are the Stirling numbers of the first kind [102]. More generally, it now follows that the reactions (2.1) following mass action kinetics must have $f_r^{(s)} = 0$ for $s > \sum_{i=1}^{N_S} \max(s_{ir}-1, 0)$. As a second example, we consider the widely used Michaelis-Menten propensity $w_r(n,\Omega) = \Omega k_r \frac{n}{n+K\Omega}$ that has $f_r^{(0)}([X]) = k_r \frac{[X]}{[X]+K}$ and $f_r^{(s)}([X]) = 0$ for $s > 0$.

(iv) Transformation of the time-derivative: Since the variable $\boldsymbol{n}$ of the CME is time-independent, we need to account for changes in $[\boldsymbol{X}](t)$ by a change in the fluctuations $\boldsymbol{\epsilon}$. The total time derivative is given by

$$\begin{aligned}\frac{\mathrm{d}}{\mathrm{d}t}P(\boldsymbol{n} = \Omega[\boldsymbol{X}] + \Omega^{1/2}\boldsymbol{\epsilon}, t) &= \left(\frac{\partial}{\partial t} + \left.\frac{\mathrm{d}\boldsymbol{\epsilon}}{\mathrm{d}t}\right|_{\boldsymbol{n}} \cdot \nabla_{\boldsymbol{\epsilon}}\right) P(\boldsymbol{n} = \Omega[\boldsymbol{X}] + \Omega^{1/2}\boldsymbol{\epsilon}, t) \\ &= \Omega^{-N_S/2}\left(\frac{\partial}{\partial t} - \Omega^{1/2}\frac{\mathrm{d}[\boldsymbol{X}]}{\mathrm{d}t} \cdot \nabla_{\boldsymbol{\epsilon}}\right)\Pi(\boldsymbol{\epsilon}, t),\end{aligned} \tag{2.18}$$

where the time-derivative of $\boldsymbol{\epsilon}$ at constant $\boldsymbol{n}$ has been obtained from Eq. (2.8). Note that we have made use of the fact that the Jacobian determinant of the transformation is time-independent.

(v) Putting it all together: Substituting now Eqs. (2.9) through (2.12) into Eq. (2.6), we find that the CME is transformed into

$$\begin{aligned}&\left(\frac{\partial}{\partial t}-\Omega^{1/2}\sum_{i=1}^{N_S}\frac{\mathrm{d}[X_i]}{\mathrm{d}t}\frac{\partial}{\partial\epsilon_i}\right)\Pi(\boldsymbol{\epsilon},t)\\&=\Omega\sum_{s=0}^{\infty}\sum_{\alpha=1}^{\infty}\sum_{\beta=0}^{\infty}(-1)^{\alpha}\Omega^{-(\alpha+\beta+2s)/2}\frac{\mathcal{D}^{j_1\ldots j_\beta}_{i_1\ldots i_\alpha,s}}{\alpha!\beta!}\partial_{\epsilon_{i_1}}\ldots\partial_{\epsilon_{i_\alpha}}\epsilon_{j_1}\ldots\epsilon_{j_\beta}\Pi(\boldsymbol{\epsilon},t),\end{aligned}\tag{2.19}$$

where we have made use of the particular summation convention that the multi-indices $i_1\ldots i_\alpha$ and $j_1\ldots j_\beta$ appearing in the coefficient $\mathcal{D}^{j_1\ldots j_\beta}_{i_1\ldots i_\alpha,s}$ are summed from 1 to N_S, i.e. the sums $\sum_{i_1=0}^{N_S}\ldots\sum_{i_\alpha=0}^{N_S}$ and $\sum_{j_1=0}^{N_S}\ldots\sum_{j_\beta=0}^{N_S}$ have been omitted. Note that the Jacobian determinant has cancelled on both sides of the above equation. The coefficients in the above equations can be given explicitly

$$\mathcal{D}^{j_1\ldots j_\beta}_{i_1\ldots i_\alpha,s}=\sum_{r=1}^{R}S_{i_1r}S_{i_2r}\ldots S_{i_\alpha r}\frac{\partial}{\partial[X_{j_1}]}\frac{\partial}{\partial[X_{j_2}]}\ldots\frac{\partial}{\partial[X_{j_\beta}]}f_r^{(s)}([\boldsymbol{X}]),\tag{2.20}$$

and depend on the stoichiometry S_{ir} and the solution of the REs. Note that is invariant under permutations of its lower (and upper) indices. Rearranging in powers of $\Omega^{-1/2}$, we have the following result:

Result 2.1. *The CME, Eq. (2.6), has the following expansion*

$$\begin{aligned}&\left(\frac{\partial}{\partial t}-\Omega^{1/2}\sum_{i=1}^{N_S}\frac{\mathrm{d}[X_i]}{\mathrm{d}t}\frac{\partial}{\partial\epsilon_i}\right)\Pi(\boldsymbol{\epsilon},t)\\&=\left(-\Omega^{1/2}\sum_{r=1}^{R}\sum_{i=1}^{N_S}S_{ir}f_r^{(0)}([\boldsymbol{X}])\frac{\partial}{\partial\epsilon_i}+\sum_{k=0}^{N}\Omega^{-k/2}\mathcal{L}_k\right)\Pi(\boldsymbol{\epsilon},t)+O(\Omega^{-(N+1)/2}),\end{aligned}\tag{2.21}$$

where

$$\mathcal{L}_k=\sum_{s=0}^{\lceil k/2\rceil}\sum_{\alpha=1}^{2+k-2s}(-1)^{\alpha}\frac{\mathcal{D}^{j_1\ldots j_{2+k-\alpha-2s}}_{i_1\ldots i_\alpha,s}}{\alpha!(2+k-\alpha-2s)!}\partial_{\epsilon_{i_1}}\ldots\partial_{\epsilon_{i_\alpha}}\epsilon_{j_1}\ldots\epsilon_{j_{2+k-\alpha-2s}},\tag{2.22}$$

and $\lceil\cdot\rceil$ denotes the ceiling value.

The first two terms of this expansion have been obtained by van Kampen for the case of single variable [44] and have later been generalized to reaction networks with up to bimolecular reactions [1]. Note that the above result has no such restrictions and, here, the expansion of the CME has been carried out to arbitrary order for the first

time. For comparison, we write out the first few terms explicitly

$$\mathcal{L}_0 = -\partial_{i_1}\mathcal{D}^{j_1}_{i_1}\epsilon_{j_1} + \frac{1}{2}\partial_{i_1}\partial_{i_2}\mathcal{D}_{i_1 i_2}, \tag{2.23a}$$

$$\mathcal{L}_1 = -\partial_{i_1}\mathcal{D}_{i_1,1} - \frac{1}{2!}\partial_{i_1}\mathcal{D}^{j_1 j_2}_{i_1}\epsilon_{j_1}\epsilon_{j_2} + \frac{1}{2!}\partial_{i_1}\partial_{i_2}\mathcal{D}^{j_1}_{i_1 i_2}\epsilon_{j_1} - \frac{1}{3!}\partial_{i_1}\partial_{i_2}\partial_{i_3}\mathcal{D}_{i_1 i_2 i_3}, \tag{2.23b}$$

$$\begin{aligned}\mathcal{L}_2 = &-\partial_{i_1}\mathcal{D}^{j_1}_{i_1,1}\epsilon_{j_1} + \frac{1}{2!}\partial_{i_1}\partial_{i_2}\mathcal{D}_{i_1 i_2,1} - \frac{1}{3!}\partial_{i_1}\mathcal{D}^{j_1 j_2 j_3}_{i_1}\epsilon_{j_1}\epsilon_{j_2}\epsilon_{j_3} + \frac{1}{2!2!}\partial_{i_1}\partial_{i_2}\mathcal{D}^{j_1 j_2}_{i_1 i_2}\epsilon_{j_1}\epsilon_{j_2} \\ &- \frac{1}{3!}\partial_{i_1}\partial_{i_2}\partial_{i_3}\mathcal{D}^{j_1}_{i_1 i_2 i_3}\epsilon_{j_1} + \frac{1}{4!}\partial_{i_1}\partial_{i_2}\partial_{i_3}\partial_{i_4}\mathcal{D}_{i_1 i_2 i_3 i_4},\end{aligned} \tag{2.23c}$$

which concludes the formal expansion of the CME.

2.4.1 Rate Equations

The dominant term in the infinite system size limit is obtained by equating terms to order $\Omega^{1/2}$ in Result 2.1. We find the deterministic equations

$$\frac{\mathrm{d}[X_i]}{\mathrm{d}t} = \sum_{r=1}^{R} S_{ir} f_r^{(0)}([\boldsymbol{X}]), \tag{2.24}$$

and we will assume that its solution is unique. Note that the right hand side of the REs is just $\mathcal{D}_{\alpha_i,0}$. Kurtz proved [79] that if the right hand side of Eq. (2.24) is Lipschitz continuous in $[\boldsymbol{X}]$, it follows that

$$\lim_{\Omega\to\infty} \Pr\left(\sup_{t\leq T}\left|\frac{X_i(t)}{\Omega} - [X_i](t,[\boldsymbol{X}]_0)\right| > \delta\right) = 0, \tag{2.25}$$

for a $\delta > 0$ and any $T > 0$ given that $\boldsymbol{X}(0) = \Omega[\boldsymbol{X}]_0$. We note however that in Kurtz's theorem we cannot take the limit $T \to \infty$ since these limit do not commute. Counterexamples for this asymptotic behaviour are well known in cases where the right hand side of Eq. (2.24) has more than a single positive fixed point which occurs for instance for multistable systems [103, 104] and close to extinction thresholds [105, 106]. We will therefore assume throughout that Eq. (2.24) has a single fixpoint that is asymptotically stable in the sense of Lyapunov.

2.4.2 Linear Noise Approximation

It then follows that the probability density has the limit

$$\pi_0(\boldsymbol{\epsilon}, t) = \lim_{\Omega\to\infty} \Pi(\boldsymbol{\epsilon}, t), \tag{2.26}$$

which is determined by terms of order Ω^0 in Eq. (2.21)

$$\frac{\partial}{\partial t}\pi_0(\boldsymbol{\epsilon}, t) = \mathcal{L}_0\pi_0(\boldsymbol{\epsilon}, t)$$

$$= \left(-\partial_\alpha \mathcal{J}_{\alpha\beta}\epsilon_\beta + \frac{1}{2}\partial_\alpha\partial_\beta D_{\alpha\beta} \right) \pi_0(\boldsymbol{\epsilon}, t). \tag{2.27}$$

This equation is a Fokker-Planck equation with linear drift and diffusion coefficients that is referred to as the LNA. Note that we have denoted by $\mathcal{J}_{\alpha\beta} = \mathcal{D}_\alpha^\beta$ the Jacobian of the REs, Eq. (2.24), and by $D_{\alpha\beta} = \mathcal{D}_{\alpha\beta}$ the so called diffusion matrix (in analogy to diffusion processes). The time evolution equations of the covariance $\Sigma_{ij}(t) = \int \mathrm{d}\boldsymbol{\epsilon}\epsilon_i\epsilon_j\pi_0(\boldsymbol{\epsilon}, t)$ are obtained by multiplying the latter by $\epsilon_i\epsilon_j$ and performing the integration over $\boldsymbol{\epsilon}$, which gives

$$\frac{\partial}{\partial t}\Sigma_{ij} = \mathcal{J}_{i\alpha}\Sigma_{\alpha j} + \Sigma_{i\alpha}\mathcal{J}_{\alpha j} + D_{ij}. \tag{2.28}$$

Solution of the Fokker-Planck equation with linear time-dependent coefficient is straightforward, and has been given for instance in [44].

Result 2.2 (Time-dependent solution of the linear noise approximation)**.** *For deterministic initial conditions the solution of the Fokker-Planck equation (2.27) is given by*

$$\pi_0(\boldsymbol{\epsilon}, t) = \frac{1}{\sqrt{(2\pi)^{N_S}|\Sigma(t)|}} e^{-\frac{1}{2}\boldsymbol{\epsilon}^T\Sigma^{-1}(t)\boldsymbol{\epsilon}}, \tag{2.29}$$

where $\Sigma(t)$ is the solution of the Lyapunov matrix equation with time-dependent coefficient matrices

$$\frac{\partial}{\partial t}\Sigma = \mathcal{J}(t)\Sigma + \Sigma\mathcal{J}^T(t) + D(t), \tag{2.30}$$

with initial condition $\Sigma(0) = 0$.

The solution can be verified by considering the characteristic function $G_0(\boldsymbol{k}, t)$ of Eq. (2.29) which is [107]

$$G_0(\boldsymbol{k}, t) = \int_{\mathbb{R}^{N_S}} \mathrm{d}\boldsymbol{\epsilon} e^{i\boldsymbol{k}\cdot\boldsymbol{\epsilon}}\pi_0(\boldsymbol{\epsilon}, t) = \exp\left(-\frac{1}{2}\boldsymbol{k}^T\Sigma(t)\boldsymbol{k} \right). \tag{2.31}$$

This function satisfies the partial differential equation

$$\frac{\partial}{\partial t}G_0(\boldsymbol{k}, t) = \left(\boldsymbol{k}^T\mathcal{J}(t)\nabla_{\boldsymbol{k}} - \frac{1}{2}\boldsymbol{k}^T D(t)\boldsymbol{k} \right) G_0(\boldsymbol{k}, t), \tag{2.32}$$

subject to the initial condition $G_0(\boldsymbol{k}, 0) = 1$, i.e. $\Sigma(0) = 0$, and the normalization condition $G_0(0, t) = 1$. The same equation is found by inserting the inverse transform $\pi_0(\boldsymbol{\epsilon}, t) = \int_{\mathbb{R}^{N_S}} \frac{\mathrm{d}\boldsymbol{k}}{2\pi} e^{-i\boldsymbol{k}\cdot\boldsymbol{\epsilon}} G_0(\boldsymbol{k}, t)$ into Eq. (2.27) which verifies Result 2.2. A simple direct calculation using the method of characteristics is as follows:

Derivation. We consider characteristic lines $(\boldsymbol{k}, G_0) = (\boldsymbol{k}(s), G_0(s))$ parametrised by s.

Inspection of Eq. (2.32) gives the characteristic equations

$$\frac{\mathrm{d}t}{\mathrm{d}s} = 1, \quad \frac{\mathrm{d}\boldsymbol{k}}{\mathrm{d}s} = -\mathcal{J}^T(s)\boldsymbol{k}, \quad \frac{\mathrm{d}G_0}{\mathrm{d}s} = -\frac{1}{2}\boldsymbol{k}^T D(s)\boldsymbol{k}\, G_0. \tag{2.33}$$

The first equation yields $s = t$, while the solution of the second equation

$$\boldsymbol{k}(t) = \mathcal{T}_{\leftarrow}\left\{e^{-\int_0^t \mathrm{d}t'\,\mathcal{J}^T(t')}\right\}\boldsymbol{c}, \tag{2.34}$$

must be expressed in terms of the operator $\mathcal{T}_{\leftarrow}$ chronological time ordering, and a constant vector $\boldsymbol{c}$ for the characteristic line. The explicit expression for the time-ordered exponential is

$$\begin{aligned}\mathcal{T}_{\leftarrow}\left\{e^{\int_0^t \mathrm{d}t'\,\mathcal{J}(t')}\right\} \equiv& \sum_{n=0}^{\infty}\frac{1}{n!}\int_0^t \mathrm{d}t_1' \cdots \int_0^t \mathrm{d}t_n' \mathcal{T}_{\leftarrow}\left\{\mathcal{J}(t_1')\cdots\mathcal{J}(t_n')\right\} \\ =& 1 + \int_0^t \mathrm{d}t_1'\,\mathcal{J}(t_1') + \int_0^t \mathrm{d}t_1' \int_0^{t_1'} \mathrm{d}t_2'\,\mathcal{J}(t_1')\mathcal{J}(t_2') + \cdots .\end{aligned} \tag{2.35}$$

Note that by this definition, we have

$$\left(\mathcal{T}_{\leftarrow}\left\{e^{\int_0^t \mathrm{d}t'\,\mathcal{J}(t')}\right\}\right)^T = \mathcal{T}_{\rightarrow}\left\{e^{\int_0^t \mathrm{d}t'\,\mathcal{J}^T(t')}\right\}, \tag{2.36}$$

$$\left(\mathcal{T}_{\leftarrow}\left\{e^{\int_0^t \mathrm{d}t'\,\mathcal{J}(t')}\right\}\right)^{-1} = \mathcal{T}_{\rightarrow}\left\{e^{-\int_0^t \mathrm{d}t'\,\mathcal{J}(t')}\right\}, \tag{2.37}$$

where the operator $\mathcal{T}_{\rightarrow}$ implements the reverse chronological ordering. Along a characteristic $\boldsymbol{c}$ the solution of the third equation in (2.33) is now obtained as

$$\ln\frac{G_0(\boldsymbol{c},t)}{G_0(\boldsymbol{c},0)} = -\frac{1}{2}\int_0^t \mathrm{d}t'\boldsymbol{c}^T\mathcal{T}_{\rightarrow}\left\{e^{-\int_0^{t'}\mathrm{d}t''\,\mathcal{J}(t'')}\right\}D(t')\mathcal{T}_{\leftarrow}\left\{e^{-\int_0^{t'}\mathrm{d}t''\,\mathcal{J}^T(t'')}\right\}\boldsymbol{c} \tag{2.38}$$

From Eqs. (2.34) and (2.37), $\boldsymbol{c} = \mathcal{T}_{\rightarrow}\left\{e^{\int_0^t \mathrm{d}t'\,\mathcal{J}^T(t')}\right\}\boldsymbol{k}(t)$, the generating function becomes

$$G_0(\boldsymbol{k},t) = \exp\left(-\frac{1}{2}\boldsymbol{k}^T\Sigma(t)\boldsymbol{k}\right), \tag{2.39}$$

which satisfies the initial condition $G_0(\boldsymbol{k},0) = 1$, and

$$\begin{aligned}\Sigma(t) = \mathcal{T}_{\leftarrow}\left\{e^{\int_0^t \mathrm{d}t'\,\mathcal{J}(t')}\right\}\Bigg[\int_0^t \mathrm{d}t'\mathcal{T}_{\rightarrow}\left\{e^{-\int_0^{t'}\mathrm{d}t''\,\mathcal{J}(t'')}\right\}D(t')\times \\ \mathcal{T}_{\leftarrow}\left\{e^{-\int_0^{t'}\mathrm{d}t''\,\mathcal{J}^T(t'')}\right\}\Bigg]\mathcal{T}_{\rightarrow}\left\{e^{\int_0^t \mathrm{d}t'\,\mathcal{J}^T(t')}\right\},\end{aligned} \tag{2.40}$$

is the solution of the Lyapunov matrix equation (2.30) with initial condition $\Sigma(0) = 0$. The result follows by inverting the generating function using Eq. (2.31). Note that since we have assumed that the REs possess an asymptotically stable fixed point ensures

that the limit $\lim_{t\to\infty} \Sigma(t)$ exists and thus a stationary solution exists. The former is obtained by the solution of Eq. (2.30) with the derivative set to zero. □

3 The expansion of the moments

The LNA is commonly used to predict how noise is regulated and exploited at the cellular level [61, 63, 65]. The predictions of its moments are exact for reaction networks of unimolecular reactions, and for networks involving bimolecular reactions but large numbers of molecules [83]. Most biochemical networks in living cells, however, involve bimolecular interactions between molecular species that are represented by a few tens to thousands of molecules under physiological conditions [11, 12]. It is therefore questionable how reliable the LNA predictions are for these systems. We here utilise the higher than LNA terms in the SSE to derive expressions for the moments that are more accurate than the LNA. This is accomplished using an asymptotic series of the moments in powers of the inverse system size that can be truncated at any desired order.

To that end, we expand the probability density $\Pi(\boldsymbol{\epsilon}, t)$ in terms of the inverse square root of the system size

$$\Pi(\boldsymbol{\epsilon}, t) = \sum_{n=0}^{N} \Omega^{-n/2} \pi_n(\boldsymbol{\epsilon}, t) + O(\Omega^{-(N+1)/2}). \tag{3.1}$$

The leading order term is given by the LNA solution. Substituting the asymptotic series (3.1) into Eq. (2.21) of Result 2.1 and equating terms to order $\Omega^{-n/2}$, we find

$$\begin{aligned} \left(\frac{\partial}{\partial t} - \mathcal{L}_0\right)\pi_n(\boldsymbol{\epsilon}, t) &= \mathcal{L}_1\pi_{n-1} + ... + \mathcal{L}_n\pi_0 \\ &= \sum_{k=1}^{n} \mathcal{L}_k \pi_{n-k}(\boldsymbol{\epsilon}, t), \end{aligned} \tag{3.2}$$

for $n > 0$. We postpone the discussion of the solution for this set of recursive equations until Chapter 4. Here, in Section 3.1 we are concerned with finding equations for the moments implied by Eq. (3.1). This allows us to perform a preliminary investigation of the convergence properties of the SSE which is carried out in Section 3.2. Specifically, we show how the expansion may be truncated to obtain biologically meaningful results. We conclude with an application of these results to a gene expression model in Section 3.3.

3.1 Construction of the moment equations

As a consequence of the asymptotic expansion of the probability density (3.1), there exists an equivalent asymptotic expansion of the γ^{th} moment

$$\langle \epsilon_{i_1} ... \epsilon_{i_\gamma} \rangle = \sum_{n=0}^{N} \Omega^{-n/2} [\epsilon_{i_1} ... \epsilon_{i_\gamma}]_n + O(\Omega^{-(N+1)/2}), \tag{3.3}$$

where the following definition has been used

$$[\epsilon_{i_1} ... \epsilon_{i_\gamma}]_n = \int \mathrm{d}\boldsymbol{\epsilon}\, \epsilon_{i_1} ... \epsilon_{i_\gamma} \pi_n(\boldsymbol{\epsilon}, t). \tag{3.4}$$

We note that only $[\epsilon_{i_1} ... \epsilon_{i_\gamma}]_0$ is a genuine statistical moment. The coefficients $[\epsilon_{i_1} ... \epsilon_{i_\gamma}]_n$, where $n \geq 1$, are not statistical moments but refer to the order $\Omega^{-n/2}$ terms in the asymptotic expansion of the true moment. This fact can been seen from the asymptotic expansion of the probability density, Eq. (3.1) since by the normalization condition, we have

$$1 = \int \mathrm{d}\boldsymbol{\epsilon}\, \Pi(\boldsymbol{\epsilon}, t) = \sum_{n=0}^{N} \Omega^{-n/2} \int \mathrm{d}\boldsymbol{\epsilon}\, \pi_n(\boldsymbol{\epsilon}, t) + O(\Omega^{-(N+1)/2}). \tag{3.5}$$

Equating terms to order $\Omega^{-n/2}$, we obtain:

$$\int \mathrm{d}\boldsymbol{\epsilon}\, \pi_0(\boldsymbol{\epsilon}, t) = 1, \quad \int \mathrm{d}\boldsymbol{\epsilon}\, \pi_n(\boldsymbol{\epsilon}, t) = 0 \quad \forall n > 0. \tag{3.6}$$

These properties are frequently encountered in the context of perturbative expansions, as for example the small noise expansions of the Fokker-Planck equation discussed by Gardiner [31]. Specifically, property (3.6) implies that only $\pi_0(\boldsymbol{\epsilon}, t)$ is a genuine probability density function but π_n for $n > 0$ can only serve as a correction to π_0 approximating the probability density $\Pi(\boldsymbol{\epsilon}, t)$ for finite values of Ω.

We remark that because the solution to the LNA is a centred Gaussian it follows that all of its moments can be expressed in terms of the second moment. Specifically, Wick's theorem [108–110] states that

$$[\epsilon_{i_1} ... \epsilon_{i_\gamma}]_0 = \sum_{\substack{\text{pairings} \\ P \text{ of } \{i_1,..,i_\gamma\}}} [\epsilon_{P_1} \epsilon_{P_2}]_0 ... [\epsilon_{P_{\gamma-1}} \epsilon_{P_\gamma}]_0, \tag{3.7}$$

and all odd order moments are zero because of the symmetry of $\pi_0(\boldsymbol{\epsilon}, t)$.

In order to obtain an equation of the moment expansion coefficients, we multiply Eq. (3.2) by $\epsilon_{i_1} ... \epsilon_{i_\gamma}$ and perform the integration over the domain of $\boldsymbol{\epsilon}$, which yields

$$\frac{\partial}{\partial t} [\epsilon_{i_1} ... \epsilon_{i_\gamma}]_n = \sum_{k=0}^{n} \sum_{s=0}^{\lceil k/2 \rceil} \int \mathrm{d}\boldsymbol{\epsilon}\, \epsilon_{i_1} ... \epsilon_{i_\gamma} \mathcal{L}_k \pi_{n-k}(\epsilon, t). \tag{3.8}$$

For obtaining explicit expressions, we note that $\mathcal{L}_k$ of Result (2.1) contains terms of the form $(-1)^\alpha \mathcal{D}^{j_1\dots j_\beta}_{k_1\dots k_\alpha} \partial_{\epsilon_{k_1}} \dots \partial_{\epsilon_{k_\alpha}} \epsilon_{j_1} \dots \epsilon_{j_\beta}$. Using partial integration, we find

$$\begin{aligned}(-1)^\alpha &\int \mathrm{d}\boldsymbol{\epsilon}\, \epsilon_{i_1}\dots\epsilon_{i_\gamma} \mathcal{D}^{j_1\dots j_\beta}_{k_1\dots k_\alpha} \partial_{\epsilon_{k_1}} \dots \partial_{\epsilon_{k_\alpha}} \epsilon_{j_1}\dots\epsilon_{j_\beta} \pi_{n-k}(\epsilon,t) \\ &= \frac{(\gamma-1)!}{(\gamma-\alpha)!}\, \mathcal{D}^{j_1\dots j_\beta}_{i_1\dots i_\alpha} [\epsilon_{i_{\alpha+1}}\dots\epsilon_{i_\gamma}\epsilon_{j_1}\dots\epsilon_{j_\beta}]_{n-k} + \text{cyclic permutations of } (i_1\dots i_\gamma),\end{aligned} \tag{3.9}$$

for $\gamma \geq \alpha$ and zero otherwise. Note that the last term denotes the sum over all possible terms that are constructed by permuting the indices $(i_1\dots i_\gamma)$ of the first term. The combinatorial factor follows from noting that by partial integration there are generally $\gamma!/(\gamma-\alpha)!$ terms in the summation, but distinct are only those terms that differ by a cyclic permutation of $(i_1\dots i_\gamma)$ because $\mathcal{D}^{j_1\dots j_\beta}_{k_1\dots k_\alpha}$ of Eq. (2.20) is invariant under permutations of its lower indices. Since there are γ of such cyclic permutations, the number of distinct terms is $(\gamma-1)!/(\gamma-\alpha)!$. Note also that the boundary terms vanish because $\pi_0(\boldsymbol{\epsilon},t)$ falls off exponentially fast as $\boldsymbol{\epsilon} \to \pm\infty$. Substituting now the expression for $\mathcal{L}_k$ given in Result (2.1) into Eq. (3.8) and using Eq. (3.9), we have the following result:

Result 3.1. *The $\Omega^{-n/2}$ expansion coefficient of the γ^{th} moment in Eq. (3.3) satisfies the ordinary differential equation*

$$\begin{aligned}\frac{\partial}{\partial t}[\epsilon_{i_1}\dots\epsilon_{i_\gamma}]_n = &\sum_{k=0}^{n} \sum_{s=0}^{\lceil k/2\rceil} \sum_{\alpha=1}^{\gamma} \frac{(\gamma-1)!}{\alpha!(\gamma-\alpha)!} \frac{\mathcal{D}^{j_1,\dots,j_{2+k-\alpha-2s}}_{i_1,\dots,i_\alpha,s}}{(2+k-\alpha-2s)!} [\epsilon_{i_{\alpha+1}}\dots\epsilon_{i_\gamma}\epsilon_{j_1}\dots\epsilon_{j_{2+k-\alpha-2s}}]_{n-k} \\ &+ \text{cyclic permutations of } (i_1\dots i_\gamma),\end{aligned} \tag{3.10}$$

where $[1]_n = \int \mathrm{d}\boldsymbol{\epsilon}\pi_n(\boldsymbol{\epsilon},t) = \delta_{n,0}$, and the coefficients are given by

$$\mathcal{D}^{j_1\dots j_\beta}_{i_1\dots i_\alpha,s} = \sum_{r=1}^{R} S_{i_1 r} S_{i_2 r} \dots S_{i_\alpha r} \frac{\partial}{\partial[X_{j_1}]} \frac{\partial}{\partial[X_{j_2}]} \dots \frac{\partial}{\partial[X_{j_\beta}]} f_r^{(s)}([\boldsymbol{X}]). \tag{3.11}$$

Note the specific summation convention introduced after Eq. (2.19) in which the multi-indices $i_1\dots i_\alpha$ and $j_1\dots j_\beta$ appearing in the coefficient $\mathcal{D}^{j_1\dots j_\beta}_{i_1\dots i_\alpha,s}$ in Eq. (3.10) are to be summed from 1 to N_S. We remark that for $k=0$ in the summation of Eq. (3.10) the highest coefficient is $[\epsilon_{i_1}\dots\epsilon_{i_\gamma}]_n$, and hence the system of equations is closed. The derived expressions fully determine the asymptotic series expansion of the moments. It is however the case that not all coefficients in the moment expansion are non-zero, as we show in the derivation of the following result:

Result 3.2. *For deterministic initial conditions, i.e. $[\epsilon_{i_1}\dots\epsilon_{i_\gamma}]_n(0) = \delta_{n,0}\delta_{\gamma,0}$, the solution of the moment coefficients yields*

$$[\epsilon_{i_1}\dots\epsilon_{i_\gamma}]_n(t) = 0 \quad \textit{if } n+\gamma \textit{ is odd} \tag{3.12}$$

for all times.

Derivation. To the $\Omega^{-n/2}$ moment coefficient $[\epsilon_{i_1}...\epsilon_{i_\gamma}]_n$ appearing on the left hand side of Eq. (3.10), we assign the symbol $\mathcal{O} = \gamma + n$. For each coefficient $[\epsilon_{j_1} \dots \epsilon_{j_{2+k-\alpha-2s}} \epsilon_{i_{\alpha+1}} \dots \epsilon_{i_\gamma}]_{n-k}$ appearing in the summation of Eq. (3.10), we then have $\mathcal{O} = 2(1-\alpha-s)+\gamma+n$. It hence follows that each coefficient, for which the symbol $\mathcal{O}$ is odd, is determined only by coefficients for which $\mathcal{O}$ is also odd. Conversely, the dynamics of any coefficient for which $\mathcal{O}$ is even, depends only on the coefficients for which $\mathcal{O}$ is also even. Considering the deterministic initial conditions, we see that the terms on the right hand side of Eq. (3.10), i.e. $[\epsilon_{j_1} \dots \epsilon_{j_{2+k-\alpha-2s}} \epsilon_{i_{\alpha+1}} \dots \epsilon_{i_\gamma}]_{n-k}(0) = \delta_{n,k}\delta_{\gamma+n,2(\alpha+s-1)}$, are non-zero only if $\gamma+n$ is even. Since initially all moments with odd $\mathcal{O}$ are zero, it follows that these must remain zero for all times. □

Remark 3.1. *For reaction networks involving only a single species, the equation determining the $\Omega^{-n/2}$ expansion coefficient of the γ^{th} moment in Result 3.1 reduces to*

$$\frac{\partial}{\partial t}[\epsilon^\gamma]_n = \sum_{k=0}^{n} \sum_{s=0}^{\lceil k/2 \rceil} \sum_{\alpha=1}^{\gamma} \binom{\gamma}{\alpha} \frac{\mathcal{D}_{\alpha,s}^{2+k-\alpha-2s}}{(2+k-\alpha-2s)!} [\epsilon^{\gamma+k+2(1-\alpha-s)}]_{n-k}, \tag{3.13}$$

where the coefficients are given by

$$\mathcal{D}_{p,s}^{q} = \sum_{r=1}^{R} (S_{1r})^p \partial_{[X_1]}^q f_r^{(s)}([X_1]), \tag{3.14}$$

and $[\epsilon^0]_n = \delta_{n,0}$.

In the following explicit expressions of the moment expansion correcting the REs and the LNA to leading order are obtained.

3.1.1 Explicit equations for the leading order moment expansion

We here investigate the leading order corrections to the LNA for the first two moments. By virtue of Result 3.1, the correction to the mean concentration is obtained from the solution of

$$\frac{\partial}{\partial t}[\epsilon_{i_1}]_1 = \mathcal{D}_{i_1,0}^{\alpha_1}[\epsilon_{\alpha_1}]_1 + \frac{1}{2}\mathcal{D}_{i_1,0}^{\alpha_1\alpha_2}[\epsilon_{\alpha_1}\epsilon_{\alpha_2}]_0 + \mathcal{D}_{i_1,1}. \tag{3.15}$$

The correction to the covariance satisfies

$$\begin{aligned}\frac{\partial}{\partial t}[\epsilon_{i_1}\epsilon_{i_2}]_2 =& \mathcal{D}_{i_1,0}^{\alpha_1}[\epsilon_{\alpha_1}\epsilon_{i_2}]_2 + \frac{1}{2}\mathcal{D}_{i_1,0}^{\alpha_1\alpha_2}[\epsilon_{\alpha_1}\epsilon_{\alpha_2}\epsilon_{i_2}]_1 + \frac{1}{6}\mathcal{D}_{i_1,0}^{\alpha_1\alpha_2\alpha_3}[\epsilon_{\alpha_1}\epsilon_{\alpha_2}\epsilon_{\alpha_3}\epsilon_{i_2}]_0 \\ &+ \frac{1}{2}\mathcal{D}_{i_1 i_2,0}^{\alpha_1}[\epsilon_{\alpha_1}]_1 + \frac{1}{4}\mathcal{D}_{i_1 i_2,0}^{\alpha_1\alpha_2}[\epsilon_{\alpha_1}\epsilon_{\alpha_2}]_0 + \frac{1}{2}\mathcal{D}_{i_1 i_2,1} \\ &+ \mathcal{D}_{i_1,1}[\epsilon_{i_2}]_1 + \mathcal{D}_{i_1,1}^{\alpha_1}[\epsilon_{\alpha_1}\epsilon_{i_2}]_0 + (i_1 \leftrightarrow i_2).\end{aligned} \tag{3.16}$$

The above depends on the leading order non-Gaussian correction of the third moment which is given by

$$\begin{aligned}\frac{\partial}{\partial t}[\epsilon_{i_1}\epsilon_{i_2}\epsilon_{i_3}]_1 =&\mathcal{D}^{\alpha_1}_{i_1,0}[\epsilon_{\alpha_1}\epsilon_{i_2}\epsilon_{i_3}]_1 + \frac{1}{2}\mathcal{D}^{\alpha_1\alpha_2}_{i_1,0}[\epsilon_{\alpha_1}\epsilon_{\alpha_2}\epsilon_{i_2}\epsilon_{i_3}]_0 + \mathcal{D}^{\alpha_1}_{i_1i_2,0}[\epsilon_{\alpha_1}\epsilon_{i_3}]_0 \\ &+ \mathcal{D}_{i_1,1}[\epsilon_{i_2}\epsilon_{i_3}]_0 + \frac{1}{3}\mathcal{D}_{i_1i_2i_3,0}[\epsilon_{i_3}]_1 + (i_1 \leftrightarrow i_2) + (i_2 \leftrightarrow i_3). \end{aligned} \tag{3.17}$$

Note that Eq. (3.16) depends also on the fourth moment as follows

$$[\epsilon_{i_1}\epsilon_{i_2}\epsilon_{i_3}\epsilon_{i_4}]_0 = [\epsilon_{i_1}\epsilon_{i_2}]_0[\epsilon_{i_3}\epsilon_{i_4}]_0 + [\epsilon_{i_1}\epsilon_{i_3}]_0[\epsilon_{i_2}\epsilon_{i_4}]_0 + [\epsilon_{i_1}\epsilon_{i_4}]_0[\epsilon_{i_2}\epsilon_{i_3}]_0, \tag{3.18}$$

by the use of Wick's theorem, Eq. (3.7).

Networks comprised of unimolecular reactions

The moment expansion coefficients in Eqs. (3.15) and (3.16) are zero for reaction networks involving up to first order reactions because the propensities are linear in the state variables, i.e. $\mathcal{D}^{j_1\ldots j_\beta}_{i_1\ldots i_\alpha,s} = 0$ for $\alpha > 1$ or $s > 0$. Hence for this case,

$$\begin{aligned}&\left\langle \frac{n_i}{\Omega} \right\rangle = [X_i], \\ &\left\langle \left(\frac{n_i}{\Omega} - \left\langle \frac{n_i}{\Omega} \right\rangle\right)\left(\frac{n_j}{\Omega} - \left\langle \frac{n_j}{\Omega} \right\rangle\right) \right\rangle = \frac{1}{\Omega}[\epsilon_i\epsilon_j]_0, \end{aligned} \tag{3.19}$$

and there are no further corrections to mean and variance as predicted by the REs and LNA, respectively. Using the exact equations for the first two moments of the CME, one can show that REs and LNA are indeed exact in this case [83].

Corrections to the rate equations for networks with bimolecular reactions

Using van Kampen's ansatz, Eq. (2.8), and Eq. (3.3), we can obtain an expression for the mean concentrations

$$\left\langle \frac{n_i}{\Omega} \right\rangle = [X_i] + \frac{1}{\Omega}[\epsilon_i]_1 + O(\Omega^{-2}). \tag{3.20}$$

The first term is given by the REs, while the second term is to be determined by Eq. (3.15) and has been given previously by Grima [86] in terms of *effective mesoscopic rate equations* (EMREs) for reaction networks involving at most bimolecular reactions. The result given here, Eq. (3.15), is slightly more general since it has no such restriction. Note that the $\Omega^{-3/2}$ coefficient $[\epsilon_i]_2$ is zero by of virtue Result 3.2. EMREs have also been used intensively to obtain expressions for the substrate concentrations in enzymatic reactions [85, 87] and gene regulatory networks [111] that are more accurate than those obtained using the REs.

Corrections to the linear noise approximation

In order to relate the above moment expansion coefficients to the covariance of the concentration variables, we use van Kampen's ansatz, Eq. (2.8), and Eq. (3.3). The result is

$$\begin{aligned}\left\langle \left(\frac{n_i}{\Omega} - \left\langle \frac{n_i}{\Omega} \right\rangle\right)\left(\frac{n_j}{\Omega} - \left\langle \frac{n_j}{\Omega} \right\rangle\right) \right\rangle \\ = \frac{1}{\Omega}[\epsilon_i\epsilon_j]_0 + \frac{1}{\Omega^2}\left([\epsilon_i\epsilon_j]_2 - [\epsilon_i]_1[\epsilon_j]_1\right) + O(\Omega^{-3}).\end{aligned} \tag{3.21}$$

The first term of the latter equation is the LNA estimate for the covariance. The terms of order Ω^{-2}, Eq. (3.15) through (3.17), determine the fluctuations about the mean concentrations given by the EMRE, Eq. (3.20), and denote the leading order corrections to the LNA. Note also that the $\Omega^{-3/2}$ coefficient $[\epsilon_i\epsilon_j]_1$ is zero by Result 3.2. Because these terms predict deviations from the behaviour expected by the central limit theorem ($\sim \Omega^{-1}$), they have been called *inverse omega squared method* (IOS). The IOS method has been applied to predict noise measures such as the coefficients of variation of gene regulatory networks [112], to investigate the validity of moment approximations [113], or to estimate the accuracy of the Fokker-Planck approximation to the CME [1, 114]. EMREs and IOS have been made available by the author in the software package *intrinsic Noise Analyzer* [111, 112]. Higher order moments such as the skewness of distributions, which can be obtained from Eq. (3.16), have been investigated by Cianci et al. for models of autocatalytic reactions [115].

Higher order terms

While higher order corrections are readily available by Result 3.1, we will here, exemplary, give an higher order estimate to the mean concentrations. The term correcting the EMRE estimate is governed by

$$\begin{aligned}\frac{\partial}{\partial t}[\epsilon_{i_1}]_3 =& \mathcal{D}^{\alpha_1}_{i_1,0}[\epsilon_{\alpha_1}]_3 + \frac{1}{2}\mathcal{D}^{\alpha_1\alpha_2}_{i_1,0}[\epsilon_{\alpha_1}\epsilon_{\alpha_2}]_2 + \frac{1}{6}\mathcal{D}^{\alpha_1\alpha_2\alpha_3}_{i_1,0}[\epsilon_{\alpha_1}\epsilon_{\alpha_2}\epsilon_{\alpha_3}]_1 \\ &+ \frac{1}{24}\mathcal{D}^{\alpha_1\alpha_2\alpha_3\alpha_4}_{i_1,0}[\epsilon_{\alpha_1}\epsilon_{\alpha_2}\epsilon_{\alpha_3}\epsilon_{\alpha_4}]_0 + \mathcal{D}^{\alpha_1}_{i_1,1}[\epsilon_{\alpha_1}]_1 + \frac{1}{2}\mathcal{D}^{\alpha_1\alpha_2}_{i_1,1}[\epsilon_{\alpha_1}\epsilon_{\alpha_2}]_0 + \mathcal{D}_{i_1,2}.\end{aligned} \tag{3.22}$$

The solution of the above equation allows us to obtain the mean concentration accurate to order Ω^{-2}

$$\left\langle \frac{n_i}{\Omega} \right\rangle = [X_i] + \Omega^{-1}[\epsilon_i]_1 + \Omega^{-2}[\epsilon_i]_3 + O(\Omega^{-3}), \tag{3.23}$$

where the first term is the RE solution, the first two terms constitute the EMRE estimate and including all three terms one obtains an estimate to order Ω^{-3}. The latter has been rarely considered to-date.

3.2 Convergence and truncation of the system size expansion

The convergence of the SSE has not been studied to date. With the derivation of closed-form expressions for the expansion coefficients of the moments, Result 3.1, one may attempt to gain insight into this question. This is however a formidable task since the coefficients of the moment expansion are coupled to the coefficients of the moments to lower order in the SSE. Moreover, the dependence on the network parameters given by relation (3.14) makes it generally difficult to find appropriate bounds on the expansion coefficients. It is therefore expected that the question must be answered on a case-by-case basis. We here discuss two examples whose propensities depend nonlinearly on the molecule numbers: (i) a metabolic reaction which leads to a finite, and hence convergent expansion of the moments; and (ii) a dimerisation reaction for which the size of the coefficients in the moment expansion increases with increasing order in the SSE. Hence in the latter case the SSE must be considered practically divergent for finite values of the system size Ω. We here present a preliminary investigation of this issue without the intention of a rigorous proof. Instead we focus on how the series can be truncated systematically to obtain biologically meaningful results.

3.2.1 An example with a convergent series expansion

As a first application of our theory, we will study the expansion of the first few concentration moments in a simplified model of a metabolic reaction in a subcellular compartment of size Ω,

$$\varnothing \xrightarrow{k_0} S \xrightarrow{k_1 \frac{n}{n+\Omega K}} \varnothing. \tag{3.24a}$$

The reactions describe substrate molecules S input with rate k_0 and their catalytic conversion by an enzyme modelled by an effective saturating propensity. The corresponding CME is given by

$$\frac{\mathrm{d}}{\mathrm{d}t}P(n) = \Omega(E^{-1}-1)k_0 P(n) + \Omega(E^{+1}-1)k_1 \frac{n}{n+\Omega K}P(n). \tag{3.25}$$

Note that K is the substrate concentration at which the catalytic rate is half of its maximum Ωk_1. The main purpose of considering such a reaction is that both its CME is exactly solvable in stationary conditions and hence it provides us with a direct test for the SSE for the first few moments.

System size expansion

The rate equation of the reactions (3.24) is given by

$$\frac{\mathrm{d}[X]}{\mathrm{d}t} = k_0 - \frac{k_1[X]}{K+[X]}, \tag{3.26}$$

and the coefficients of the SSE given in Remark 3.1 can be written as

$$\mathcal{D}_p^q = \delta_{q,0} k_0 + (-1)^p k_1 \frac{\partial^q}{\partial [X]^q} \frac{[X]}{K + [X]}. \tag{3.27}$$

and $\mathcal{D}_{p,s}^q = 0$ for $s > 0$. Assuming steady state conditions and $k_1 > k_0$, we denote by

$$\varsigma = \frac{[X]}{K} = \frac{k_0}{k_1 - k_0}, \tag{3.28}$$

the reduced substrate concentration that is obtained by setting the time-derivative in Eq. (3.26) to zero. The SSE of the first concentration moment is then obtained using Eq. (3.27), yielding

$$\left\langle \frac{n}{\Omega} \right\rangle = \varsigma \left(K + \frac{1}{\Omega} \right). \tag{3.29}$$

One can show that there is no term higher than Ω^{-1}. The second, third, and fourth central moments are obtained correspondingly. The result is given by

$$\begin{aligned}
\left\langle \left(\frac{n}{\Omega} - \left\langle \frac{n}{\Omega} \right\rangle \right)^2 \right\rangle &= \frac{\varsigma(\varsigma+1)}{\Omega} \left(K + \frac{1}{\Omega} \right), \\
\left\langle \left(\frac{n}{\Omega} - \left\langle \frac{n}{\Omega} \right\rangle \right)^3 \right\rangle &= \frac{\varsigma(\varsigma+1)(2\varsigma+1)}{\Omega^2} \left(K + \frac{1}{\Omega} \right), \\
\left\langle \left(\frac{n}{\Omega} - \left\langle \frac{n}{\Omega} \right\rangle \right)^4 \right\rangle &= \frac{\varsigma(\varsigma+1)}{\Omega^2} \left(3K^2 \varsigma(\varsigma+1) + K \frac{12\varsigma(\varsigma+1)+1}{\Omega} + \frac{9\varsigma(\varsigma+1)+1}{\Omega^2} \right).
\end{aligned} \tag{3.30}$$

Similarly, one can show that there are no further terms. Hence the system size of the first four moments leads to a finite series in Ω. In the following we show that Eqs. (3.29) and (3.30) are indeed exact.

Comparison with exact moments

In stationary conditions, the CME (3.25) is solved exactly by the negative binomial distribution [116]. The cumulant generating function of the concentrations is given by

$$\phi(z) = \ln \sum_{n=0}^{\infty} e^{z \frac{n}{\Omega}} P(n) = -(1 + \Omega K) \ln \left(\varsigma \left(1 - e^{\frac{z}{\Omega}} \right) + 1 \right). \tag{3.31}$$

The concentration cumulants κ_n are then identified as its Taylor coefficients, i.e. $\phi(z) = \sum_{n=0}^{\infty} \kappa_n \frac{z^n}{n!}$. By employing the Taylor expansion of the logarithm about 1, the n^{th} concentration cumulant is found to be

$$\kappa_n = \left(\frac{1}{\Omega^n} + \frac{K}{\Omega^{n-1}} \right) \mathrm{Li}_{1-n} \left(\frac{\varsigma}{1+\varsigma} \right), \tag{3.32}$$

where $\mathrm{Li}_{-n}(x) = \sum_{k=1}^{\infty} k^n x^k$ is the polylogarithm function. Using the well-known relation between cumulants and moments [31] we recover Eqs. (3.29) and (3.30). It also follows from this exact expression that the concentration moments have a finite series expansion in Ω.

3.2.2 An example with divergent series expansion

As a second application of our theory, we will estimate the moments for a dimerisation reaction. This is the simplest case of a bimolecular reaction mechanism. The set of reactions under study are:

$$\begin{aligned} &\varnothing \xrightarrow{k_1} X, \\ &2X \xrightarrow{k_2} \varnothing. \end{aligned} \tag{3.33}$$

Monomers, denoted as X, are pumped into a compartment of volume Ω at rate k_1. Pairs of monomers react with rate constant k_2 to form a dimer molecule. The latter is not explicitly considered in our model. The CME for this reaction reads

$$\frac{\mathrm{d}}{\mathrm{d}t}P(n,t) = k_1\Omega(E^{-1}-1)P(n,t) + \frac{k_2}{\Omega}(E^2-1)n(n-1)P(n_1,t). \tag{3.34}$$

The SSE of this CME is analysed in the following.

System size expansion of the moments

The SSE of the moments is obtained by solving the equations given in Remark 3.1 with the coefficients for the reactions (3.33):

$$\begin{aligned} \mathcal{D}^q_{p,0} &= k_1\delta_{q0} + (-2)^p\left([X]^2\delta_{q,0} + 2[X]\delta_{q,1} + 2\delta_{q,2}\right), \\ \mathcal{D}^q_{p,1} &= -(-2)^p\left([X]\delta_{q,0} + \delta_{q,1}\right), \end{aligned} \tag{3.35}$$

and $\mathcal{D}_{p,s} = 0$ for $s > 1$. Solving $\mathcal{D}^0_{1,0}([X]) = 0$ gives the RE solution $[X] = \sqrt{\frac{k_1}{2k_2}}$. The asymptotic series expansion for the mean obtained using this procedure is given by

$$\begin{aligned} \left\langle \frac{n}{\Omega} \right\rangle = [X]\Bigg(1 + \frac{1}{8\Omega[X]} + \frac{3}{128[X]^2\Omega^2} + \frac{3}{512[X]^3\Omega^3} \\ + \frac{63}{32768[X]^4\Omega^4} + \frac{27}{32768[X]^5\Omega^5}\Bigg) + O(\Omega^{-6}). \end{aligned} \tag{3.36}$$

Fig. 3.1A shows the prediction of the mean molecule number as obtained using Eq. (3.36). We observe that increasing the number of terms in the series expansion does not generally give more accurate results. It is is instructive to note that the coefficients in the above series exhibit the typical factorial growth of the coefficients in divergent series [117]. In particular, its coefficients are not smaller than those of the series $[X]\sum_{k=0}^{\infty}(1+k)!(16\Omega[X])^{-k}$, which diverges for all finite values of $\Omega[X]$. A systematic

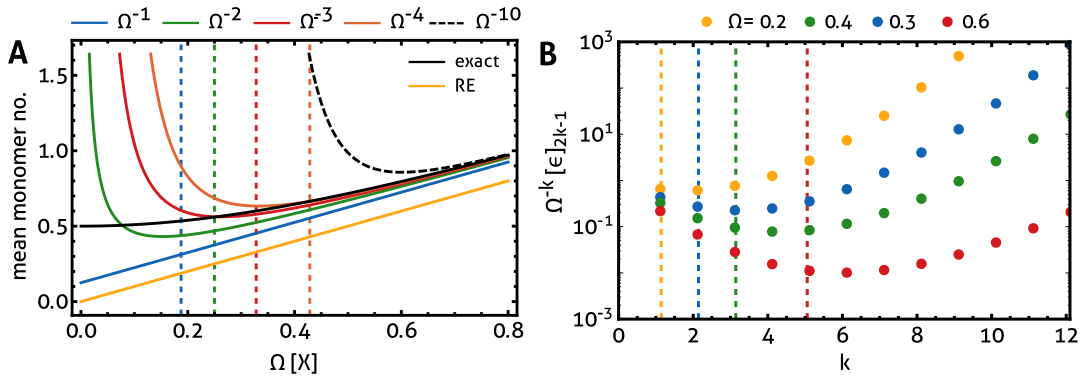

Figure 3.1:

Optimal truncation of the system size expansion. (A) The SSE mean monomer number in the dimerisation reaction (3.33) when truncated after the Ω^{-1} (solid blue line), Ω^{-2} (green), Ω^{-3} (red), Ω^{-4} (orange) in Eq. (3.36). For comparison the RE solution (solid yellow), and the exact result (solid black) given by Eq. (3.51) are shown. The truncated series diverges for decreasing system size and increasing truncation order. This trend is exacerbated when the series is truncated after Ω^{-10} terms (dashed black). The critical parameter $[X]\Omega_k$ as given in Tab. (3.41) is indicated by vertical lines for $k = 1$ (dashed blue), 2 (green), 3 (red) 4 (orange). This confirms that the series truncated after k terms can generally not be trusted for values $\Omega < \Omega_k$. (B) The size of successive non-zero terms in the summation of Eq. (3.36) is shown. These terms first decrease in size and then increase without bound for different values of the parameter $[X]\Omega$. Optimal truncation orders estimated graphically are in agreement with the analytical values given in Tab. (3.41).

approach that allows to control this behaviour is proposed in the following section. For completeness, we also give the corresponding expression for the variance

$$\left\langle \left(\frac{n}{\Omega}\right)^2 - \left\langle \frac{n}{\Omega}\right\rangle^2 \right\rangle = \frac{[X]}{\Omega}\left(\frac{3}{4} + \frac{1}{16\Omega[X]} + \frac{3}{512[X]^2\Omega^2} - \frac{63}{131072[X]^4\Omega^4}\right) + O(\Omega^{-6}). \tag{3.37}$$

Note that in the above expression the Ω^{-4}-term is zero.

Optimal truncation of the system size expansion

We now turn our attention to the accuracy of these series when it is truncated after the N^{th} term. We therefore recast the expansion of the mean concentration in the form

$$\left\langle \frac{n}{\Omega}\right\rangle = [X] + \sum_{k=1}^{N} \Omega^{-k}[\epsilon]_{2k-1} + O(\Omega^{-(N+1)}), \tag{3.38}$$

where we have made use of the fact that $[\epsilon]_{2k} = 0$. Generally, we presume that for a given Ω the terms of this series will first decrease in absolute value such that

$$\left| \frac{[\epsilon]_{2k+1}}{[\epsilon]_{2k-1}} \right| \leq \Omega, \tag{3.39}$$

for $k \leq N_*$ and they then increase after that point so that

$$\left| \frac{[\epsilon]_{2k+1}}{[\epsilon]_{2k-1}} \right| > \Omega, \tag{3.40}$$

for $k > N_*$. We will consider such asymptotic series formally divergent although not all terms can, of course, be evaluated. The value of N_* for which this transition occurs is called *optimal truncation order* [117, 118] and depends naturally on Ω. Specifically, this implies the existence of a critical system size Ω_k for which $N_*(\Omega_k) = k$. Hence the series truncated after k terms may not be trusted for values smaller than Ω_k.

In Fig. 3.1B we compare the size of the successive terms in Eq. (3.36) for different values of $\Omega[X]$, which confirms that the stipulated behaviour is observed. The optimal truncation orders (vertical dashed lines) can also be obtained graphically by determining the order for which a minimum is observed in Fig. 3.1B. The optimal truncation order is the value of k before this minimum occurs.

We note that by inspection of the CME, Eq. (3.34), the only free parameter is the number of molecules predicted by the rate equation given by $\Omega[X] = \Omega\sqrt{\frac{k_1}{2k_2}}$. Therefore, we employed the condition $N_*([X]\Omega_k) = k$ to determine the critical system size Ω_k. The analytical values for consecutive terms of Eq. (3.36) are as follows:

truncation order k	1	2	3	4
$\Omega_k[X]$ (mean)	$\frac{3}{16}$ (≈ 0.19)	$\frac{1}{4}$($= 0.25$)	$\frac{21}{64}$(≈ 0.33)	$\frac{3}{7}$(≈ 0.43)

(3.41)

Most notably, the critical system size increases with increasing truncation order. The above values are indicated by vertical dashed lines in Fig. 3.1A and agree exactly with those graphically determined in B.

More generally, the procedure can be applied to the estimates of the $\boldsymbol{\epsilon}$-moments

$$\langle \epsilon_{i_1} ... \epsilon_{i_\gamma} \rangle = \sum_{j=0}^{N} \Omega^{-j/2} [\epsilon_{i_1} ... \epsilon_{i_\gamma}]_j + O(\Omega^{-(N+1)/2}), \tag{3.42}$$

where $[\epsilon_{i_1} ... \epsilon_{i_\gamma}]_j = 0$ when $\gamma + j$ is odd. Analogously to the expansion of the mean concentration, for the above series we presume that

$$\left| \frac{[\epsilon_{i_1} ... \epsilon_{i_\gamma}]_{j+2}}{[\epsilon_{i_1} ... \epsilon_{i_\gamma}]_j} \right| \leq \Omega, \tag{3.43}$$

for $j \leq N_*(\Omega)$ and $j+\gamma$ even, and

$$\left| \frac{[\epsilon_{i_1} \ldots \epsilon_{i_\gamma}]_{j+2}}{[\epsilon_{i_1} \ldots \epsilon_{i_\gamma}]_j} \right| > \Omega, \tag{3.44}$$

for $j > N_*(\Omega)$. The critical value of Ω for this transition can now be determined. The result for the variance of the dimerisation reaction, Eq. (3.37), is

truncation order j	2	4	6	8
$\Omega_j[X]$ (variance)	$\frac{1}{12}$ $(= 0.08)$	$\frac{3}{32}$ (≈ 0.09)	–	$\frac{\sqrt{21}}{16}$ (≈ 0.29)

(3.45)

Note that the value for $j = 6$ is missing since the term proportional to Ω^{-4} is absent from Eq. (3.37). The proposed procedure hence provides a systematic procedure for the validation of the SSE.

Exact moments and their asymptotic series expansion

Next, we will verify the result of the previous paragraphs by comparing it with an exact solution of the CME and the asymptotics thereof. To that end, we make use of the probability generating function defined as $F(s,t) = \sum_n s^n P(n,t)$. Using this definition in Eq. (3.34) one can show by multiplying Eq. (3.34) from both sides by s^n and summing over n from 0 to infinity that $F(s)$ obeys the partial differential equation

$$\frac{\partial}{\partial t} F(s,t) = k_1 \Omega (s-1) F(s,t) + \frac{k_2}{\Omega}(1-s^2)\frac{\partial^2 F(s,t)}{\partial s^2}. \tag{3.46}$$

Note that we must have $F(1) = 1$ by normalization of the probability distribution. In steady state conditions, i.e. setting the time-derivative to zero, we find by inspection of Eq. (3.46) that $F(-1) = 0$. These conditions have been used in [32] to obtain the steady state solution:

$$F(s) = \sqrt{\frac{s+1}{2}} \frac{I_1\left(2\sqrt{2(s+1)}X\right)}{I_1(4X)}, \tag{3.47}$$

where $X = \Omega[X] = \Omega(k_1/2k_2)^{1/2}$ is the number of molecules predicted by the rate equations and I_n is the modified Bessel function of the first kind and order n. Mean and variance can then be obtained exactly and are given by the following expressions

$$\langle n \rangle = \left.\frac{\partial F(s)}{\partial s}\right|_{s=1} = X \frac{I_0(4X)}{I_1(4X)}, \tag{3.48}$$

$$\begin{aligned} \langle n^2 \rangle - \langle n \rangle^2 &= \left(\left.\frac{\partial^2 F(s)}{\partial s^2}\right|_{s=1} + \left.\frac{\partial F(s)}{\partial s}\right|_{s=1} - \left[\left.\frac{\partial F(s)}{\partial s}\right|_{s=1}\right]^2 \right) \\ &= X\left(X + \frac{I_0(4X)(I_1(4X) - X I_0(4X))}{I_1(4X)^2} \right). \end{aligned} \tag{3.49}$$

Parameter	(i)	(ii)	(iii)
$k_0[G]\,(\mathrm{min}^{-1}\mu M)$	2.4	0.024	0.024
$k_{\mathrm{dM}}\,(\mathrm{min}^{-1})$	20	0.2	0.2
$k_s\,(\mathrm{min}^{-1})$	1.5	1.5	15
$k_{-1}, k_2\,(\mathrm{min}^{-1})$	2	2	20
$k_1((\mu M\mathrm{min})^{-1})$	400	400	4000

Tab. 3.1:
Kinetic parameters used for the gene expression model, scheme 3.53, as discussed in the main text. The volume is fixed to $10^{-15}l$ with an enzyme concentration of $0.1\mu M$ corresponding to 60 enzyme molecules. The Michaelis-Menten constant is $0.01\mu M$ in all cases.

For large arguments X, implying large Ω, we can use the asymptotics of the modified Bessel functions [119], which are given by

$$I_\alpha(z) = \frac{e^z}{\sqrt{2\pi z}} \sum_{m=0}^{p} \frac{\Gamma(\alpha+m+1/2)}{m!\Gamma(\alpha-m+1/2)} \frac{(-1)^m}{(2z)^m} + O(e^{-z} z^{-1/2-p}), \tag{3.50}$$

where $\Gamma(n)$ denotes the gamma function, to obtain the asymptotic expansions of the concentration moments. The result for the mean concentration is

$$\left\langle \frac{n}{\Omega} \right\rangle = [X] \left(1 + \frac{1}{8\Omega[X]} + \frac{3}{128[X]^2\Omega^2} + \frac{3}{512[X]^3\Omega^3} + \frac{63}{32768[X]^4\Omega^4} + \frac{27}{32768[X]^5\Omega^5} \right) + O(\Omega^{-6}), \tag{3.51}$$

while the variance follows

$$\left\langle \left(\frac{n}{\Omega}\right)^2 - \left\langle \frac{n}{\Omega} \right\rangle^2 \right\rangle = \frac{[X]}{\Omega} \left(\frac{3}{4} + \frac{1}{16\Omega[X]} + \frac{3}{512[X]^2\Omega^2} - \frac{63}{131072[X]^4\Omega^4} \right) + O(\Omega^{-6}). \tag{3.52}$$

Note that Eqs. (3.51) and (3.52) agree exactly with Eqs. (3.36) and (3.37), respectively. The asymptotic expansion obtained using the SSE is however significantly simpler since it does not require an exact solution for the probability generating functions. Finally, we note that that the asymptotic series for $I_\alpha(z)$, Eq. (3.50), is divergent for all finite values of z [118, 119]. The fact that the SSE produces the exact asymptotic expansion of the moments, Eqs. (3.51) and (3.52), indicates that it is also a purely asymptotic expansion.

3.3 A case study: gene expression with enzymatic degradation

The aim of this section is to demonstrate how the equations for the first two moments can be used to gain qualitative as well as quantitative insights into stochasticity in biochemical reaction dynamics. To that end, we carry out a comparative study of the

moment estimates derived from the SSE and exact stochastic simulations. Specifically, we consider the two-stage model of gene expression with an enzymatic degradation mechanism:

$$\begin{aligned}
&\text{Gene} \xrightarrow{k_0} \text{Gene} + \text{mRNA}, \quad \text{mRNA} \xrightarrow{k_{\text{dM}}} \varnothing, \\
&\text{mRNA} \xrightarrow{k_s} \text{mRNA} + \text{Protein}, \\
&\text{Protein} + \text{Enzyme} \underset{k_{-1}}{\overset{k_1}{\rightleftharpoons}} \text{Complex} \xrightarrow{k_2} \text{Enzyme} + \varnothing.
\end{aligned} \tag{3.53}$$

The scheme involves the transcription of mRNA, its translation to protein and subsequent degradation of both mRNA and protein. Note that while mRNA is degraded via an unspecific linear reaction, the degradation of protein occurs via an enzyme catalysed reaction. The latter may model proteolysis, the consumption of protein by a metabolic pathway or other post-translational modifications. A simplified version of this model is obtained when the protein degradation is replaced by the linear reaction: Protein $\rightarrow \varnothing$. Over the past decade the latter model has been the subject of numerous studies, principally because the scheme is composed of purely first-order reactions and can be solved exactly [65, 120–122]. However, an analytical solution to the former model as given by scheme (3.53), is not known because of the bimolecular association reaction between enzyme and protein. Hence in what follows we demonstrate the power of the derived approximation methods to infer useful information regarding the network's intrinsic noise properties.

We consider the model with three different parameter sets (see Tab. 3.1) and fix the compartment volume to one femtoliter (one micron cubed). For all three cases, the REs predict the same steady state mRNA and protein concentrations: $[\text{mRNA}] = 0.12\mu M$ and $[\text{Protein}] = 0.09\mu M$. In these dimensional units the system size corresponds $\Omega = 600(\mu M)^{-1}$ such that these concentrations correspond to 72 and 54 molecule numbers, respectively.

Fast transcription

In Fig. 3.2, we show the mean concentrations and the variance of fluctuations obtained using the REs and the LNA for parameter set (i) for which transcription is fast. Also shown are the SSA estimates. In comparison we find that the REs and LNA provide reasonably accurate results for these parameters. However, the scenario considered may not be particularly realistic. This is since the ratio of protein and mRNA lifetimes in this example is approximately 100 (as estimated from the time taken for the concentrations to reach 90% of their steady state values) while an evaluation of 1,962 genes in budding yeast showed that the ratios have median and mode close to 3 [121].

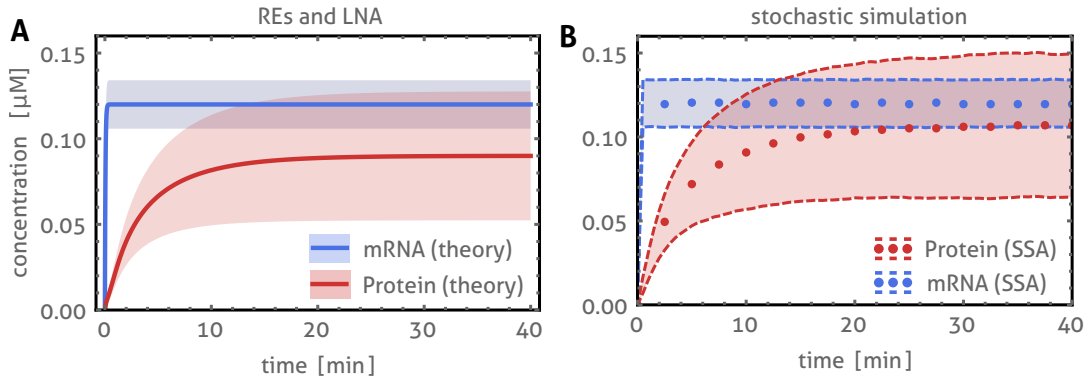

Figure 3.2:
Gene expression model with fast transcription rate. In (A) and (B) we compare the RE predictions of mean concentrations with those obtained from ensemble averaging 3,000 SSA trajectories (dots). The shaded areas denote the region of one standard deviation around the average concentrations which in (A) has been computed using the LNA and in (B) using the SSA. The results in (A) and (B) are in good qualitative agreement.

Moderate transcription

We now consider parameter set (ii), the case of moderate transcription. In Fig. 3.3A we compare the RE and LNA predictions of mean concentrations and variance of fluctuations with that obtained from the SSA. Notice that in this case, the two are in severe disagreement. The SSA predicts that the mean concentration of protein is larger than that of the mRNA while the REs predict the opposite. It is also the case that the variance estimate of the LNA is considerably smaller than that of the SSA. In Fig. 3.3B we show the mean concentrations computed using the EMRE and the variance computed using the IOS method. Note that the latter are in good agreement with the SSA. The transient times for this case are given by 37 minutes for protein and 12 minutes for mRNA concentrations with a ratio of approximately 3 in agreement with the median and mode of experimentally measured ratios. Hence this example provides clear evidence for the need to go beyond the RE and LNA level of approximation for physiologically relevant parameters of the gene expression model.

Using the method described in Section 3.2.2, we computed the critical system size for the truncated series of the mean. The value for the EMRE is $\approx 165(\mu M)^{-1}$ while the value for the next term in the expansion of the mean, given by Eq. (3.23), is $\approx 606(\mu M)^{-1}$. Hence including the latter term corresponds to an optimally truncated series which is shown Fig. 3.3C. Therein we also show the variance prediction corresponding to the next term beyond the IOS approximation. The excellent agreement with simulations using the SSA validates our truncation procedure. Note that no further improvement is achieved by including even higher order terms.

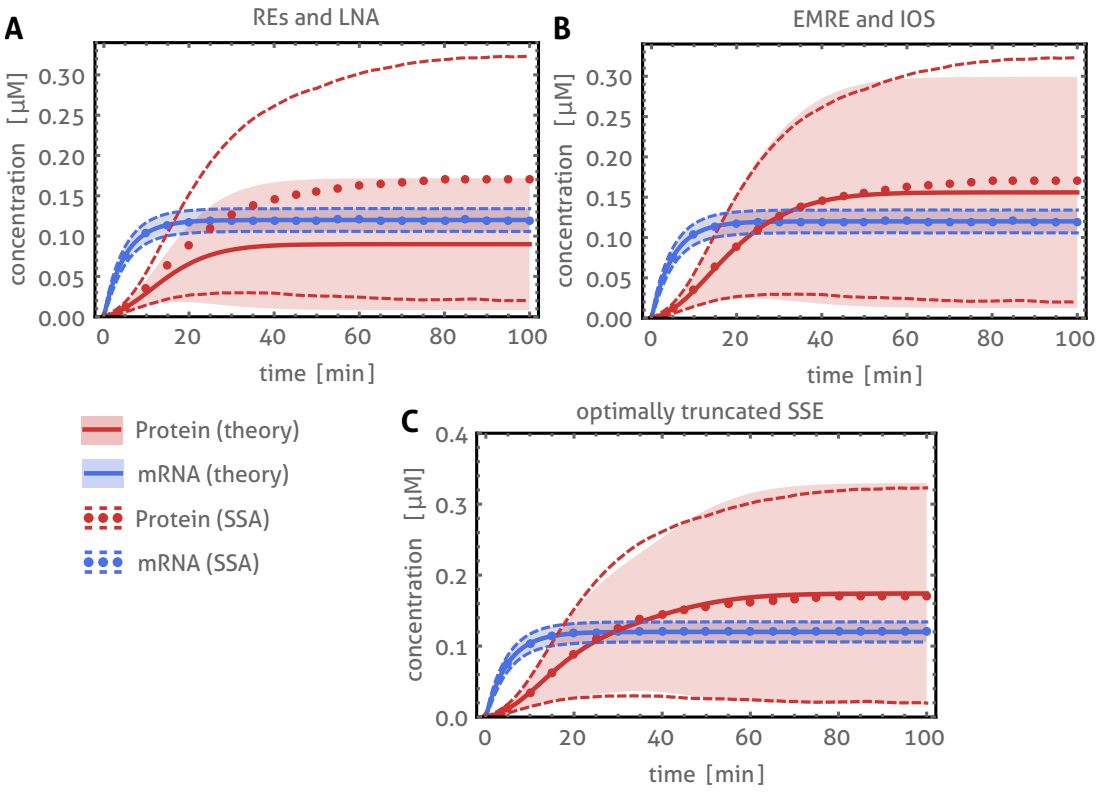

Figure 3.3:
Gene expression model with moderate transcription rate. (A) We compare the RE and LNA predictions of mean concentrations and variance of fluctuations with those obtained from ensemble averaging of 30,000 stochastic realizations computed using the SSA (dots: mean, dashed: area of one standard deviation). Note that the RE and LNA predictions differ significantly from the simulated values. (B) we show the mean concentration prediction according to the EMRE and the variance prediction according to IOS. These are in good agreement with those obtained from the SSA. (C) Excellent agreement with the SSA is obtained using the optimally truncated SSE which includes the next order terms beyond the EMRE and IOS approximations.

Moderate transcription and fast translation

Finally we consider parameter set (iii), the case of moderate transcription and fast translation (k_s is an order of magnitude larger in (iii) compared to (ii)). Previous studies have shown that increased translation efficiency leads to increased noise in the protein abundance [120] due to the proteins being produced in bursts [121]. Indeed individual realizations of the SSA show proteins expressed in sharply peaked bursts (Fig. 3.4A). Note that in this case the critical system sizes for the EMRE and higher order terms are much larger than the value of Ω considered here. Hence the accuracy of the expansion must be accessed by comparison against simulations.

We computed the mean concentrations of mRNA and protein according to RE/LNA, EMRE/IOS approximation methods and compared them to the prediction of the SSA

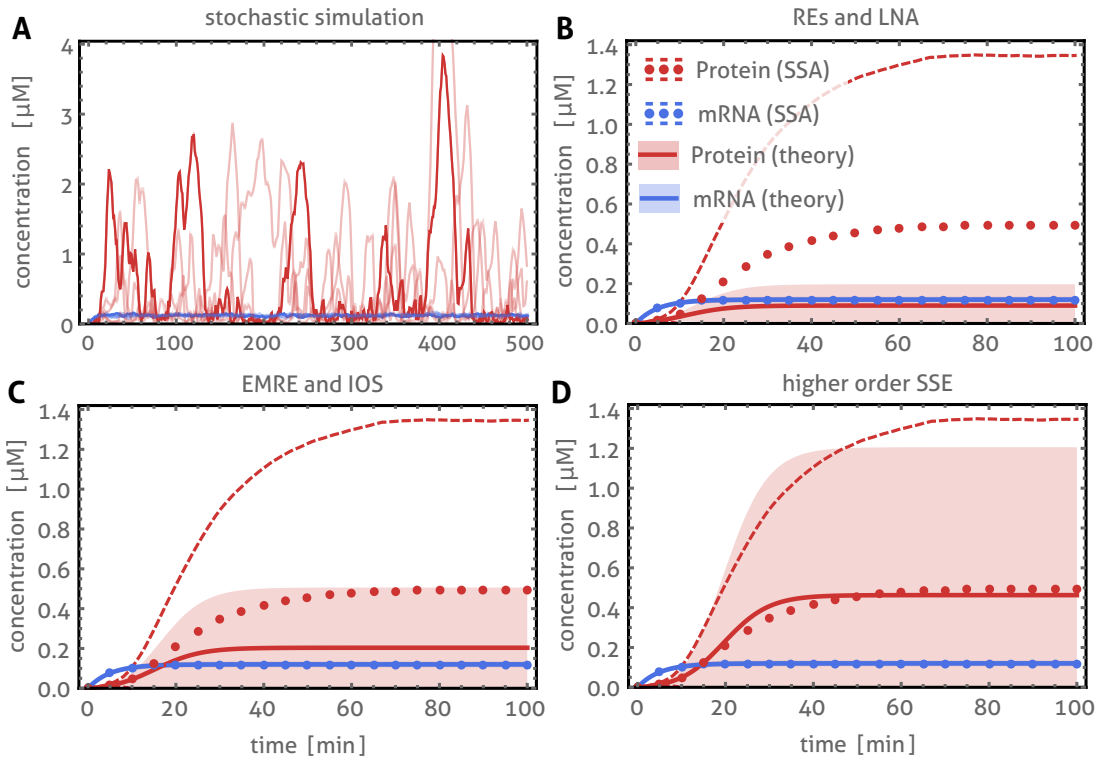

Figure 3.4:

Gene expression model with efficient translation. (A) Individual SSA trajectories illustrate that large bursts are observed in the protein concentrations. In (B), (C) and (D) we show the mean estimates predicted by REs, EMREs and their higher order correction, respectively. The corresponding standard deviations predicted by LNA, IOS and their higher order corrections are indicated by shaded areas. These are compared against stochastic simulations obtained from ensemble averaging 30,000 SSA trajectories (dots: mean, dashed: area of one standard deviation). Note that only the estimates with higher accuracy than EMRE and IOS, shown in (D), are in good quantitative agreement with the SSA predictions. These predictions are over 5 times larger than those of REs, this discrepancy stems from the fact that the latter do not take into account contributions due to large fluctuations.

(Figs. 3.4B and C). Note that neither accurately predicts the mean concentrations but the approximation that goes one order beyond the EMRE, Eq. (3.23), shown in Fig. 3.4D provides the most accurate result. Note that also the variance obtained from truncating after one term beyond the IOS approximation is in reasonable agreement. However, no further improvement could be obtained by including even higher order terms. Transient times of 48 minutes and 12 minutes for protein and mRNA concentrations have been extracted from the time course data as for previous cases; these are similar to those observed in the expression of the *E. coli* proteome [7], once again showing the necessity of approximation methods beyond the conventional REs and LNA to study physiologically relevant cases.

4 The expansion of the probability distributions

In the previous chapter we have employed the higher than LNA terms in the SSE to calculate non-Gaussian corrections to the LNA for the first few moments. A systematic investigation of the distributions implied by these higher order terms in the SSE is however still missing. Resolution of this problem is crucial because it allows assessing to which extent the asymptotic series of the SSE captures the non-Gaussian fluctuations predicted by the CME, but also because it provides a generic and particularly simple means of solution in closed form. The aim of this chapter is therefore to provide an asymptotic series solution to the probability distribution underlying the CME that can be truncated systematically to any desired order in the inverse system size.

For simplicity, we focus on the case of a single species for which the CME, Eq. (2.6), reduces to

$$\frac{\mathrm{d}P(n,t)}{\mathrm{d}t} = \sum_{r=1}^{R}\left(E^{-S_r} - 1\right) w_r\left(n,\Omega\right) P(n,t), \tag{4.1}$$

with stoichiometry $S_r = r_{1r} - s_{1r}$. While commonly only the LNA terms of the SSE are considered, see Section 2.4.2, we show that the higher order terms can be obtained using an asymptotic expansion of the continuous probability density in Section 4.1. The resulting series is given in terms of orthogonal polynomials and can be truncated systematically to any desired order in the inverse system size. Analytical expressions are given for the expansion coefficients capturing the full time-dependence. The stationary solution is recovered as a particular case.

In Section 4.2, we introduce an alternative discrete approximation of the probability distribution and show that it also satisfies the expansion of the CME. This is motivated because, as we show, the continuous approximation often fails to converge reasonably fast even for biochemical networks involving only unimolecular reactions, i.e. linear birth-death processes. In contrast, the discrete approximation converges rapidly to the true distribution with increasing truncation order. In Section 4.3, we show that for networks with bimolecular reactions, i.e. nonlinear birth-death processes, renormalisation is required for achieving rapid convergence of the series. We conclude in Section 4.4 that the new method allows to predict the full time-dependence of the molecule number distribution of a gene expression model.

4.1 Continuous probability density approximation

In Section 2.4 it was assumed that there exists a probability density function approximating the probability distribution solution $P(n,t)$ of the CME. For the case of a single species, Eq. (2.9) becomes

$$\Pi(\epsilon,t) = \Omega^{1/2} P(n = \Omega[X] + \Omega^{1/2}\epsilon, t), \tag{4.2}$$

where $[X]$ is obtained from solving the RE

$$\frac{\mathrm{d}[X]}{\mathrm{d}t} = \sum_{r=1}^{R} f_r^{(0)}([X]). \tag{4.3}$$

In Result 2.1, we have shown that the expansion of the CME for $\Pi(\epsilon,t)$ satisfies the PDE

$$\frac{\partial}{\partial t}\Pi(\epsilon,t) = \sum_{k=0}^{N} \Omega^{-k/2}\mathcal{L}_k \Pi(\epsilon,t) + O(\Omega^{-(N+1)/2}), \tag{4.4}$$

where the differential operators

$$\mathcal{L}_k = \sum_{s=0}^{\lceil k/2 \rceil} \sum_{p=1}^{k-2(s-1)} \frac{\mathcal{D}_{p,s}^{k-p-2(s-1)}}{p!(k-p-2(s-1))!} (-\partial_\epsilon)^p \epsilon^{k-p-2(s-1)}, \tag{4.5}$$

are parametrized by the time-dependent coefficients

$$\mathcal{D}_{p,s}^{q} = \sum_{r=1}^{R} (S_r)^p \partial_{[X]}^q f_r^{(s)}([X]), \tag{4.6}$$

that depend explicitly on the solution of the RE (4.3). In the following, we omit the subscript for $s = 0$, i.e. $\mathcal{D}_{p,0}^{q} = \mathcal{D}_p^q$.

For solving the PDE approximation (4.4) perturbatively, we will make use of the asymptotic expansion

$$\Pi(\epsilon,t) = \pi_0(\epsilon,t) + \sum_{j=1}^{N} \Omega^{-j/2}\pi_j(\epsilon,t) + O(\Omega^{-(N+1)/2}), \tag{4.7}$$

that has already been employed in Eq. (3.1) for the calculation of moments in Chapter 3. Using Eq. (4.7) in (4.4), the higher order terms satisfy the system of PDEs

$$\left(\frac{\partial}{\partial t} - \mathcal{L}_0\right)\pi_0(\epsilon,t) = 0, \tag{4.8}$$

$$\left(\frac{\partial}{\partial t} - \mathcal{L}_0\right)\pi_j(\epsilon,t) = \sum_{k=1}^{j} \mathcal{L}_k \pi_{j-k}(\epsilon,t), \tag{4.9}$$

for $j > 0$, where

$$\mathcal{L}_0 = -\partial_\epsilon \mathcal{J}(t)\epsilon + \mathcal{D}_2^0(t)\partial_\epsilon^2. \tag{4.10}$$

By Result 2.2 the solution of Eq. (4.8) is given by the Gaussian

$$\pi_0(\epsilon, t) = \frac{1}{\sqrt{2\pi\sigma^2(t)}} \exp\left[-\frac{\epsilon^2}{2\sigma^2(t)}\right], \tag{4.11}$$

which acquires time-dependence via its variance $\sigma^2(t)$. Assuming deterministic initial conditions and denoting by $\mathcal{J}(t) = \mathcal{D}_1^1(t)$ the Jacobian of the deterministic RE, the variance as in the derivation of Result 2.2 is given by

$$\sigma^2(t) = \int_0^t \mathrm{d}t' e^{\int_{t'}^t \mathrm{d}t'' \mathcal{J}(t'')} \mathcal{D}_2^0(t'), \tag{4.12}$$

which satisfies the inhomogeneous ODE

$$\frac{\partial \sigma^2}{\partial t} = 2\mathcal{J}(t)\sigma^2 + \mathcal{D}_2^0(t). \tag{4.13}$$

Note that in the following we will drop the time-dependence of the coefficients for convenience of notation. For investigating higher order terms, it is convenient to introduce the following eigenvalue problem:

Result 4.1. *The eigenvalue problem*

$$\left(\frac{\partial}{\partial t} - \mathcal{L}_0\right) \Psi_m = \lambda_m \Psi_m, \tag{4.14}$$

subject to the boundary conditions $\lim_{\epsilon \to \pm\infty} \Psi_m(\epsilon, t)$*, is solved by* $\lambda_m = -m\mathcal{J}$ *and* $\Psi_m(\epsilon, t) = \psi_m(\epsilon, t)\pi_0(\epsilon, t)$ *where*

$$\psi_m(\epsilon, t) = \pi_0^{-1}(-\partial_\epsilon)^m \pi_0 = \frac{1}{\sigma^m} H_m\left(\frac{\epsilon}{\sigma}\right), \tag{4.15}$$

and H_m *are the Hermite orthogonal polynomials.*

Derivation. Suppose $\Psi_{m+1} = (-\partial_\epsilon)\Psi_m$ and observe that $(\partial_t - \mathcal{L}_0)\Psi_{m+1} = -\mathcal{J}\Psi_{m+1} - \partial_\epsilon(\partial_t - \mathcal{L}_0)\Psi_m$ by Eq. (4.10). Using the latter together with Eq. (4.14), we obtain $\lambda_{m+1} = (-\mathcal{J} + \lambda_m)$ from which the result follows using $\lambda_0 = 0$ and $\Psi_0 = \pi_0$. □

The properties of the Hermite polynomials are reviewed in the following section.

4.1.1 Properties of the Hermite orthogonal polynomials

Here, we briefly review some properties of the Hermite orthogonal polynomials. The polynomials can be defined in terms of the derivatives of a centred Gaussian $\pi_0(\epsilon)$ with

variance σ^2,

$$H_n\left(\frac{\epsilon}{\sigma}\right) = \pi_0^{-1}(\epsilon)(-\sigma\partial_\epsilon)^n\pi_0(\epsilon). \tag{4.16}$$

An explicit formula [123, Ch. 22] is

$$H_n\left(\frac{\epsilon}{\sigma}\right) = \sum_{k=0}^{\lfloor n/2\rfloor}\binom{n}{2k}(-1)^k\left(\frac{\epsilon}{\sigma}\right)^{n-2k}(2k-1)!!\,, \tag{4.17}$$

where $(2k-1)!!$ is the double factorial. These functions are orthogonal

$$\frac{1}{n!}\int_{-\infty}^{\infty}\mathrm{d}\epsilon\, H_m\left(\frac{\epsilon}{\sigma}\right)H_n\left(\frac{\epsilon}{\sigma}\right)\pi_0(\epsilon) = \delta_{nm}, \tag{4.18}$$

with respect to the Gaussian measure π_0. Their derivatives satisfy

$$(\sigma\partial_\epsilon)^m H_n\left(\frac{\epsilon}{\sigma}\right) = \frac{n!}{(n-m)!}H_{n-m}\left(\frac{\epsilon}{\sigma}\right). \tag{4.19}$$

Since these polynomials are complete, every function $g(\epsilon)$ satisfying

$$\int_{-\infty}^{\infty}\mathrm{d}\epsilon\left(\frac{|g(\epsilon)|^2}{\pi_0(\epsilon)}\right) < \infty \tag{4.20}$$

can be expanded as

$$g(\epsilon) = \sum_{n=0}^{\infty} b_n H_n\left(\frac{\epsilon}{\sigma}\right)\pi_0(\epsilon), \tag{4.21}$$

where the coefficients are given by $b_n = \frac{1}{n!}\int \mathrm{d}\epsilon\, H_n\left(\frac{\epsilon}{\sigma}\right)g(\epsilon)$. We note because $H_0\left(\frac{\epsilon}{\sigma}\right) = 1$ and π_0 is normalized, we must have $b_0 = 1$ if $\int \mathrm{d}\epsilon\, g(\epsilon) = 1$.

4.1.2 Higher order terms

The system of PDEs given by Eq. (4.9) can now be solved using the eigenfunction approach. Using the completeness of the eigenfunctions of $\mathcal{L}_0$, we can write

$$\pi_j(\epsilon, t) = \sum_{m=0}^{N_j} a_m^{(j)}(t)\psi_m(\epsilon, t)\pi_0(\epsilon, t), \tag{4.22}$$

where we have anticipated that to each order j only the first N_j eigenfunctions are required. We verify in the following section, by the derivation of Result 4.2, that the j^{th} order term in the expansion involves in fact only the first $N_j = 3j$ eigenfunctions.

The continuous SSE approximation is consequently given by the asymptotic expansion

$$\Pi(\epsilon,t) = \pi_0(\epsilon,t)\left(1+\sum_{j=1}^{N}\Omega^{-j/2}\sum_{m=1}^{N_j}a_m^{(j)}(t)\psi_m(\epsilon,t)\right)+O(\Omega^{-(N+1)/2}), \tag{4.23}$$

for which the coefficients can be determined using the orthogonality of the ψ_m, i.e.

$$\frac{\sigma^{2n}}{n!}\int \mathrm{d}\epsilon\,\psi_n(\epsilon,t)\psi_m(\epsilon,t)\pi_0(\epsilon,t) = \delta_{m,n}, \tag{4.24}$$

which follows from Eq. (4.18) and the definition of the eigenfunctions, Eq. (4.15).

4.1.3 The equation for the expansion coefficients

The coefficients $a_n^{(j)}$ are now determined by inserting Eq. (4.22) into Eq. (4.9), multiplying the result by $\frac{\sigma^{2n}}{n!}\int \mathrm{d}\epsilon\,\psi_n(\epsilon,t)$, and performing the integration. Using Eq. (4.14) of Result 4.1, the left hand side of Eq. (4.9) becomes

$$\begin{aligned}\frac{\sigma^{2n}}{n!}\sum_m\int d\epsilon\,\psi_n(\epsilon,t)\left(\frac{\partial}{\partial t}-\mathcal{L}_0\right)a_m^{(j)}\psi_m(\epsilon,t)\,\pi_0(\epsilon,t)\\ =\left(\frac{\partial}{\partial t}-n\mathcal{J}\right)a_n^{(j)}.\end{aligned} \tag{4.25}$$

The calculation of terms in the summation on the right hand side of Eq. (4.9) is greatly simplified by defining the integral

$$\mathcal{I}_{mn}^{\alpha\beta} = \frac{\sigma^{2n}}{n!\alpha!\beta!}\int \mathrm{d}\epsilon\,\psi_n(\epsilon,t)(-\partial_\epsilon)^\alpha\epsilon^\beta\psi_m(\epsilon,t)\pi_0(\epsilon,t), \tag{4.26}$$

which yields

$$\begin{aligned}\frac{\sigma^{2n}}{n!}\int \mathrm{d}\epsilon\psi_n(\epsilon,t)\mathcal{L}_k\psi_m(\epsilon,t)\pi_0(\epsilon,t)\\ =\sum_{s=0}^{\lceil k/2\rceil}\sum_{p=1}^{k-2(s-1)}\mathcal{D}_{p,s}^{k-p-2(s-1)}\mathcal{I}_{mn}^{p,k-p-2(s-1)},\end{aligned} \tag{4.27}$$

where the definition of $\mathcal{L}_k$ in Eq. (4.5) has been substituted. Using Eq. (4.25) and (4.27) in Eq. (4.9), we have the following result:

Result 4.2. *The coefficients in the asymptotic expansion of the probability density, Eq. (4.23), satisfy the following set of ordinary differential equations*

$$\left(\frac{\partial}{\partial t}-n\mathcal{J}\right)a_n^{(j)} = \sum_{k=1}^{j}\sum_{m=0}^{3(j-k)}a_m^{(j-k)}\sum_{s=0}^{\lceil k/2\rceil}\sum_{p=1}^{k-2(s-1)}\mathcal{D}_{p,s}^{k-p-2(s-1)}\mathcal{I}_{mn}^{p,k-p-2(s-1)}, \tag{4.28}$$

where $a_n^{(j)} = 0$ *for* $n > 3j$ *and the non-zero integrals are given by*

$$\mathcal{I}_{mn}^{\alpha\beta} = \frac{\sigma^{\beta-\alpha+n-m}}{\alpha!} \sum_{s=0}^{\min(n-\alpha,m)} \binom{m}{s} \frac{(\beta+\alpha+2s-(m+n)-1)!!}{(\beta+\alpha+2s-(m+n))!(n-\alpha-s)!}, \tag{4.29}$$

and zero for odd $(\alpha+\beta)-(m+n)$*. The integral is non-zero only if* $n = m+\alpha\pm 2l$ *for even* $\beta = 2k$ *or* $n = m+\alpha\pm(2l+1)$ *when* $\beta = (2k+1)$ *is odd, where* $l = 0, ..., k$*.*

Explicit expressions for the approximate probability density can now be evaluated to any desired order. Note that in the above equation, $\mathcal{D}_{p,s}^{q}$ and $\mathcal{I}_{mn}^{pq}$ are time-dependent because they depend on the solution of the RE and the LNA variance.

Derivation. We first note that changing variables $\epsilon = x\sigma$ and defining $\tilde{\mathcal{I}}_{mn}^{\alpha\beta} = \sigma^{\alpha-\beta+m-n}\mathcal{I}_{mn}^{\alpha\beta}$, the related integral can be written

$$\tilde{\mathcal{I}}_{mn}^{\alpha\beta} = \frac{1}{n!\alpha!\beta!}\int \mathrm{d}x H_n(x)(-\partial_x)^\alpha x^\beta H_m(x)\pi_0(x), \tag{4.30}$$

where $\pi_0(x)$ is a centred Gaussian with unit variance. Using partial integration, property (4.19), and the relation

$$H_\alpha(x)H_\beta(x) = \alpha!\beta!\sum_{s=0}^{\min(\alpha,\beta)}\frac{H_{\alpha+\beta-2s}(x)}{s!(\alpha-s)!(\beta-s)!}, \tag{4.31}$$

given in Ref. [124, Ch. 4, p. 96], one obtains

$$\tilde{\mathcal{I}}_{mn}^{\alpha\beta} = \frac{1}{\alpha!\beta!}\sum_{s=0}^{\min(n-\alpha,m)}\binom{m}{s}\frac{\int \mathrm{d}x\, x^\beta H_{m+n-\alpha-2s}(x)\pi_0(x)}{(n-\alpha-s)!}. \tag{4.32}$$

The remaining integral can now be evaluated in terms of the moments of the unit Gaussian as follows

$$\begin{aligned}\int \mathrm{d}x\, x^b H_a(x)\pi_0(x) &= \frac{b!}{(b-a)!}\int \mathrm{d}x\, x^{b-a}\pi_0(x)\\ &= \begin{cases}\frac{b!}{(b-a)!}(b-a-1)!! & \text{if } (b-a)\geq 0 \text{ and even},\\ 0 & \text{otherwise.}\end{cases}\end{aligned} \tag{4.33}$$

Explicitly, the matrix elements are given by

$$\tilde{\mathcal{I}}_{mn}^{\alpha\beta} = \frac{1}{\alpha!}\sum_{s=0}^{\min(n-\alpha,m)}\binom{m}{s}\frac{(\beta+\alpha+2s-(m+n)-1)!!}{(\beta+\alpha+2s-(m+n))!(n-\alpha-s)!}, \tag{4.34}$$

for even $(\alpha+\beta)-(m+n)$ and zero otherwise. Note that the above quantity is strictly positive. Note also that the argument of the double factorial is taken to be positive and hence the summation is non-zero only if $\alpha+\beta+2\min(n-\alpha,m)\geq m+n$. Consequently, for even $\beta = 2k$, we have $n = m+\alpha\pm 2l$, while for odd $\beta = (2k+1)$, we have

$n = m + \alpha \pm (2l+1)$, with $l = 0, ..., k$.

It remains to verify that Eq. (4.28) indeed yields a finite number of equations. Let N_j be the index of the highest eigenfunction required to order $\Omega^{-j/2}$. Using Eq. (4.28) one can show that $a^{(j)}_{N_j} \sim a^{(j-1)}_{N_{j-1}} \mathcal{I}^{p,3-p}_{N_{j-1},N_j}$ for $p \in \{1,2,3\}$. By virtue of the properties given after Eq. (4.29), we find $N_j = N_{j-1} + 3$. Because for deterministic initial conditions we have $N_0 = 0$, it follows that $N_j = 3j$. □

Result 4.3. *For deterministic initial conditions, i.e.* $a^{(j)}_n = \delta_{n,0}\delta_{j,0}$*, it holds that* $a^{(j)}_n = 0$ *for all times when* $(n+j)$ *is odd.*

Derivation. We note that the right hand side of Eq. (4.28) can contain only terms for which $\mathcal{I}^{p,k-p-2(s-1)}_{mn}$ is non-zero. Hence, by the condition given after Eq. (4.29), the non-zero terms in the summation are those for which $k-(m+n)$ is even. Assuming now that $n+j$ in Eq. (4.28) is even, it follows together with the latter condition that for the non-zero terms in the summation $m+(j-k)$ must be even. Conversely, if $n+j$ is odd it follows that $m+(j-k)$ must be odd. Hence the pair of equations for $a^{(j)}_n$ with even and odd $(n+j)$ is mutually uncoupled. Using the fact that, initially, $a^{(j)}_n = 0$ when $j+n$ is odd, we must have $a^{(j)}_n = 0$ for all times. □

The relation of Result 4.3 to Result 3.2 will be clarified in the following.

4.1.4 Moments of the probability distribution

The solution for the probability density enables one to derive closed-form expressions for the moments. These are obtained by multiplying Eq. (4.23) by $\int \mathrm{d}\epsilon\, \epsilon^\beta$ and performing the integration using Eq. (4.33). The result is

$$\langle \epsilon^\beta \rangle = \sum_{j=0}^{N} \Omega^{-j/2} \sum_{k=0}^{\lfloor \beta/2 \rfloor} \frac{\beta!}{2^k k!} \sigma^{2k} a^{(j)}_{\beta-2k} + O(\Omega^{-(N+1)/2}), \tag{4.35}$$

and $a^{(j)}_0 = \delta_{0,j}$. In particular, it follows that

$$\langle \epsilon \rangle = \sum_{j=1}^{N} \Omega^{-j/2} a^{(j)}_1 + O(\Omega^{-(N+1)/2}), \tag{4.36a}$$

$$\langle \epsilon^2 \rangle = \sigma^2 + 2\sum_{j=1}^{N} \Omega^{-j/2} a^{(j)}_2 + O(\Omega^{-(N+1)/2}), \tag{4.36b}$$

for the first and second moment, respectively. Finally, note that using Result 4.3 it follows that the moment expansion coefficients in Eq. (4.35), i.e.

$$[\epsilon^\beta]_j = \sum_{k=0}^{\lfloor \beta/2 \rfloor} \frac{\beta!}{2^k k!} \sigma^{2k} a^{(j)}_{\beta-2k}, \tag{4.37}$$

are non-zero only when $\beta + j$ is even as stated in Result 3.2.

4.1.5 Relation to the inverse problem

It is now evident that the coefficients of the expansion are intricately related to the system size expansion of the distribution moments. Naturally, one may seek to invert this relation. Here, we show that the coefficients in Eq. (4.23) are uniquely determined by the expansion for a finite set moments. In particular, to construct the probability density to order $\Omega^{-j/2}$ one requires the expansion of the first $3j$ moments to the same order. Thus the problem of moments provides an equivalent route of systematically constructing solutions to the CME.

Result 4.4 (Reconstruction of the distributions from the system size expansion of the moments)**.** *Given the asymptotic expansion of the moments in powers of* $\Omega^{-1/2}$*,*

$$\langle \epsilon^\beta \rangle = \sum_{j=0}^{N} \Omega^{-j/2} [\epsilon^\beta]_j + O(\Omega^{-(N+1)/2}), \tag{4.38}$$

whose coefficients are uniquely determined by Remark 3.1, the coefficients in the asymptotic expansion of the probability density, Eq. (4.23), are uniquely determined and given by

$$a_n^{(j)} = \frac{1}{n!} \sum_{k=0}^{\lfloor n/2 \rfloor} \binom{n}{2k} (-1)^k \sigma^{2k} [\epsilon^{n-2k}]_j (2k-1)!!\,, \tag{4.39}$$

with $[\epsilon^0]_j = \delta_{j,0}$.

The above result relates the expansion of the moments, as given by Remark 3.1, to the expansion of distribution functions. It is now evident that the system size expansion of the distribution can be constructed from the system size expansion for a finite set of moments.

Derivation. Using the completeness of the Hermite polynomials, one can write the probability density as $\Pi(\epsilon) = \sum_{n=0}^{\infty} b_n H_n\left(\frac{\epsilon}{\sigma}\right)\pi_0(\epsilon)$, where the $b_n = \frac{1}{n!}\int d\epsilon H_n\left(\frac{\epsilon}{\sigma}\right)\Pi(\epsilon)$ can be expressed in terms of the moments using the explicit definition of the Hermite polynomials given in Eq. (4.17)

$$b_n = \frac{1}{n!} \sum_{k=0}^{\lfloor n/2 \rfloor} \binom{n}{2k} (-1)^k \frac{\langle \epsilon^{n-2k} \rangle}{\sigma^{n-2k}} (2k-1)!!. \tag{4.40}$$

Inserting now Eq. (4.38), the coefficients in the expansion of the b_n can be related to the coefficients a_n in Eq. (4.23) by equating equal powers of Ω in $\sigma^n b_n = \sum_{j=0}^{N} \Omega^{-j/2} a_n^{(j)} + O(\Omega^{-(N+1)/2})$. The result is given by Eq. (4.39). □

Specifically, to order $\Omega^{-1/2}$ the non-zero coefficients evaluate to

$$a_1^{(1)} = [\epsilon]_1, \quad a_3^{(1)} = \frac{1}{3!}\left([\epsilon^3]_1^3 - 3\sigma^2[\epsilon]_1\right), \tag{4.41}$$

while the coefficients to order Ω^{-1} are given by

$$a_2^{(2)} = \frac{1}{2}[\epsilon^2]_2, \quad a_4^{(2)} = \frac{1}{4!}\left([\epsilon^4]_2 - 6\sigma^2[\epsilon^2]_2\right),$$
$$a_6^{(2)} = \frac{1}{6!}\left(45\sigma^4[\epsilon^2]_2 - 15\sigma^2[\epsilon^4]_2 + [\epsilon^6]_2\right). \tag{4.42}$$

4.1.6 Solution in stationary conditions

Of particular interest is the expansion of the density under stationary conditions. Implicitly, we assume here that the RE, Eq. (4.3), has a single asymptotically stable fixed point, and hence the LNA variance is given by $\sigma^2 = \mathcal{D}_2^0/(-2\mathcal{J})$. Setting the time-derivative on the left hand side of Eq. (4.28) to zero, we find that the coefficients of Eq. (4.23) can be expressed in terms of lower order ones

$$a_n^{(j)} = -\frac{1}{n\mathcal{J}} \sum_{k=1}^{j} \sum_{s=0}^{\lceil k/2 \rceil} \sum_{p=1}^{k-2(s-1)} \mathcal{D}_{p,s}^{k-p-2(s-1)} \sum_{m=0}^{3(j-k)} a_m^{(j-k)} \mathcal{I}_{mn}^{p,k-p-2(s-1)}. \tag{4.43}$$

For example, truncating after terms of order Ω^{-1}, we obtain

$$\begin{aligned}\Pi(\epsilon) = &\pi_0(\epsilon) + \Omega^{-1/2}\left(a_1^{(1)}\psi_1(\epsilon) + a_3^{(1)}\psi_3(\epsilon)\right)\pi_0(\epsilon) \\ &+ \Omega^{-1}\left(a_2^{(2)}\psi_2(\epsilon) + a_4^{(2)}\psi_4(\epsilon) + a_6^{(2)}\psi_6(\epsilon)\right)\pi_0(\epsilon) + O(\Omega^{-3/2}).\end{aligned} \tag{4.44}$$

The non-zero coefficients to order $\Omega^{-1/2}$ are given by

$$a_1^{(1)} = -\frac{\sigma^2\mathcal{D}_1^2 + 2\mathcal{D}_{1,1}^0}{2\mathcal{J}},$$
$$a_3^{(1)} = -\frac{3\sigma^4\mathcal{D}_1^2 + 3\sigma^2\mathcal{D}_2^1 + \mathcal{D}_3^0}{18\mathcal{J}}, \tag{4.45}$$

while those to order Ω^{-1} are

$$\begin{aligned}a_2^{(2)} = &- a_1^{(1)}\left(\frac{\mathcal{D}_{1,1}^0}{2\mathcal{J}} + \frac{\mathcal{D}_2^1}{4\mathcal{J}} + \frac{3\sigma^2\mathcal{D}_1^2}{4\mathcal{J}}\right) \\ &- \frac{3a_3^{(1)}\mathcal{D}_1^2}{2\mathcal{J}} - \frac{\mathcal{D}_{2,1}^0}{4\mathcal{J}} - \frac{\sigma^2\mathcal{D}_{1,1}^1}{2\mathcal{J}} - \frac{\sigma^2\mathcal{D}_2^2}{8\mathcal{J}} - \frac{\sigma^4\mathcal{D}_1^3}{4\mathcal{J}}, \\ a_4^{(2)} = &- a_1^{(1)}\left(\frac{\mathcal{D}_3^0}{24\mathcal{J}} + \frac{\sigma^2\mathcal{D}_2^1}{8\mathcal{J}} + \frac{\sigma^4\mathcal{D}_1^2}{8\mathcal{J}}\right) - \frac{\mathcal{D}_4^0}{96\mathcal{J}} - \frac{\sigma^2\mathcal{D}_3^1}{24\mathcal{J}} \\ &- \frac{\sigma^4\mathcal{D}_2^2}{16\mathcal{J}} - \frac{\sigma^6\mathcal{D}_1^3}{24\mathcal{J}} - a_3^{(1)}\left(\frac{\mathcal{D}_{1,1}^0}{4\mathcal{J}} + \frac{3\mathcal{D}_2^1}{8\mathcal{J}} + \frac{7\sigma^2\mathcal{D}_1^2}{8\mathcal{J}}\right), \\ a_6^{(2)} = &\frac{1}{2}(a_3^{(1)})^2.\end{aligned} \tag{4.46}$$

The accuracy of this distribution approximation is studied through an example in the following.

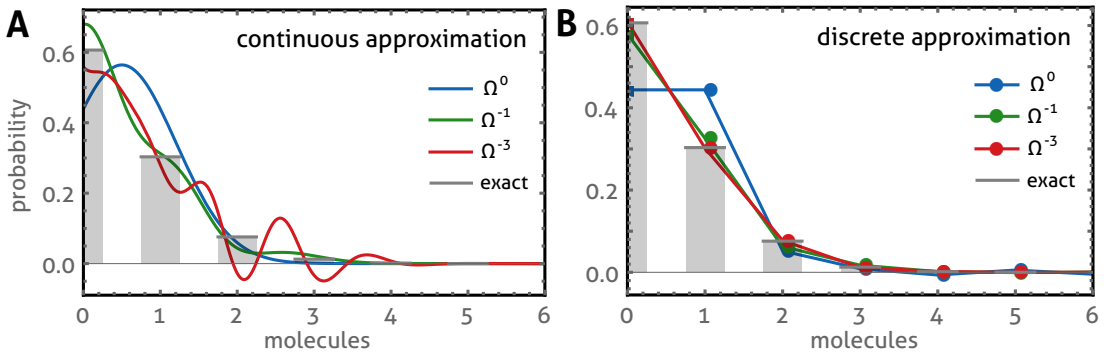

Figure 4.1:
Linear birth-death process. We consider the reaction system (4.47) in stationary conditions. (A) We compare the exact Poisson distribution (grey) to the continuous SSE approximation [Eq. (4.23) together with Eqs. (4.43) and (4.48)] truncated after Ω^0 (LNA, blue line), Ω^{-1} (green), and Ω^{-3}-terms (red) for parameter values $k_0 = 0.5$, $k_1 = 1$ and $\Omega = 1$ giving half a molecule on average. We observe that the continuous approximation becomes increasingly negative and tends to oscillate with increasing truncation order. (B) In contrast, the discrete approximation shows no oscillations and the overall agreement with the exact Poisson distribution (grey bars) improves with increasing truncation order.

4.1.7 The continuous approximation fails under low molecule number conditions

We now study the SSE solution for a linear birth-death process, i.e. processes whose propensities depend at most linearly on the molecular populations. Specifically, we consider the synthesis and decay of a molecular species X,

$$\varnothing \underset{k_1}{\overset{k_0}{\rightleftharpoons}} X. \tag{4.47}$$

The CME is constructed using $S_1 = +1$, $w_1 = \Omega k_0$, $S_2 = -1$, $w_2 = k_1 n$, and $R = 2$ in Eq. (4.1). The exact stationary solution of the CME is a simple Poisson distribution with mean $\Omega[X]$ where $[X] = k_0/k_1$. The coefficients in Eq. (4.6) are then given by

$$\mathcal{D}_n^m = \delta_{m,0} k_0 + (-1)^n k_1 \left(\delta_{m,0}[X] + \delta_{m,1}\right), \tag{4.48}$$

and $\mathcal{D}_{n,s}^m = 0$ for $s > 0$. The leading order corrections to the LNA given by Eqs. (4.44-4.46) lead to very compact expressions for the expansion coefficients and are given by

$$a_3^{(1)} = \frac{[X]}{6}, \quad a_4^{(2)} = \frac{[X]}{24}, \quad a_6^{(2)} = \frac{[X]^2}{72}, \tag{4.49}$$

and $a_1^{(1)} = a_2^{(2)} = 0$. Note that by Eqs. (4.36) this implies that there are no corrections to mean and variance predicted by the LNA.

Though the continuous approximation is expected to perform well at large values of Ω, we are particularly interested in its performance when the value of Ω is decreased. Since the expansion is carried out at constant average concentration, low values of Ω typically imply low numbers of molecules and non-Gaussian distributions. In Fig. 4.1A we show that for parameters yielding half a molecule on average, the continuous approximation obtained in this section, given by Eq. (4.23) together with Eqs. (4.43) and (4.48), is unsatisfactory since as higher orders are taken into account, one observes large oscillations in the tails of the distribution. In the following section we show that the disagreement arises due to the assumption that the support of the distribution is continuous rather than discrete as implied by the CME.

4.2 Discrete approximation of the probability distribution

The aim of this section is to generalize the SSE to discrete distribution approximations. An intuitive approach considers the exact characteristic function $G(k,t) = \sum_{n=0}^{\infty} e^{ikn} P(n,t)$ that is necessarily a 2π-periodic function. It can hence be inverted as follows

$$P(n,t) = \int_{-\pi}^{\pi} \frac{\mathrm{d}k}{2\pi} e^{-ikn} G(k,t). \tag{4.50}$$

We now associate the continuous approximation, Eq. (4.23), with this characteristic function

$$G(k,t) = \int_{-\infty}^{\infty} \mathrm{d}\epsilon \, e^{ik\Omega([X]+\Omega^{-1/2}\epsilon)} \Pi(\epsilon,t). \tag{4.51}$$

Substituting this together with Eq. (4.7) into Eq. (4.50) one establishes a connection formula between these discrete and continuous approximations via the convolution

$$P(n,t) = \sum_{j=0}^{N} \Omega^{-j/2} \int_{-\infty}^{\infty} \mathrm{d}\epsilon \, K(n - \Omega[X] - \Omega^{1/2}\epsilon) \pi_j(\epsilon,t) + O(\Omega^{-(N+1)/2}), \tag{4.52}$$

with convolution kernel

$$K(s) = \int_{-\pi}^{\pi} \frac{\mathrm{d}k}{2\pi} e^{-iks} = \frac{\sin(\pi s)}{\pi s}. \tag{4.53}$$

For example, to leading order Ω^0, Eq. (4.52) replaces the conventional continuous LNA estimate, π_0 given by Eq. (4.11), with the discrete approximation

$$P_0(n,t) = \frac{1}{2} \frac{e^{-\frac{y^2}{2\Sigma^2}}}{\sqrt{2\pi}\Sigma} \left(\mathrm{erf}\left(\frac{iy + \pi\Sigma^2}{\sqrt{2}\Sigma} \right) - \mathrm{erf}\left(\frac{iy - \pi\Sigma^2}{\sqrt{2}\Sigma} \right) \right), \tag{4.54}$$

where $y = n - \Omega[X]$, $\Sigma^2 = \Omega\sigma^2$ is the LNA's estimate for the variance of molecule numbers, and erf is the error function defined by $\mathrm{erf}(x) = \frac{2}{\sqrt{\pi}} \int_0^x e^{-t^2} \, \mathrm{d}t$. For consistency,

we study the two limiting cases: (i) as $\Omega \to \infty$ with y/Σ constant, the probability distribution P_0 reduces to the density π_0 given by Eq. (4.11); (ii) as $\Sigma \to 0$ and $\Omega[X]$ being integer-valued, then $P_0(n) = K(n - \Omega[X])$ reduces to the Kronecker delta $\delta_{n,\Omega[X]}$ which is consistent with deterministic initial conditions.

Associating the $\Omega^{-j/2}$-term of Eq. (4.23) with π_j in Eq. (4.52), we have the following result that we refer to as the discrete approximation:

Result 4.5 (Discrete approximation)**.** *The discrete approximation of the probability distribution given by*

$$P(n,t) = P_0(n,t) + \sum_{j=1}^{N} \Omega^{-j/2} \sum_{m=1}^{3j} a_m^{(j)} \left(-\Omega^{1/2}\partial_n\right)^m P_0(n,t) + O(\Omega^{-(N+1)/2}), \tag{4.55}$$

is an asymptotic series solution to the CME (4.1), where $P_0(n,t)$ is given by Eq. (4.54) and the coefficients $a_m^{(j)}$ are given by Result 4.2.

Derivation. Eq. (4.55) follows from substituting Eq. (4.23) into (4.52), and using the fact that convolution preserves the derivative, i.e.

$$\partial_n P_0(n,t) = \int_{-\infty}^{\infty} \mathrm{d}\epsilon\, K(n - \Omega[X] - \Omega^{1/2}\epsilon)(\Omega^{-1/2}\partial_\epsilon)\pi_0(\epsilon,t). \tag{4.56}$$

Since by construction $P(n,t)$ given by Eq. (4.55) and $\Omega^{1/2}\Pi(\Omega^{-1/2}(n-\Omega[X]),t)$ have the same expansion of the characteristic function expansion, it follows that the continuous approximation, Eq. (4.23), and the discrete approximation possess the same asymptotic expansion of their moments.

It remains to verify that Eq. (4.55) solves the expansion of the CME. We therefore suppose that $P(n,t) = \int_{-\infty}^{\infty} \mathrm{d}\epsilon\, K(n-\Omega[X]-\Omega^{1/2}\epsilon)\Pi(\epsilon,t)$ and inspect the action of the step operator

$$E^{-S_r} P(n,t) = \int_{-\infty}^{\infty} \mathrm{d}\epsilon\, K(n - \Omega[X] - \Omega^{1/2}\epsilon) e^{-\Omega^{-1/2}\partial_\epsilon S_r}\Pi(\epsilon,t), \tag{4.57}$$

which follows from the fact that the integral kernel K given by Eq. (4.53) is analytic, i.e. $K(n - S_r - \Omega[X] - \Omega^{1/2}\epsilon) = \mathrm{e}^{-S_r\partial_n} K(n - \Omega[X] - \Omega^{1/2}\epsilon)$, and partial integration. One the other hand, presuming that $w_r(n,\Omega)$ is analytic in n, we have

$$w_r(n,\Omega)P(n,t) = \int_{-\infty}^{\infty} \mathrm{d}\epsilon\, K(n - \Omega[X] - \Omega^{1/2}\epsilon) w_r(\Omega[X] + \Omega^{1/2}\epsilon, \Omega)\Pi(\epsilon,t). \tag{4.58}$$

The above remarks are then used in the CME, Eq. (4.1), to find

$$\begin{aligned}
0 =& \frac{\mathrm{d}}{\mathrm{d}t}P(n,t) - \sum_{r=1}^{R}(E^{-S_r}-1)w_j(n,\Omega)P(n,t) \\
=& \int_{-\infty}^{\infty}\mathrm{d}\epsilon\, K(n-\Omega[X]-\Omega^{1/2}\epsilon)\left(\frac{\partial}{\partial t} - \Omega^{1/2}\frac{\mathrm{d}[X]}{\mathrm{d}t}\partial_\epsilon\right)\Pi(\epsilon,t), \\
& - \int_{-\infty}^{\infty}\mathrm{d}\epsilon\, K(n-\Omega[X]-\Omega^{1/2}\epsilon)\times \\
& \qquad \left[\sum_{r=1}^{R}(e^{-\Omega^{-1/2}\partial_\epsilon S_r}-1)w_r(\Omega[X]+\Omega^{1/2}\epsilon,\Omega)\right]\Pi(\epsilon,t). \qquad (4.59)
\end{aligned}$$

Proceeding along the lines in Section 2.4, the term in the angled brackets is expanded in a series of the inverse square root of Ω. Since $\Pi(\epsilon,t)$ given by Eq. (4.23) solves this expansion to each order, the result follows. □

It is important to note that the asymptotic errors of the continuous approximation, Eq. (4.23), and the discrete approximation given by Result 4.5 are the same. It is however the case that the discrete approximation takes into account exponentially small terms in Ω, which are beyond the scope of perturbation theory, and are therefore dismissed in a continuous approximation of $P(n,t)$, i.e. Eq. (2.9) in Section 2.4, as obtained in the original derivation of the SSE due to van Kampen [44, 76]. However, we will demonstrate in the following that these terms are relevant in applications.

4.2.1 The discrete approximation fares well for linear birth-death processes

For the linear birth-death process in the previous section, Fig. 4.1B shows that the discrete approximation given by Eq. (4.55) with Eq. (4.43) and (4.48) is in reasonable agreement with the true distribution when truncated after terms of order Ω^{-1} and shows no oscillations. The approximation is almost indistinguishable from the exact result when the series is truncated after Ω^{-3}-terms. We hence conclude that the discrete series better approximates the underlying distribution of the CME than the continuous approximation.

4.2.2 The discrete approximation fails for nonlinear birth-death process

Next, we turn our attention to the analysis of nonlinear birth-death processes, i.e. a process whose propensities depend nonlinearly on the number of molecules. A particular feature of such processes is that the LNA estimates for mean and variances are generally no longer exact, but agree with those of the true distribution only in the limit of large system size [1].

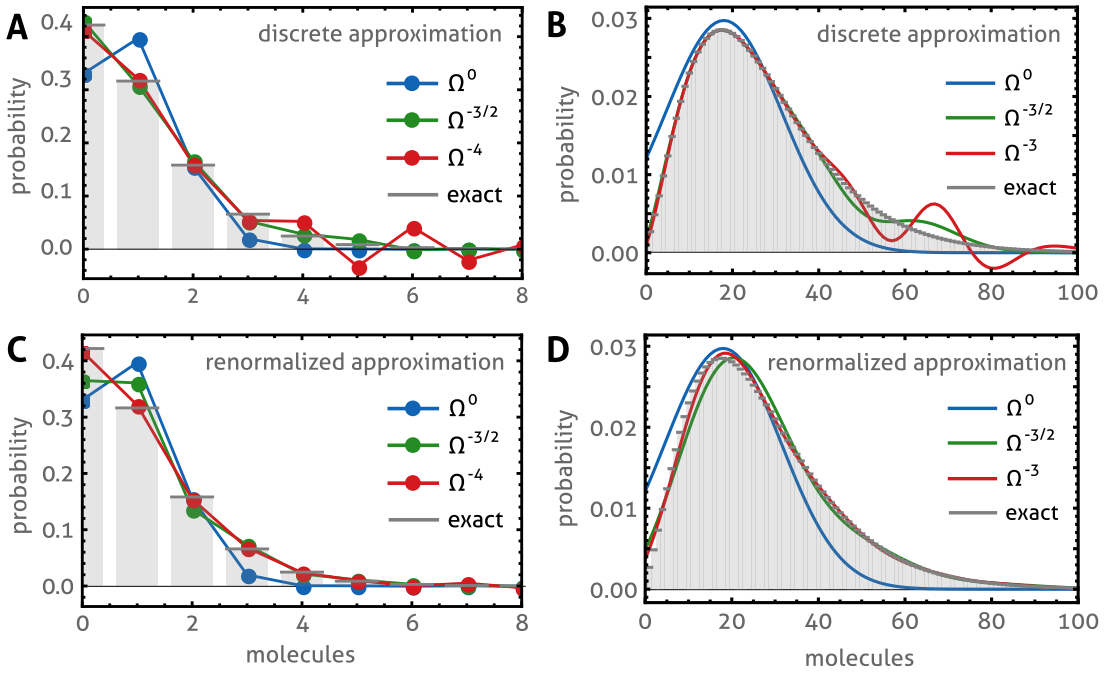

Figure 4.2:

Nonlinear birth-death process. A metabolic reaction with Michaelis-Menten kinetics, scheme (4.60), is studied using the reduced model described in Sec. 4.2.2. The exact stationary distribution is a negative binomial (shown in gray). (A) The discrete SSE approximation given by Eq. (4.55) with Eq. (4.43) and (4.48) is shown in the low molecule number regime ($k_0/k_1 = 0.25$, 1 molecule on average) when truncated after Ω^0 (blue), $\Omega^{-3/2}$ (green) and Ω^{-4}-terms (red dots). We observe that the expansion tends to oscillations and negative values of probability as the truncation order is increased. (B) Similar oscillations are observed in the moderate molecule numbers ($k_0/k_1 = 0.9$, 27 molecules on average) for the discrete series truncated after Ω^0 (blue), $\Omega^{-3/2}$ (green) and Ω^{-3}-terms (red lines). In (C) and (D) we show the approximations corresponding to the same parameters used in (A) and (B), respectively, but obtained using the renormalisation procedure given by Result 4.6 with Eq. (4.67). The renormalized approximations avoid oscillations and are in excellent agreement with the true probability distributions (grey bars). We note that for the cases (B) and (D) the continuous and discrete approximations give essentially the same result. The remaining parameters are given by $\Omega = 10$ and $K = 0.1$.

As an example, we here consider a simple metabolic reaction confined to a small subcellular compartment of size Ω with substrate input,

$$\varnothing \xrightarrow{h_0} S, \tag{4.60a}$$

$$S + E \underset{h_2}{\overset{h_1}{\rightleftharpoons}} C \xrightarrow{h_3} E. \tag{4.60b}$$

The reactions describe substrate molecules S input and their catalytic conversion by enzyme species E via the enzyme-substrate complex C. The SSE of the average concentrations correcting the macroscopic REs have been intensively studied [85]. Since our theory applies to a single species only, we here consider a reduced model in which reaction (4.60b) is modelled via an effective propensity: this gives $S_1 = +1$, $w_1 = \Omega k_0$, and $S_2 = -1$, $w_2 = \Omega k_1 \frac{n}{n+\Omega K}$ as studied in Section 3.2.1. This simplification is valid when the enzyme-substrate association is in rapid equilibrium, which holds when $[E_T] \ll K$ and $h_3 \ll h_2$ where $[E_T]$ is the total enzyme concentration [125, 126]. The parameters in the reduced model are related to those in the developed model by $k_0 = h_1$, $k_1 = h_3[E_T]$, and $K = h_2/h_1$. The reduced CME is solved exactly by a negative binomial distribution [116].

The system size coefficients are obtained from Eq. (4.6), and are given by $\mathcal{D}^m_{n,s} = 0$ for $s > 0$ and

$$\mathcal{D}^m_n = \delta_{m,0} k_0 + (-1)^n k_1 \frac{\partial^m}{\partial [X]^m} \frac{[X]}{K + [X]}. \tag{4.61}$$

In Fig. 4.2A and 4.2B, we consider two parameter sets corresponding to low and moderate numbers of substrate molecules, respectively. We observe that in contrast to the linear case, the discrete approximation of the nonlinear birth-death process tends to oscillate with increasing truncation order. This issue is addressed in the following section.

4.3 Renormalisation of nonlinear birth-death processes

Van Kampen's ansatz, Eq. (2.8) in Section 2.4, bears the particularly simple interpretation that for linear birth-death processes ϵ denotes the fluctuations about the average given by the solution of the RE $[X]$. As noted in the previous example, for nonlinear birth-death processes these estimates are only approximate. Their asymptotic series expansions will therefore require additional terms that compensate for the deviations of the LNA from the true concentration mean and variance. It would therefore be desirable to find an approximation for nonlinear processes that yields more accurate estimates for mean and variance than the LNA. For instance by rewriting van Kampen's ansatz as

$$\frac{n}{\Omega} = \underbrace{\left\langle \frac{n}{\Omega} \right\rangle}_{\text{mean}} + \underbrace{\Omega^{-1/2} \bar{\epsilon}}_{\text{fluctuations}} . \tag{4.62}$$

Here, the first term is $\left\langle \frac{n}{\Omega} \right\rangle = [X] + \Omega^{-1/2} \langle \epsilon \rangle$ and the second $\bar{\epsilon} = \epsilon - \langle \epsilon \rangle$ denotes a centred variable that quantifies the fluctuations about the true average which, of course, is a priori unknown. Estimates can however be obtained using the SSE beforehand, and the asymptotic expansion of the distributions can then be performed about these new

values. This idea is called renormalisation and makes use of the fact that the terms correcting mean and variances can be summed exactly. As we show in the following, the resummation allows to better control the convergence by effectively reducing the number of terms in the summation while at the same time it retains the accuracy of the expansion. We note that while the order of the asymptotic error is the same, the renormalisation scheme leads to a smaller absolute error which we will demonstrate through the use of examples.

The system size expansion of the moments, Eq. (4.35), yields the following estimates for mean and variance of the fluctuations

$$\langle \epsilon \rangle = \sum_{j=0}^{N} \Omega^{-j/2} a_1^{(j)} + O(\Omega^{-(N+1)/2}), \tag{4.63a}$$

$$\bar{\sigma}^2 = \sigma^2 + \sum_{j=1}^{N} \Omega^{-j/2} \sigma_{(j)}^2 + O(\Omega^{-(N+1)/2}), \tag{4.63b}$$

respectively, where $\bar{\sigma}^2_{(j)} = 2(a_2^{(j)} - B_{j,2}(\{\zeta! a_1^{(\zeta)}\})/j!)$ and $B_{j,n}(\{x_\zeta\})$ is short-hand for the partial Bell polynomials[1] [102, Ch. III] defined as

$$B_{n,k}(\{x_\zeta\}_{\zeta=1}^{n-k+1}) = \sum{}' \frac{n!}{j_1!...j_{n-k+1}!} \left(\frac{x_1}{1!}\right)^{j_1} ... \left(\frac{x_{n-k+1}}{(n-k+1)!}\right)^{j_{n-k+1}}, \tag{4.64}$$

where $\sum'$ denotes the summation over all sequences $j_1, ..., j_{n-k+1}$ of non-negative integers such that $j_1 + ... + j_{n-k+1} = k$ and $j_1 + 2j_2 + ... + (n-k+1)j_{n-k+1} = n$. The renormalisation procedure amounts to replacing y by $(n - \Omega[X] - \Omega^{1/2}\langle\epsilon\rangle)$, Σ^2 by $\bar{\Sigma}^2 = \Omega\bar{\sigma}^2$ in Eq. (4.54) and associating a new Gaussian $\bar{P}_0(n)$ with these estimates. Note that henceforth we will refer to the approximation without renormalisation as the bare approximation.

Result 4.6 (The renormalised expansion)**.** *The renormalised asymptotic expansion for the discrete probability distribution is given by*

$$P(n,t) = \bar{P}_0(n,t) + \sum_{j=1}^{N} \Omega^{-j/2} \sum_{m=1}^{3j} \bar{a}_m^{(j)} \left(-\Omega^{1/2}\partial_n\right)^m \bar{P}_0(n,t) + O(\Omega^{-(N+1)/2}), \tag{4.65}$$

with

$$\bar{P}_0(n,t) = \frac{1}{2} \frac{e^{-\frac{\bar{y}^2}{2\bar{\Sigma}^2}}}{\sqrt{2\pi}\bar{\Sigma}} \left[\mathrm{erf}\left(\frac{i\bar{y} + \pi\bar{\Sigma}^2}{\sqrt{2}\bar{\Sigma}}\right) - \mathrm{erf}\left(\frac{i\bar{y} - \pi\bar{\Sigma}^2}{\sqrt{2}\bar{\Sigma}}\right)\right], \tag{4.66}$$

where $\bar{y} = (n - \Omega[X] - \Omega^{1/2}\langle\epsilon\rangle)$ *and* $\bar{\Sigma}^2 = \Omega\bar{\sigma}^2$*. The renormalised coefficients* $\bar{a}_m^{(j)}$ *are*

[1] These are available in Mathematica via the function BellY$[n, k, \{x_1, \ldots, x_{n-k+1}\}]$

obtained from the bare ones using

$$\bar{a}_m^{(j)} = \sum_{k=0}^{j} \sum_{n=0}^{3k} a_n^{(k)} \kappa_{m-n}^{(j-k)}, \tag{4.67}$$

and

$$\kappa_j^{(n)} = \frac{1}{n!} \sum_{m=0}^{\lfloor j/2 \rfloor} (-1)^{(j+m)} \sum_{k=j-2m}^{n-m} \binom{n}{k} \times B_{n-k,m}\left(\left\{\frac{\zeta!}{2}\bar{\sigma}^2_{(\zeta)}\right\}\right) B_{k,j-2m}\left(\left\{\zeta! a_1^{(\zeta)}\right\}\right). \tag{4.68}$$

It is important to note that while the order of the expansions in Result 4.5 and 4.6 are the same, the renormalised expansion leads to a smaller absolute error because it has generally less non-zero coefficients. In particular, it follows by construction that $\bar{a}_1^{(j)} = \bar{a}_2^{(j)} = 0$ for all j. Note also that for linear birth-processes, mean and variance are exact to order Ω^0 (LNA), and hence for this case expansion (4.55) coincides with (4.65).

For example, truncating after Ω^{-1}-terms, from Eq. (4.63) it follows that $\langle \epsilon \rangle = \Omega^{-1/2} a_1^{(1)} + O(\Omega^{-3/2})$ and $\bar{\sigma}^2 = \sigma^2 + \Omega^{-1}(2a_2^2 - (a_1^{(1)})^2) + O(\Omega^{-3/2})$. Using Eq. (4.67) the renormalised coefficients can be expressed in terms of the bare ones

$$\bar{a}_1^{(1)} = 0, \quad \bar{a}_3^{(1)} = a_3^{(1)}, \tag{4.69a}$$

$$\bar{a}_2^{(2)} = 0, \quad \bar{a}_4^{(2)} = a_4^{(2)} - a_1^{(1)} a_3^{(1)}, \quad \bar{a}_6^{(2)} = a_6^{(2)}. \tag{4.69b}$$

This result can for instance be used to renormalise the stationary solution using the bare coefficients given in Section 4.1.6, Eqs. (4.45-4.46). The non-zero renormalised coefficients evaluate to

$$\bar{a}_3^{(1)} = -\frac{\sigma^4 \mathcal{D}_1^2}{6\mathcal{J}} + \frac{\sigma^2 \mathcal{D}_2^1}{6\mathcal{J}} + \frac{\mathcal{D}_3^0}{18\mathcal{J}}, \tag{4.70a}$$

$$\bar{a}_4^{(2)} = -\frac{\mathcal{D}_4^0}{96\mathcal{J}} - \frac{\sigma^2 \mathcal{D}_3^1}{24\mathcal{J}} - \frac{\sigma^4 \mathcal{D}_2^2}{16\mathcal{J}} - \frac{\sigma^6 \mathcal{D}_1^3}{24\mathcal{J}} - \bar{a}_3^{(1)}\left(\frac{3\mathcal{D}_2^1}{8\mathcal{J}} + \frac{3\sigma^2 \mathcal{D}_1^2}{4\mathcal{J}}\right),$$

$$\bar{a}_6^{(2)} = \frac{1}{2}(\bar{a}_3^{(1)})^2. \tag{4.70b}$$

Note that for linear birth-death processes, we have $\mathcal{D}_{n,s}^m = 0$ for $s > 0$ and $m > 1$ and hence the above equations reduce to Eqs. (4.45-4.46).

Derivation. The renormalised coefficients can in principle be obtained by matching the expansions given by Eq. (4.55) and (4.65) via their characteristic functions. For

convenience, let us consider the characteristic function of the series (4.23)

$$G(k) = G_0(k)\left(1 + \sum_{j=1}^{\infty} \Omega^{-j/2} \sum_{n=1}^{3j} a_n^{(j)} (ik)^n\right), \tag{4.71}$$

with $G_0(k) = e^{-(k\sigma)^2/2}$ being the characteristic function solution of the LNA, $\pi_0(\epsilon)$. We have omitted the explicit time-dependence to ease the notation. Next, we are looking for a different expansion with corrected estimates for the mean and variance that can be written as follows

$$\bar{G}(k) = \bar{G}_0(k)\left(1 + \sum_{j=1}^{\infty} \Omega^{-j/2} \sum_{n=1}^{3j} \bar{a}_n^{(j)} (ik)^n\right), \tag{4.72}$$

Note that $\bar{G}_0(k) = e^{ik\langle\epsilon\rangle} e^{-(k\bar{\sigma})^2/2}$ is the characteristic function for a Gaussian random variable with mean $\langle\epsilon\rangle$ and variance $\bar{\sigma}^2$ given by Eq. (4.63). Equating now Eq. (4.71) and (4.72), we find

$$\begin{aligned} &1 + \sum_{j=1}^{\infty} \Omega^{-j/2} \sum_{n=1}^{3j} \bar{a}_n^{(j)} (ik)^n \\ &\quad = \frac{G_0(k)}{\bar{G}_0(k)}\left(1 + \sum_{j=1}^{\infty} \Omega^{-j/2} \sum_{n=1}^{3j} a_n^{(j)} (ik)^n\right). \end{aligned} \tag{4.73}$$

Expanding the prefactor in the above equation in powers of k and then in Ω, we have

$$\frac{G_0(k)}{\bar{G}_0(k)} = \sum_{j=0}^{\infty} (ik)^j \kappa_j = \sum_{n=0}^{\infty} \Omega^{-n/2} \sum_{j=0}^{2n} (ik)^j \kappa_j^{(n)}, \tag{4.74}$$

from which Eq. (4.67) follows, which expresses the new coefficients $\bar{a}_n^{(j)}$ in terms of the bare ones $a_n^{(j)}$. It remains to derive an explicit expression for the $\kappa_j^{(n)}$. The expansion in powers of (ik) yields

$$\kappa_j = \sum_{m=0}^{\lfloor j/2 \rfloor} (-1)^{(j+m)} \frac{\langle\epsilon\rangle^{j-2m}}{(j-2m)!} \frac{\left(\frac{\bar{\sigma}^2 - \sigma^2}{2}\right)^m}{m!}. \tag{4.75}$$

We now expand the first term in inverse powers of Ω using the partial Bell polynomials

$$\begin{aligned} &\frac{1}{(j-2m)!}\left(\sum_{n=1}^{\infty} \Omega^{-n/2} a_1^{(n)}\right)^{j-2m} \\ &\quad = \sum_{n=1}^{\infty} \frac{\Omega^{-n/2}}{n!} \sum_{k=0}^{n} \delta_{j-2m,k} B_{n,k}\left(\left\{\zeta! a_1^{(\zeta)}\right\}\right), \end{aligned} \tag{4.76}$$

and similarly for the second term

$$\frac{1}{m!}\left(\frac{1}{2}\sum_{n=1}^{\infty}\Omega^{-n/2}\bar{\sigma}^2_{(n)}\right)^m = \sum_{n=0}^{\infty}\frac{\Omega^{-n/2}}{n!}\sum_{k=0}^{n}\delta_{m,k}B_{n,k}\left(\left\{\frac{\zeta!}{2}\bar{\sigma}^2_{(\zeta)}\right\}\right). \tag{4.77}$$

Using the above expansions in Eq. (4.75) and rearranging in powers of $\Omega^{-1/2}$, Eq. (4.68) for the coefficients $\kappa_j^{(n)}$ follows.

Finally, one associates with the centred variable $\bar{\epsilon} = \epsilon - \langle\epsilon\rangle$, a Gaussian $\bar{\pi}_0(\bar{\epsilon})$ with variance $\bar{\sigma}^2$. Inverting Eq. (4.72), we have

$$\Pi(\bar{\epsilon}) = \bar{\pi}_0(\bar{\epsilon}) + \sum_{j=1}^{N}\Omega^{-j/2}\sum_{n=1}^{3j}\bar{a}_n^{(j)}\psi_n\left(\bar{\epsilon}\right)\bar{\pi}_0(\bar{\epsilon}) + O(\Omega^{-(N+1)/2}). \tag{4.78}$$

Associating now the $\Omega^{-j/2}$-term of this equation with π_j in Eq. (4.52), the discrete series for $P(n,t)$ as given by Eq. (4.65) is obtained. □

4.3.1 The renormalised discrete approximation performs well for nonlinear birth-death process

For the metabolic reaction (4.60), mean and variance can be obtained to be $\langle\epsilon\rangle = \Omega^{-1/2}\varsigma + O(\Omega^{-2})$, $\bar{\sigma}^2 = \sigma^2 + \Omega^{-1}\varsigma(\varsigma+1) + O(\Omega^{-2})$, where $\varsigma = [X]/K$ is the reduced substrate concentration and $\sigma^2 = K\varsigma(\varsigma+1)$. Substituting now Eq. (4.61) into Eqs. (4.70), we obtain the expansion coefficients

$$\bar{a}_3^{(1)} = \frac{\sigma^2}{6}(2\varsigma+1), \tag{4.79a}$$

$$\bar{a}_4^{(2)} = \frac{\sigma^2}{24}\left(6\varsigma(\varsigma+1)+1\right), \quad \bar{a}_6^{(2)} = \frac{1}{2}(\bar{a}_3^{(1)})^2, \tag{4.79b}$$

which determine the renormalised series expansion to order Ω^{-1}. Using Eq. (4.43), (4.61) and (4.67) we can give the next order terms to order $\Omega^{-3/2}$ analytically

$$\bar{a}_3^{(3)} = \frac{\bar{a}_3^{(1)}}{K}, \quad \bar{a}_5^{(3)} = \frac{\bar{a}_3^{(1)}}{20}(12\varsigma(\varsigma+1)+1),$$
$$\bar{a}_7^{(3)} = \bar{a}_3^{(1)}\bar{a}_4^{(2)}, \quad \bar{a}_9^{(3)} = \frac{1}{6}(\bar{a}_3^{(1)})^3. \tag{4.79c}$$

In Fig. 4.2C and 4.2D we compare the renormalised approximation given by Eq. (4.65) with the respective bare approximations in Fig. 4.2A and 4.2B. We observe that the renormalisation technique avoids oscillations and even the simple analytical approximation given by Eqs. (4.79) is in reasonable agreement with the exact result. We note that the asymptotic approximations shown in C and D are almost indistinguishable when higher truncation orders are taken into account.

4.4 Application: Time-dependent solution of the CME

The models studied so far have been useful to develop the method. It remains however to be demonstrated that it remains accurate in cases where analytical solution is not feasible, as for instance, for out-of-steady-state and non-detailed balance systems. We here consider the synthesis of a protein P which is degraded by an enzyme

$$\varnothing \xrightarrow{h_0} M \xrightarrow{h_1} \varnothing, \quad M \xrightarrow{h_2} M + P, \tag{4.80a}$$

$$P + E \underset{h_4}{\overset{h_3}{\rightleftharpoons}} C \xrightarrow{h_5} E, \tag{4.80b}$$

where M denotes the transcript, E the enzyme and C complex species as has been studied in Section 3.3. Since our theory applies only to a single species, we consider the limiting case in which the protein dynamics represents the slowest timescale of the system. It has be shown [121] that when species M is degraded much faster than the protein P, the protein synthesis (4.80a) reduces to the transition $S_1 = +z$, $w_1 = \Omega k_0$ in which z is a random variable following the geometric distribution $\varphi(z) = \frac{1}{1+b}\left(\frac{b}{1+b}\right)^z$ with average b, which is called the burst approximation. Similarly to the metabolic reaction studied in Section 4.2, the enzymatic degradation process (4.80b) can be reduced to $S_2 = -1$, $w_2 = \Omega k_1 \frac{n}{\Omega K + n}$ with a nonlinear dependence on the protein number n. The CME describing the protein number distribution is then given by

$$\frac{\mathrm{d}}{\mathrm{d}t}P(n) = \Omega \sum_{z=0}^{\infty} (E^{-z} - 1) k_0 \varphi(z) P(n) + \Omega (E^{+1} - 1) k_1 \frac{n}{\Omega K + n} P(n). \tag{4.81}$$

The relation between the parameters in the reduced and the developed models are given by $k_0 = h_0 h_2 / h_1$, $b = h_2/h_1$, $k_1 = h_5[E_T]$, $K = h_5/h_3$, where $[E_T]$ denotes the total enzyme concentration. This description involves infinitely many reactions: one for the degradation of the protein, and one for each value of z. Therefore, the reactions cannot obey detailed balance in steady state. The system size coefficients now follow from definition (4.6), and are given by $\mathcal{D}^m_{n,s} = 0$ for $s > 0$ and

$$\mathcal{D}^m_n = \delta_{m,0} k_0 \langle z^n \rangle_\varphi + (-1)^n k_1 \frac{\partial^m}{\partial [X]^m} \frac{[X]}{K + [X]}, \tag{4.82}$$

where $\langle z^n \rangle_\varphi = \sum_{z=0}^{\infty} z^n \varphi(z) = \frac{1}{1+b} \mathrm{Li}_{-n}(\frac{b}{1+b})$ denotes the average over the geometric distribution in terms of the polylogarithm function, $\mathrm{Li}_{-n}(x) = \sum_{k=1}^{\infty} k^n x^k$. The deterministic equation is given by

$$\frac{\mathrm{d}[X]}{\mathrm{d}t} = k_0 b - \frac{k_1 [X]}{K + [X]}, \tag{4.83}$$

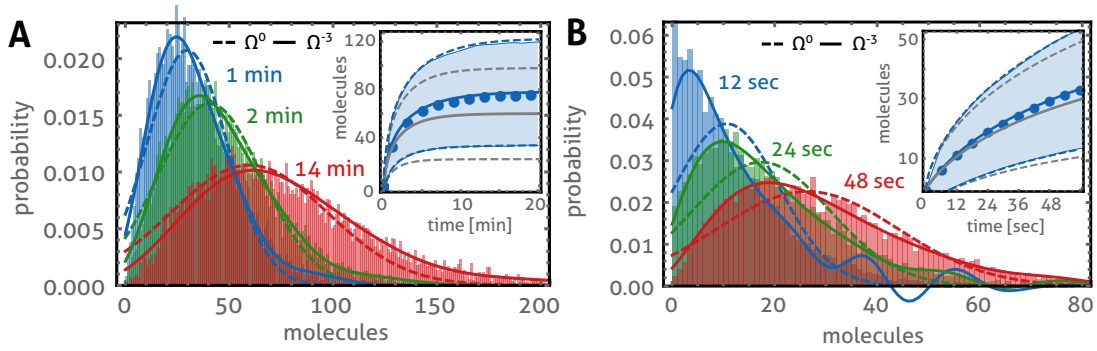

Figure 4.3:

Predicting transient distributions of gene expression. The dynamics of protein synthesis with enzymatic degradation, scheme (4.80), is studied using the burst approximation (4.81). (A) We compare the time-dependence of the renormalised discrete approximations to exact stochastic simulations at times 1, 2, and $14min$. The overall shape (mode, skewness, distribution tails) of the simulated distributions (bars) is in excellent agreement with the series approximation when truncated after Ω^{-3}-terms (solid lines) but not when only Ω^0 are taken into account (dashed lines). This agreement is also observed for the first two moments shown in the inset: while the Ω^{-3}-approximation (blue solid line) agrees with the moment dynamics of the simulated distributions (dots) of the reduced model (4.81), the Ω^0-approximation underestimates the mean (grey solid line) and variance by 25%. The area within one standard deviation of the mean obtained from simulations is shown in blue, the boundaries obtained from the approximations are shown as dashed lines (Ω^0 grey, Ω^{-3} blue). (B) Despite the good agreement shown in (A) we found that at very short times ($12s$ – blue solid line) the series truncated after Ω^{-3}-terms tends to oscillations which quickly disappear for later times ($24s$ – green, $48s$ – red solid line). See main text for discussion. Parameters are $k_0\Omega = 15min^{-1}$, $k_1\Omega = 100min^{-1}$, $K\Omega = 20$, $\Omega = 100$, and $b = 5$. Histograms were obtained from $10,000$ stochastic simulations.

as obtained from the expression for $\mathcal{D}_1^0$. Using the Jacobian $\mathcal{J} = \mathcal{D}_1^1$ and $\mathcal{D}_2$ in Eq. (4.13), we find that the LNA variance obeys

$$\frac{\partial\sigma^2}{\partial t} = -\frac{2k_1K}{([X]+K)^2}\sigma^2 + k_0b(1+2b) + \frac{k_1[X]}{K+[X]}. \tag{4.84}$$

The ODEs given by Eq. (4.83) and (4.84) can be integrated numerically and used in Eq. (4.54) from which the leading order approximation follows. Higher order approximations are now be obtained by using Eq. (4.82) in (4.28), numerically obtaining the time-dependent coefficients $a_m^{(j)}(t)$ and using the result in Eq. (4.67) and (4.65). We assume deterministic initial conditions with zero proteins meaning $a_m^{(j)}(0) = \delta_{m,0}\delta_{j,0}$.

In Fig. 4.3A we show the time-evolution obtained by the leading order approximation P_0 to Eq. (4.65) truncated after the Ω^{-3}-term. The latter distributions are in excellent

agreement with the distributions sampled using the stochastic simulation algorithm [15]. In particular, unlike the leading order approximation, these approximate well mode, skewness, and tails of the distribution. We note that also the mean and variance of these distribution approximation approximations are in excellent agreement as verified in inset of Fig. 4.3A.

Despite the overall good agreement, in Fig. 4.3B we show that there are discrepancies at very short times where, again, the distribution approximations tend to oscillations. Motivated by this numerical observation, we speculate that this behaviour of the expansion is due a temporal boundary layer as commonly observed in singular perturbation expansions [127]. Theoretically, the layer must be located at times of the same order as the expansion parameter, i.e. $t = (\Omega K)^{-1/2} min \approx 13s$, coinciding with the simulation in Fig. 4.3B. This suggests that our approach does only describe the outer solution. Further analysis is required to investigate also the inner solution which is beyond the scope of the present analysis.

5 Diagrammatic expansion of power spectra and correlation functions

This chapter presents an diagrammatic approach for the approximate calculation of correlation functions and their associated power spectra from the CME. A common obstacle for the requisite analysis on the basis of the SSE is the increasing algebraic complexity of the resulting equations, as is often encountered with higher order perturbation theories. A method commonly used for the purpose of a two-point correlation function is for instance to determine the time-dependent solution of the first moment subject to a specific initial condition, $\langle n_i(t)|\boldsymbol{n}(t')\rangle$ for $t \geq t'$ and then performing the average $\langle\langle n_i(t)|\boldsymbol{n}(t')\rangle n_j(t')\rangle$. For unimolecular reaction networks this method has been applied successfully [51]. In practice, however, analytical studies for bimolecular reactions are limited to particularly simple examples [76, 128] or numerical studies [129] because of the difficulty involved in solving these differential equations with increasing numbers of terms and relations.

In physics, in particular in the theory of elementary particles, condensed matter, and statistical fields, a powerful technique that can handle this complexity is the Feynman diagram method and the associated rules from which these diagrams are constructed [130]. Feynman's perturbation theory [131] (and equivalently the Green's functions approach of Schwinger [132]) represents interactions between particles as small perturbations of non-interacting particle systems. The concept which allows us to replace particles with fluctuations and develop a systematic perturbation theory of the CME is given by the generalized fluctuation-dissipation theorem, following Keizer's notion [105]. It states that the response of a deterministic system to a small perturbation is equal to a small fluctuation in a stochastic system. A more precise relation is given in Section 5.2.1. The diagrammatic method for multi-time correlation functions is here adapted through the path-integral approach.

The path-integral is developed in Section 5.1 from an operator representation of the CME. In Section 5.2.1, we present an alternative derivation for the SSE from a path-integral point-of-view, paralleling the expansion performed in Chapter 2. In Section 5.2.2, we show that – to each order – the expansion of these functions can be expressed as a finite sum of diagrams. We then provide a set of *Feynman rules* in Section 5.2.3 from which the SSE can be constructed algorithmically, or simply "drawn" in diagrammatic form. These rules are then used to derive the leading order corrections to the LNA estimate of the power spectra in Section 5.3. We apply this

result to the Brusselator reaction scheme in Section 5.4 and demonstrate that the theory predicts noise-induced oscillations that are not described by the LNA. We conclude by deriving an effective theory for the power spectra of biochemical systems close to a Hopf bifurcation in Section 5.5.

5.1 The generating functional of the Chemical Master Equation

In this section we describe the path-integral approach to the CME. While the construction of path-integrals for master equations is common practice for instance via the Doi-Peliti formalism or similar techniques [38–40, 42], we build on the Martin-Siggia-Rose formalism [41, 133–135] because it allows a straightforward SSE [136]. This allows us to derive the generating functional of correlation functions, an exact statistic that can be expressed as a weighted sum over all possible trajectories and hence contains the statistics of the underlying stochastic process at all times.

5.1.1 Path-integral and generating functional of correlation functions

We make use of the random time-change representation [137] that corresponds to the SSA

$$\boldsymbol{n}(t_f) = \boldsymbol{n}(t_0) + \sum_{r=1}^{R} \boldsymbol{S}_r Y_r \left(\int_{t_0}^{t_f} \mathrm{d}t\, w_r(\boldsymbol{n}(t), \Omega) \right), \tag{5.1}$$

where $\boldsymbol{S}_r$ is the vector formed by the columns of the stoichiometric matrix S and $(Y_1, ..., Y_R)$ are independent unit rate Poisson processes. We continue by slicing the time evolution from t_0 to t_f into L pieces of length $\delta t = (t_f - t_0)/L$ and let $Y_{r,k-1} = Y_r(\delta t\, w_r(\boldsymbol{n}_{k-1}, \Omega))$. The Ito-discretisation of Eq. (5.1) is then given by $\boldsymbol{n}_k = \boldsymbol{n}_{k-1} + \sum_{r=1}^{R} \boldsymbol{S}_r Y_{r,k-1}$. The expectation value of a functional $\mathcal{O}[\boldsymbol{Q}]$ of the concentration process $\boldsymbol{Q}(t) = \frac{\boldsymbol{n}(t)}{\Omega}$, whose discretisation is $\mathcal{O}(\boldsymbol{Q}_0, ..., \boldsymbol{Q}_L)$, can then be calculated using the path-integral

$$\begin{aligned}
\langle \mathcal{O}[\boldsymbol{Q}] \rangle = \lim_{L\to\infty} & \left(\prod_{k=0}^{L} \Omega^{N_S} \int \mathrm{d}\boldsymbol{Q}_k \right) \mathcal{O}(\boldsymbol{Q}_0, ..., \boldsymbol{Q}_L) \\
& \times \delta\left(\Omega \boldsymbol{Q}_0 - \Omega[\boldsymbol{X}](t_0)\right) \left\langle \prod_{k=1}^{L} \delta \left(\Omega \boldsymbol{Q}_k - \Omega \boldsymbol{Q}_{k-1} - \sum_{r=1}^{R} \boldsymbol{S}_r Y_{r,k-1} \right) \right\rangle \\
= \lim_{L\to\infty} & \left(\prod_{k=0}^{L} \Omega^{N_S} \int \mathrm{d}\boldsymbol{Q}_k \right) \left(\prod_{k=1}^{L} \int \frac{\mathrm{d}\boldsymbol{P}_k}{2\pi i} \right) \mathcal{O}(\boldsymbol{Q}_0, ..., \boldsymbol{Q}_L)\, \delta\left(\Omega \boldsymbol{Q}_0 - \Omega[\boldsymbol{X}](t_0)\right) \\
& \times \exp\left[\delta t \sum_{k=1}^{L} \left(-\Omega \boldsymbol{P}_k \frac{(\boldsymbol{Q}_k - \boldsymbol{Q}_{k-1})}{\delta t} + \mathcal{H}(\boldsymbol{P}_k, \Omega \boldsymbol{Q}_{k-1}) \right) \right],
\end{aligned} \tag{5.2}$$

where deterministic initial conditions have been assumed. Note that the function

$$\mathcal{H}(\boldsymbol{P},\Omega\boldsymbol{Q}) = \sum_{r=1}^{R}\left[\mathrm{e}^{(\boldsymbol{P}\,\mathrm{S})_r}-1\right] w_r\left(\Omega\boldsymbol{Q},\Omega\right), \tag{5.3}$$

corresponds to the transition matrix of the CME (2.6) with the step operator E_i^{-1} being replaced by e^{P_i} and $\boldsymbol{n}$ being replaced by $\Omega\boldsymbol{Q}$. Note that throughout we implicitly assume $\boldsymbol{Q}$ to be a column vector and $\boldsymbol{P}_k$ to be a row vector with imaginary unit. Eq. (5.2) can be obtained using the procedure described in Refs. [41] and [134], and follows from taking the average over the Poisson variables $Y_{r,k-1}$ to order δt:

$$\begin{aligned}
&\left\langle \delta\left(\Omega\boldsymbol{Q}_k - \Omega\boldsymbol{Q}_{k-1} - \sum\nolimits_{r=1}^{R}\boldsymbol{S}_r Y_{r,k-1}\right)\right\rangle \\
&\quad= \int \frac{\mathrm{d}\boldsymbol{P}_k}{2\pi i}\, e^{-\Omega\boldsymbol{P}_k(\boldsymbol{Q}_k-\boldsymbol{Q}_{k-1})}\prod_{r=1}^{R}\left\langle e^{\boldsymbol{P}_k\boldsymbol{S}_r Y_{r,k-1}}\right\rangle \\
&\quad= \int \frac{\mathrm{d}\boldsymbol{P}_k}{2\pi i}\, e^{-\Omega\boldsymbol{P}_k(\boldsymbol{Q}_k-\boldsymbol{Q}_{k-1})}\prod_{r=1}^{R}\left[1+(e^{\boldsymbol{P}_k\boldsymbol{S}_r}-1)w_r(\Omega\boldsymbol{Q}_{k-1},\Omega)\delta t\right] + O(\delta t^2) \\
&\quad= \int \frac{\mathrm{d}\boldsymbol{P}_k}{2\pi i}\, e^{-\Omega\boldsymbol{P}_k(\boldsymbol{Q}_k-\boldsymbol{Q}_{k-1})+\mathcal{H}(\boldsymbol{P}_k,\Omega\boldsymbol{Q}_{k-1})\delta t} + O(\delta t^2),
\end{aligned} \tag{5.4}$$

where in the second line we have inserted the Fourier transform of the delta function and we have made use of the fact that the $Y_{r,k-1}$ are independent. In the third line, we have used the property of the Poisson variables $\Pr(Y_{r,k-1}=0) = 1-\delta t\, w_r(\Omega\boldsymbol{Q}_{k-1},\Omega)+O(\delta t^2)$, $\Pr(Y_{r,k-1}=1) = \delta t\, w_r(\Omega\boldsymbol{Q}_{k-1},\Omega)+O(\delta t^2)$ and $\Pr(Y_{r,k-1}=j) = O(\delta t^j)$ for $j>1$, while in the last line the term in the square brackets was expressed as an exponential which is correct to order δt.

The integration in Eq. (5.2) cannot be done analytically since $\mathcal{H}$ is not quadratic in the $\boldsymbol{P}_k$ variables. It is therefore convenient to augment concentration process by $(\boldsymbol{P}_1,...,\boldsymbol{P}_L)$ for which an expression analogous to Eq. (5.2) can be written. In order not to complicate the issue, we here restrict our discussion to the generating functional of correlation functions defined as

$$Z[\boldsymbol{j},\boldsymbol{j}^\star] = \left\langle \exp\int_{t_0}^{t_f}\mathrm{d}t\left(\boldsymbol{P}(t)\boldsymbol{j}^*(t)+\boldsymbol{j}^T(t)\boldsymbol{Q}(t)\right)\right\rangle, \tag{5.5}$$

and simply note that such an expression can be obtained by replacing $\mathcal{H}\to\mathcal{H}+\boldsymbol{P}\boldsymbol{j}^\star+\boldsymbol{j}^T\boldsymbol{Q}$ and setting $\mathcal{O}(\boldsymbol{Q}_0,...,\boldsymbol{Q}_L)=1$ on the right hand side of Eq. (5.2). The result is:

Result 5.1. *The exact generating functional for the concentrations of the CME is given by*

$$Z[\boldsymbol{j},\boldsymbol{j}^\star] = \lim_{L\to\infty}\left(\prod_{k=0}^{L}\Omega^{N_S}\int\mathrm{d}\boldsymbol{Q}_k\right)\left(\prod_{k=1}^{L}\int\frac{\mathrm{d}\boldsymbol{P}_k}{2\pi i}\right)\delta\left(\Omega\boldsymbol{Q}_0-\Omega[\boldsymbol{X}](t_0)\right)\times$$

$$\exp \delta t \sum_{k=1}^{L} \left(-\Omega \boldsymbol{P}_k \frac{(\boldsymbol{Q}_k - \boldsymbol{Q}_{k-1})}{\delta t} + \mathcal{H}(\boldsymbol{P}_k, \Omega \boldsymbol{Q}_{k-1}) + \boldsymbol{P}_k \boldsymbol{j}^\star + \boldsymbol{j}^T \boldsymbol{Q}_{k-1} \right)$$

$$\equiv \int \mathcal{D}\boldsymbol{P}\mathcal{D}\boldsymbol{Q}\ \delta(\boldsymbol{Q}(t_0) - [\boldsymbol{X}](t_0)) \times$$

$$\exp \int_{t_0}^{t_f} \mathrm{d}t \left(-\Omega \boldsymbol{P}\dot{\boldsymbol{Q}} + \mathcal{H}(\boldsymbol{P}, \Omega \boldsymbol{Q}) + \boldsymbol{P}\boldsymbol{j}^\star + \boldsymbol{j}^T \boldsymbol{Q} \right), \tag{5.6}$$

where the measure $\mathcal{D}\boldsymbol{P}\mathcal{D}\boldsymbol{Q}$ denotes the integral obtained by the limiting procedure above.

This result has also been given by Calisto and Tirapegui [136]. Note that in the above formulation $\boldsymbol{j}$ and $\boldsymbol{j}^\star$ are two independent functions of time. The generating functional contains the full information of the underlying stochastic process at all times and can hence be used to formally define arbitrary time-correlation functions.

5.1.2 Correlation functions and power spectra

We now introduce the exact connected generating functional W as

$$W[\boldsymbol{j}, \boldsymbol{j}^\star] = \ln Z[\boldsymbol{j}, \boldsymbol{j}^\star]. \tag{5.7}$$

Note that the above definition is convenient, since the first and second cumulants of $\hat{\boldsymbol{Q}}$ are given by the mean concentrations and the centred second moments, respectively. We will henceforth restrict our discussion to cumulant correlation functions. The *m-point correlation* functions can be defined in both the time and the frequency domain, as follows:

$$\begin{aligned} \mathrm{G}_m(t_1, t_2, \ldots, t_m) &= \left[\prod_{k=1}^{m} \delta_{\boldsymbol{j}(t_k)} W[\boldsymbol{j}, \boldsymbol{j}^\star] \right]_{[\boldsymbol{j}, \boldsymbol{j}^\star]=(0,0)} \\ &= \int_{-\infty}^{\infty} \left(\prod_{k=1}^{m} \frac{\mathrm{d}\omega_k}{2\pi} \mathrm{e}^{i\omega_k t_k} \right) \left[\prod_{k=1}^{m} \delta_{\boldsymbol{j}(\omega_k)} W[\boldsymbol{j}, \boldsymbol{j}^\star] \right]_{[\boldsymbol{j}, \boldsymbol{j}^\star]=(0,0)}, \end{aligned} \tag{5.8}$$

where $\delta_{\boldsymbol{j}(t)} \equiv \delta / \delta \boldsymbol{j}(t)$ is the functional derivative which, augmented by $\delta_{\boldsymbol{j}(t')} \boldsymbol{j}(t) = \delta(t - t')\mathbb{I}$, follows the usual rules of differentiation. With the diagrammatic method in mind we can represent such m-point functions graphically. For example, the exact one-point function corresponding to the mean concentration may be represented symbolically by a diagram with one external line

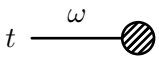

(5.9)

where the blob, which remains to be specified, arises from differentiation of the cumulant generating functional W. Similarly, the exact two-point function can be represented by

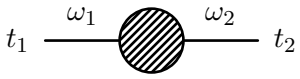

(5.10)

Under stationarity, the two-point correlation function only depends on the distance between the two time points. Hence,

$$\begin{aligned} \mathrm{G}_2(t_1 - t_2) &= \left[\delta_{\boldsymbol{j}(t_1)}\delta_{\boldsymbol{j}(t_2)}W[\boldsymbol{j},\boldsymbol{j}^\star]\right]_{[\boldsymbol{j},\boldsymbol{j}^\star]=(0,0)} \\ &= \int_{-\infty}^{\infty}\frac{\mathrm{d}\omega}{2\pi}\mathrm{e}^{i\omega(t_1-t_2)}\delta_{\boldsymbol{j}(\omega)}\delta_{\boldsymbol{j}(-\omega)}W[\boldsymbol{j},\boldsymbol{j}^\star], \end{aligned} \tag{5.11}$$

which implies that the frequency over the whole diagram in Eq. (5.10) is conserved in the sense that $\omega = \omega_1 = -\omega_2$. Analogous definitions as given after Eq. (5.8) apply for the functional derivative in the frequency domain representation. The *intrinsic noise power spectral matrix* is then defined by the Fourier transform of G_2,

$$\mathcal{S}(\omega) = \left[\delta_{\boldsymbol{j}(\omega)}\delta_{\boldsymbol{j}(-\omega)}W[\boldsymbol{j},\boldsymbol{j}^\star]\right]_{[\boldsymbol{j},\boldsymbol{j}^\star]=(0,0)}. \tag{5.12}$$

Its diagonal elements are typically referred to as the power spectrum. General stationary m-point functions can be defined analogously in the Fourier domain, via

$$\mathrm{G}_m(\omega_1,\omega_2,\ldots,\omega_{m-1}) = \int_{-\infty}^{\infty}\frac{\mathrm{d}\omega_m}{2\pi}\,\delta\left(\sum_{k=1}^{m}\omega_k\right)\left[\prod_{k=1}^{m}\delta_{\boldsymbol{j}(\omega_k)}W[\boldsymbol{j},\boldsymbol{j}^\star]\right]_{[\boldsymbol{j},\boldsymbol{j}^\star]=(0,0)}. \tag{5.13}$$

Hence, the one-point function in Eq. (5.9) contributes only at zero frequency, as expected. It is important to note that the derivatives of the cumulant generating functional W involve only diagrams which are fully connected [138]. Specifically, in the case of $m = 3$, the stationary three-point function is represented by

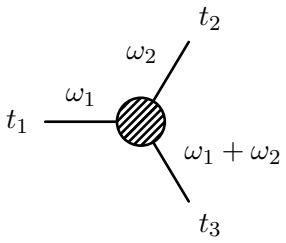

(5.14)

which concludes the formal diagrammatic representation of these m-point correlations.

We remark that even though the generating functional in Eq. (5.6) is an exact representation of the CME, it does not provide analytical insight into these correlation

functions. The reason is that the integration in (5.6) cannot be carried out analytically in general because Eq. (5.3) does not represent a quadratic form, which typically prevents one from obtaining exact expressions for the intrinsic noise power spectrum. Simple approximations for these functions on the basis of the SSE are developed in the following.

5.2 System size expansion using Feynman rules

5.2.1 The expansion of the generating functional

In the limit as $\Omega \to \infty$, the variational principle tells us that the integral in Eq. (5.6) is dominated by the minimum of the exponential therein, which is determined from the variational equations

$$\begin{aligned}\dot{Q}_i &= \lim_{\Omega\to\infty} \frac{1}{\Omega}\frac{\partial \mathcal{H}}{\partial P_i} = \sum_{r=1}^{R} \mathrm{e}^{(\boldsymbol{P}\,\mathrm{S})_r} S_{ir} f_r^{(0)}(\boldsymbol{Q}),\\ \dot{P}_i &= -\lim_{\Omega\to\infty} \frac{1}{\Omega}\frac{\partial \mathcal{H}}{\partial Q_i} = \sum_{r=1}^{R} (1 - \mathrm{e}^{(\boldsymbol{P}\,\mathrm{S})_r}) \frac{\partial}{\partial Q_i} f_r^{(0)}(\boldsymbol{Q}).\end{aligned} \tag{5.15}$$

Here, $f_r^{(0)}(\boldsymbol{Q}) = \lim_{\Omega\to\infty} \frac{w_r(\boldsymbol{Q},\Omega)}{\Omega}$ denote the deterministic rate functions that are obtained as the leading order term in the expansion of the propensity, Eq. (2.13). The above equations constitute the exact description of well-mixed reaction networks in the limit of infinite system size. A particular solution of these is given by the REs

$$\frac{\mathrm{d}[\boldsymbol{X}]}{\mathrm{d}t} = \mathrm{S}\, \boldsymbol{f}^{(0)}([\boldsymbol{X}]), \tag{5.16}$$

which is found by letting $\boldsymbol{P} = 0$ and $\boldsymbol{Q} = [\boldsymbol{X}]$. The REs are exactly as given in Chapter 2 but, here, their solution represents the saddle point of the generating functional. We now proceed by expanding the exponent in Eq. (5.6) around this point. Again we assume that the REs given by Eq. (5.16) have a single positive fixed point that is asymptotically stable.

The SSE is obtained from the scaling assumption that the fluctuations about the deterministic state $[\boldsymbol{X}]$ decay as the inverse square root of the system size

$$\boldsymbol{Q} = [\boldsymbol{X}] + \Omega^{-1/2}\boldsymbol{q}, \quad \boldsymbol{P} = \Omega^{-1/2}\boldsymbol{p}, \tag{5.17}$$

which is akin to van Kampen's ansatz (2.8). Note that applying the latter to Eq. (5.6) provides a local approximation for the generating functional which is valid only in the vicinity of a stable fixed point of Eq. (5.16). Here, we restrict our analysis to that case. We also rescale $\boldsymbol{j} = \sqrt{\Omega}\boldsymbol{J}$ and $\boldsymbol{j}^\star = \sqrt{\Omega}\boldsymbol{J}^\star$ correspondingly. The generating functional

for $\boldsymbol{q}$ and $\boldsymbol{p}$ is now given by

$$Z[\boldsymbol{J},\boldsymbol{J}^\star] = \int \mathcal{D}\boldsymbol{q}\mathcal{D}\boldsymbol{p}\exp\Big[\int_{t_0}^{t_f} \mathrm{d}t\big(-\boldsymbol{p}\dot{\boldsymbol{q}} + \mathcal{H}(\Omega^{-1/2}\boldsymbol{p},\Omega[\boldsymbol{X}]+\Omega^{1/2}\boldsymbol{q}) - \sqrt{\Omega}\boldsymbol{p}[\dot{\boldsymbol{X}}] + \boldsymbol{J}^T\boldsymbol{q} + \boldsymbol{p}\boldsymbol{J}^\star\big)\Big]\delta(\boldsymbol{q}(t_0)), \tag{5.18}$$

and is related to $Z[\boldsymbol{j},\boldsymbol{j}^\star]$ through

$$Z[\boldsymbol{j},\boldsymbol{j}^\star] = \left(\exp\int_{t_0}^{t_f}\mathrm{d}t[\boldsymbol{X}]^T\boldsymbol{j}\right)Z[\boldsymbol{J},\boldsymbol{J}^\star]. \tag{5.19}$$

It remains to expand $\mathcal{H}$ in powers of the system size Ω. Expanding $\mathcal{H}$ in terms of $\Omega^{-1/2}$, one obtains

$$\begin{aligned}\mathcal{H}(\Omega^{-1/2}\boldsymbol{p},\Omega[\boldsymbol{X}]+\Omega^{1/2}\boldsymbol{q}) =& \Omega^{1/2}\sum_{\alpha=1}^{N_S} p_\alpha[\dot{X}]_\alpha + \mathcal{L}_0 \\ &+ \sum_{k=1}^{N}\Omega^{-k/2}\mathcal{L}_k + O(\Omega^{-(N+1)/2}),\end{aligned} \tag{5.20}$$

which follows along the same lines as in Section 2.4. In the first term $[\dot{X}]_\alpha$ simply equals $\mathrm{S}\,\boldsymbol{f}^{(0)}$. The next term of order Ω^0 is given by the quadratic form

$$\mathcal{L}_0 = \mathcal{D}^\beta_\alpha p_\alpha q_\beta + \frac{1}{2!}\mathcal{D}_{\alpha\beta}p_\alpha p_\beta, \tag{5.21}$$

and the higher order terms are given by

$$\mathcal{L}_k = \sum_{s=0}^{\lceil k/2\rceil}\sum_{u=1}^{2+k-2s}\frac{\mathcal{D}^{\beta_1\ldots\beta_{2+k-u-2s}}_{\alpha_1\ldots\alpha_u,s}}{u!(2+k-u-2s)!}p_{\alpha_1}\ldots p_{\alpha_u}q_{\beta_1}\ldots q_{\beta_{2+k-u-2s}}. \tag{5.22}$$

Note the particular summation convention used, in which the multi-indices $i_1\ldots i_\alpha$ and $j_1\ldots j_\beta$ appearing in the coefficient $\mathcal{D}^{j_1\ldots j_\beta}_{i_1\ldots i_\alpha,s}$ in the above equation are to be summed from 1 to N_S; as it was introduced after Eq. (2.19) in Chapter 2. Note that the above equations are exactly the same as Eqs. (2.22) and (2.23a) but with $(-\partial_\alpha)$ replaced by p_α and ϵ_β replaced by q_β. Equivalently, also the system size coefficients are defined as before

$$\mathcal{D}^{j_1\ldots j_\beta}_{i_1\ldots i_\alpha,s} = \sum_{r=1}^{R} S_{i_1r}S_{i_2r}\ldots S_{i_\alpha r}\frac{\partial}{\partial[X]_{j_1}}\frac{\partial}{\partial[X]_{j_2}}\cdots\frac{\partial}{\partial[X]_{j_\beta}}f_r^{(s)}([\boldsymbol{X}]), \tag{5.23}$$

compare Eq. (2.20) in Section 2.4.

Note that by Eqs. (5.21) and (5.22), the expansion of $\mathcal{H}$ in Eq. (5.20) vanishes for $\boldsymbol{p}=0$ to each order in the system size, thus ensuring conservation of probability. By the expansion (5.20) it follows that in the limit as $\Omega\to\infty$, we can approximate the

generating functional $Z[\boldsymbol{J},\boldsymbol{J}^\star]$ defined in Eq. (5.18) by the Gaussian integral

$$\begin{aligned} Z_0[\boldsymbol{J},\boldsymbol{J}^\star] &= \lim_{\Omega\to\infty} Z[\boldsymbol{J},\boldsymbol{J}^\star] \\ &= \int \mathcal{D}\boldsymbol{q}\mathcal{D}\boldsymbol{p}\exp\int_{t_0}^{t_f}\mathrm{d}t\left(-\boldsymbol{p}\dot{\boldsymbol{q}}+\boldsymbol{p}\,\mathcal{J}\,\boldsymbol{q}+\frac{1}{2}\boldsymbol{p}\,\mathrm{D}\,\boldsymbol{p}^T+\boldsymbol{J}^T\boldsymbol{q}+\boldsymbol{p}\boldsymbol{J}^\star\right)\delta(\boldsymbol{q}(t_0)), \end{aligned} \tag{5.24}$$

which is the LNA and which has also been obtained by Calisto and Tirapegui [136]. Here, the matrix $[\,\mathcal{J}\,]_{\alpha\beta}=\mathcal{D}^{\beta}_{\alpha}$ is the Jacobian of the REs, Eq. (5.16), while $[\,\mathrm{D}\,]_{\alpha\beta}=\mathcal{D}_{\alpha\beta}$ denotes the diffusion matrix.

Frequency-domain representation of the linear noise approximation

Gaussian integrals can in most cases be evaluated exactly. For simplicity, we will assume stationary conditions such that the integral will omit the explicit dependence on the initial condition. In consequence we can safely take $t_0\to-\infty$ and $t_f\to\infty$ in Eq. (5.24). The corresponding Fourier representations

$$\boldsymbol{q}(t)=\int_{-\infty}^{\infty}\frac{\mathrm{d}\omega}{2\pi}\,\mathrm{e}^{i\omega t}\boldsymbol{q}(\omega),\quad \boldsymbol{p}(t)=\int_{-\infty}^{\infty}\frac{\mathrm{d}\omega}{2\pi}\,\mathrm{e}^{i\omega t}\boldsymbol{p}(\omega), \tag{5.25}$$

can then be used to perform the integration in the frequency domain explicitly. The result is:

Result 5.2. *The LNA of the generating functional for the stationary statistics is given by*

$$Z_0[\boldsymbol{J},\boldsymbol{J}^\star]=\exp\int_{-\infty}^{\infty}\frac{\mathrm{d}\omega}{2\pi}\left(\boldsymbol{J}(\omega)^T\,\mathrm{F}\,(\omega)\boldsymbol{J}^\star(-\omega)+\frac{1}{2}\boldsymbol{J}^T(\omega)\,\Delta\,(\omega)\boldsymbol{J}(-\omega)\right), \tag{5.26}$$

where the coefficient matrices

$$\mathrm{F}\,(\omega)=(i\omega-\,\mathcal{J}\,)^{-1}\mathrm{e}^{-i\omega 0^+}, \tag{5.27a}$$

$$\Delta\,(\omega)=\,\mathrm{F}\,(\omega)\,\mathrm{D}\,\mathrm{F}^{\,\dagger}(\omega), \tag{5.27b}$$

are the linear response and the spectral matrix, respectively.

Derivation. We first transform Eq. (5.24) into the frequency domain. Inserting Eq. (5.25) into Eq. (5.24) and omitting the initial condition, we find

$$Z_0[\boldsymbol{J},\boldsymbol{J}^\star]=\int\mathcal{D}\boldsymbol{q}\mathcal{D}\boldsymbol{p}\,\mathrm{e}^{\mathcal{K}_0(\boldsymbol{p},\boldsymbol{q})}, \tag{5.28}$$

where the exponential $\mathcal{K}_0$ is given by

$$\mathcal{K}_0(\boldsymbol{p},\boldsymbol{q}) = \int_{-\infty}^{\infty} \frac{\mathrm{d}\omega}{2\pi} \Big(-i\omega \boldsymbol{p}(\omega)\boldsymbol{q}(-\omega) + \boldsymbol{p}(\omega)\,\mathcal{J}\,\boldsymbol{q}(-\omega) + \frac{1}{2}\boldsymbol{p}(\omega)\,\mathrm{D}\,\boldsymbol{p}^T(-\omega) + \mathrm{e}^{-i\omega 0^+}\boldsymbol{J}^T(\omega)\boldsymbol{q}(-\omega) + \boldsymbol{p}(\omega)\boldsymbol{J}^\star(-\omega)\Big). \tag{5.29}$$

Note that we have included a factor of $\mathrm{e}^{-i\omega 0^+}$ here, which appears because of the discretisation scheme of the time integral given by Result (5.1). Specifically, considering the term $\sum_k \delta t \boldsymbol{J}_k^T \boldsymbol{q}_{k-1}$ in the exponential of Eq. (5.6), inserting Eq. (5.25), and taking the limit as $\delta t \to 0$ yields $\int \frac{\mathrm{d}\omega}{2\pi}\,\mathrm{e}^{-i\omega 0^+}\boldsymbol{J}^T(\omega)\boldsymbol{q}(-\omega)$. The Gaussian integral in Eq. (5.28) may be performed directly by completing the square in the exponential. Alternatively, by partial integration, we can utilize the two relations

$$\int \mathcal{D}\boldsymbol{q}\mathcal{D}\boldsymbol{p}\,\frac{\delta}{\delta \boldsymbol{q}}\mathrm{e}^{\mathcal{K}_0(\boldsymbol{p},\boldsymbol{q})} = 0, \int \mathcal{D}\boldsymbol{q}\mathcal{D}\boldsymbol{p}\,\frac{\delta}{\delta \boldsymbol{p}}\mathrm{e}^{\mathcal{K}_0(\boldsymbol{p},\boldsymbol{q})} = 0. \tag{5.30}$$

The first relation can be used to derive

$$\frac{\delta Z_0}{\delta \boldsymbol{J}^\star(-\omega)} = \boldsymbol{J}^T(\omega)\,\mathrm{F}\,(\omega) Z_0, \tag{5.31}$$

which, together with the second relation, yields

$$\frac{\delta Z_0}{\delta \boldsymbol{J}(\omega)} = (\,\mathrm{F}\,(\omega)\boldsymbol{J}^\star(-\omega) + \,\Delta\,(\omega)\boldsymbol{J}(-\omega))Z_0, \tag{5.32}$$

where we have made use of the definitions (5.27a) and (5.27b). This pair of equations can be integrated to obtain Eq. (5.26) with $Z_0[0,0] = 1$ due to conservation of probability. □

Linear noise approximation of the power spectra and correlation functions

Using the cumulant generating functional $W_0 = \ln Z_0$, we now verify that the functional in Eq. (5.26) agrees with well-known results obtained from the LNA. The first cumulant is calculated as

$$\langle \hat{\boldsymbol{q}}(\omega)\rangle_0 = \delta_{\boldsymbol{J}(\omega)} W_0|_{[\boldsymbol{J},\boldsymbol{J}^\star]=(0,0)} = 0. \tag{5.33}$$

Hence, it follows from Eq. (5.17) that the average concentrations are well predicted by the REs. The second cumulant is given by the Fourier transform of the correlation function, as discussed earlier, and evaluates to

$$\langle \hat{\boldsymbol{q}}(\omega)\hat{\boldsymbol{q}}^T(-\omega)\rangle_0 = \delta_{\boldsymbol{J}(\omega)}\delta_{\boldsymbol{J}(-\omega)} W_0|_{[\boldsymbol{J},\boldsymbol{J}^\star]=(0,0)} = \,\Delta\,(\omega), \tag{5.34}$$

where $\Delta(\omega)$ is given by Eq. (5.27b). The above is the well-known result for the spectral matrix, which can be found in [31].

We further have $\delta_{\boldsymbol{J}(\omega)}\delta_{\boldsymbol{J}^\star(-\omega)}W_0|_{[\boldsymbol{J},\boldsymbol{J}^\star]=(0,0)} = \mathrm{F}(\omega)$, which is given by the Green's function of the linearised REs, as is seen by inverting the Fourier transform of Eq. (5.27a):

$$\mathrm{F}(\tau) = \int \frac{\mathrm{d}\omega}{2\pi} \mathrm{e}^{i\omega\tau}\,\mathrm{F}(\omega) = H(\tau - 0^+)\mathrm{e}^{\mathcal{J}\tau}, \tag{5.35}$$

where $H(\tau)$ denotes the Heaviside step-function and we have made use of the fact that $(i\omega - \mathcal{J})^{-1} = \int_0^\infty \mathrm{d}s\, \mathrm{e}^{(\mathcal{J}-i\omega)s}$ for asymptotically stable $\mathcal{J}$. Note that the factor of $\mathrm{e}^{-i\omega 0^+}$ in Eq. (5.27a) ensures that the contour of the Fourier integral has to be closed in the lower half of the complex plane on which $\mathrm{F}(\tau = 0)$ vanishes, thus precluding an instantaneous action of the linear response. The latter fact is a consequence of the Ito-discretisation. Similarly, the expression for Δ in the time domain, $\Delta(\tau) = \int \frac{\mathrm{d}\omega}{2\pi}\mathrm{e}^{i\omega\tau}\Delta(\omega)$, can be obtained from

$$\Delta(\tau) = \mathrm{F}(\tau)\,\Sigma + \Sigma\,\mathrm{F}^T(-\tau), \tag{5.36}$$

where $\Delta(0) = \Sigma$ is just the covariance matrix of $\boldsymbol{q}$ [31].

This relation between the size of fluctuations $\Delta(\tau)$ and the linear response function $\mathrm{F}(\tau)$, or equivalently its frequency domain representation, Eq. (5.27b), is commonly obtained in dynamic perturbation theories of equilibrium and non-equilibrium steady states and referred to as the *generalized fluctuation-dissipation theorem* [42, 105].

Setting up the perturbation expansion

Next, we make use of a well-known trick [130] to express the exact generating functional in terms of the Gaussian integral $Z_0[\boldsymbol{J},\boldsymbol{J}^\star]$, Eq. (5.24). For any analytic function $f(\hat{\boldsymbol{p}},\hat{\boldsymbol{q}})$, the Gaussian expectation value can be written as

$$\langle f(\hat{\boldsymbol{p}}(t),\hat{\boldsymbol{q}}(t'))\rangle_0 = \int \mathcal{D}\boldsymbol{q}\mathcal{D}\boldsymbol{p}\, f(\boldsymbol{p}(t),\boldsymbol{q}(t'))\mathrm{e}^{\mathcal{K}_0(\boldsymbol{p},\boldsymbol{q})} = f(\delta_{\boldsymbol{J}(t)},\delta_{\boldsymbol{J}^\star(t')})Z_0[\boldsymbol{J},\boldsymbol{J}^\star], \tag{5.37}$$

where we have used Eq. (5.28). We thus define the function

$$\mathcal{K}_N(\boldsymbol{p},\boldsymbol{q}) = \exp\sum_{k=1}^{N}\Omega^{-N/2}\int_{-\infty}^{\infty}\mathrm{d}t\,\mathcal{L}_k(\boldsymbol{p},\boldsymbol{q}), \tag{5.38}$$

and note that, using Eq. (5.37), the exact generating functional can be expressed as

$$\begin{aligned} Z[\boldsymbol{J},\boldsymbol{J}^\star] =& \mathcal{K}_N(\delta_{\boldsymbol{J}^\star},\delta_{\boldsymbol{J}})Z_0[\boldsymbol{J},\boldsymbol{J}^\star] + O(\Omega^{-(N+1)/2}) \\ =& \exp\left[\sum_{k=1}^{N}\Omega^{-N/2}\int_{-\infty}^{\infty}\mathrm{d}t\,\mathcal{L}_k(\delta_{\boldsymbol{J}^\star(t)},\delta_{\boldsymbol{J}(t)})\right]Z_0[\boldsymbol{J},\boldsymbol{J}^\star] \end{aligned}$$

$$+ O(\Omega^{-(N+1)/2}). \tag{5.39}$$

Analogous expressions are common to dynamical perturbation theories [130, 138]. The first few of the higher order terms in the expansion of $\mathcal{L}$ are as follows

$$\begin{aligned}
\mathcal{L}_1 =& \frac{1}{2!} p_\alpha \mathcal{D}_\alpha^{\beta\gamma} q_\beta q_\gamma + \frac{1}{2!} p_\alpha p_\beta \mathcal{D}_{\alpha\beta}^{\gamma} q_\gamma + \frac{1}{3!} p_\alpha p_\beta p_\gamma \mathcal{D}_{\alpha\beta\gamma} + p_\alpha \mathcal{D}_{\alpha,1}, \\
\mathcal{L}_2 =& \frac{1}{3!} p_\alpha \mathcal{D}_{\alpha\beta}^{\beta\gamma\delta} q_\beta q_\gamma q_\delta + \frac{1}{2!}\frac{1}{2!} p_\alpha p_\beta \mathcal{D}_{\alpha\beta}^{\gamma\delta} q_\gamma q_\delta + \frac{1}{3!} p_\alpha p_\beta p_\gamma \mathcal{D}_{\alpha\beta\gamma}^{\delta} q_\delta \\
&+ \frac{1}{4!} p_\alpha p_\beta p_\gamma p_\delta \mathcal{D}_{\alpha\beta\gamma\delta} + p_\alpha \mathcal{D}_{\alpha,1}^{\beta} q_\beta + \frac{1}{2!} p_\alpha p_\beta \mathcal{D}_{\alpha\beta,1}.
\end{aligned} \tag{5.40}$$

These terms denote the leading order corrections to the LNA. Eq. (5.39) represents an ideal starting point for the purposes of detailed calculation, since the exponential is expanded in powers of the inverse square root of the system size. More generally, using $\mathcal{L}_k$ given by Eq. (5.22) in Eq. (5.39), we find that

Result 5.3. *The stationary generating functional of the CME has the following asymptotic expansion*

$$Z[\boldsymbol{J}, \boldsymbol{J}^\star] = \mathcal{K}_N(\delta_{\boldsymbol{J}^\star}, \delta_{\boldsymbol{J}}) Z_0[\boldsymbol{J}, \boldsymbol{J}^\star] + O(\Omega^{-(N+1)/2}), \tag{5.41}$$

where in the frequency domain

$$\begin{aligned}
&\mathcal{K}_N(\delta_{\boldsymbol{J}^\star}, \delta_{\boldsymbol{J}}) = \\
&\quad \exp\Bigg[\sum_{j=1}^{N} \sum_{s=0}^{\lceil k/2 \rceil} \sum_{u=1}^{2+k-2s} \Omega^{-j/2} \frac{\mathcal{D}_{\alpha_1 \ldots \alpha_u, s}^{\beta_1 \ldots \beta_{2+j-u-2s}}}{u!(2+j-u-2s)!} \int_{-\infty}^{\infty} \left(\prod_{k=1}^{n} \frac{\mathrm{d}\omega_k}{2\pi} \right) \times \\
&\qquad \delta\left(\sum_{k=1}^{n} \omega_k \right) \delta_{J^\star_{\alpha_1}(\omega_1)} \ldots \delta_{J^\star_{\alpha_u}(\omega_u)} \delta_{J_{\beta_1}(\omega_{u+1})} \ldots \delta_{J_{\beta_{2+j-u-2s}}(\omega_{2+j-u-2s})} \Bigg],
\end{aligned} \tag{5.42}$$

and $Z_0[\boldsymbol{J}, \boldsymbol{J}^\star]$ is given by Result 5.2.

This result can in principle be used to evaluate expectation values explicitly to any order in the SSE.

5.2.2 Explicit calculations and diagrams

In order to illustrate the utility of Feynman diagrams for the evaluation of expectation values, we here outline the calculation of the mean concentrations up to order Ω^{-1}. The analysis is carried out in parallel both analytically and using the diagrammatic method. To that end, we expand

$$\begin{aligned}
\langle \hat{q}_i \rangle &= \delta_{J_i(\omega)} Z[\boldsymbol{J}, \boldsymbol{J}^\star]\big|_{[\boldsymbol{J}, \boldsymbol{J}^\star]=(0,0)} \\
&= \Omega^{-1/2} \delta(\omega)\ \delta_{J_i(\omega)} Z_0[\boldsymbol{J}, \boldsymbol{J}^\star]\big|_{[\boldsymbol{J}, \boldsymbol{J}^\star]=(0,0)}
\end{aligned}$$

$$
\begin{aligned}
&+\Omega^{-1/2}\delta(\omega)\int_{-\infty}^{\infty}\left(\prod_{k=1}^{3}\frac{\mathrm{d}\ell_k}{2\pi}\right)\,\delta\left(\sum_{k=1}^{3}\ell_k\right)\times\\
&\qquad\mathcal{D}_{\alpha}^{\beta\gamma}\left(\delta_{J_\alpha^\star(\ell_1)}\delta_{J_\beta(\ell_2)}\delta_{J_\gamma(\ell_3)}\delta_{J_i(\omega)}Z_0[\boldsymbol{J},\boldsymbol{J}^\star]\right)_{[\boldsymbol{J},\boldsymbol{J}^\star]=(0,0)}\\
&+\Omega^{-1/2}\delta(\omega)\int_{-\infty}^{\infty}\left(\prod_{k=1}^{3}\frac{\mathrm{d}\ell_k}{2\pi}\right)\,\delta\left(\sum_{k=1}^{3}\ell_k\right)\times\\
&\qquad\mathcal{D}_{\alpha\beta}^{\gamma}\left(\delta_{J_\alpha^\star(\ell_1)}\delta_{J_\beta^\star(\ell_2)}\delta_{J_\gamma(\ell_3)}\delta_{J_i(\omega)}Z_0[\boldsymbol{J},\boldsymbol{J}^\star]\right)_{[\boldsymbol{J},\boldsymbol{J}^\star]=(0,0)}\\
&+\Omega^{-1/2}\delta(\omega)\int_{-\infty}^{\infty}\left(\frac{\mathrm{d}\ell}{2\pi}\right)\,\delta\left(\ell\right)\times\\
&\qquad\mathcal{D}_{\alpha,1}\left(\delta_{J_\alpha^\star(\ell)}\delta_{J_i(\omega)}Z_0[\boldsymbol{J},\boldsymbol{J}^\star]\right)_{[\boldsymbol{J},\boldsymbol{J}^\star]=(0,0)}\\
&+\Omega^{-1/2}\delta(\omega)\int_{-\infty}^{\infty}\left(\prod_{k=1}^{3}\frac{\mathrm{d}\ell_k}{2\pi}\right)\,\delta\left(\sum_{k=1}^{3}\ell_k\right)\times\\
&\qquad\mathcal{D}_{\alpha\beta\gamma}\left(\delta_{J_\alpha^\star(\ell_1)}\delta_{J_\beta^\star(\ell_2)}\delta_{J_\gamma^\star(\ell_3)}\delta_{J_i(\omega)}Z_0[\boldsymbol{J},\boldsymbol{J}^\star]\right)_{[\boldsymbol{J},\boldsymbol{J}^\star]=(0,0)}\\
&+O(\Omega^{-1}).
\end{aligned}
\tag{5.43}
$$

Since $\delta_{J_i(\omega)}Z_0[\boldsymbol{J},\boldsymbol{J}^\star]\big|_{[\boldsymbol{J},\boldsymbol{J}^\star]=(0,0)}=0$, we are left with four integrals. These integrals can be evaluated analytically from the identities

$$
\begin{aligned}
\left(\delta_{\boldsymbol{J}(\omega)}\delta_{\boldsymbol{J}(\omega')}Z_0[\boldsymbol{J},\boldsymbol{J}^\star]\right)_{[\boldsymbol{J},\boldsymbol{J}^\star]=(0,0)}&=\delta(\omega+\omega')\,\Delta\left(\omega\right),\\
\left(\delta_{\boldsymbol{J}^\star(\omega)}\delta_{\boldsymbol{J}(\omega')}Z_0[\boldsymbol{J},\boldsymbol{J}^\star]\right)_{[\boldsymbol{J},\boldsymbol{J}^\star]=(0,0)}&=\delta(\omega+\omega')\,\mathrm{F}\left(\omega\right),\\
\left(\delta_{\boldsymbol{J}^\star(\omega)}\delta_{\boldsymbol{J}^\star(\omega')}Z_0[\boldsymbol{J},\boldsymbol{J}^\star]\right)_{[\boldsymbol{J},\boldsymbol{J}^\star]=(0,0)}&=0,
\end{aligned}
\tag{5.44}
$$

in combination with Wick's theorem [138, 139], which states that the expectation value of a Gaussian distribution is given by the sum over all possible products of pairs:

$$
\begin{aligned}
&\left(\delta_{\chi_1(\omega_1)}...\delta_{\chi_{2n}(\omega_n)}Z_0\right)_{[\boldsymbol{J},\boldsymbol{J}^\star]=(0,0)}=\\
&\qquad\sum_{\text{pairings}}\left(\delta_{\chi_{i_1}}\delta_{\chi_{i_2}}Z_0\right)_{[\boldsymbol{J},\boldsymbol{J}^\star]=(0,0)}...\left(\delta_{\chi_{i_{m-1}}}\delta_{\chi_{i_m}}Z_0\right)_{[\boldsymbol{J},\boldsymbol{J}^\star]=(0,0)},
\end{aligned}
\tag{5.45}
$$

which is analogue to Eq. (3.7) given in Section 3.1 but slightly more general since, here, $\chi_i(\omega_i)$ may denote either $J_i(\omega_i)$ or $J_i^\star(\omega_i)$.

There is, however, a simpler way which is based on a representation of these integrals in diagrammatic form. We begin by assigning the line ~~~~~ to $\Delta\left(\omega\right)$ and the line ⟶ to $\mathrm{F}\left(\omega\right)$, while denoting the matrices $\mathcal{D}_{\alpha}^{\beta\gamma}$, $\mathcal{D}_{\alpha\beta}^{\gamma}$, $\mathcal{D}_{\alpha\beta\gamma}$ by $\bullet$. The second term in Eq. (5.43) thus becomes

$$
\delta(\omega)\int_{-\infty}^{\infty}\left(\prod_{k=1}^{3}\frac{\mathrm{d}\ell_k}{2\pi}\right)\,\delta\left(\sum_{k=1}^{3}\ell_k\right)\mathcal{D}_{\alpha}^{\beta\gamma}\left(\delta_{J_\alpha^\star(\ell_1)}\delta_{J_\beta(\ell_2)}\delta_{J_\gamma(\ell_3)}\delta_{J_i(\omega)}Z_0[\boldsymbol{J},\boldsymbol{J}^\star]\right)
$$

$$
\begin{aligned}
=&\delta(\omega)[\,\mathrm{F}\,(\omega)]_{i\alpha}\left(\frac{1}{2!}\mathcal{D}_{\alpha}^{\beta\gamma}\int\frac{\mathrm{d}\ell}{2\pi}[\,\Delta\,(\ell)]_{\beta\gamma}\right)\\
&+\delta(\omega)[\,\Delta\,(\omega)]_{i\alpha}\left(\frac{2}{2!}\mathcal{D}_{\alpha}^{\beta\gamma}\int\frac{\mathrm{d}\ell}{2\pi}[\,\mathrm{F}\,(\ell)]_{\beta\gamma}\right)\\
=&\frac{1}{2!}\,i\;\underset{\omega}{\longrightarrow}\boxed{\mathcal{D}_{\alpha}^{\beta\gamma}}\;\ell\;+\;\underbrace{\frac{2}{2!}\,i\;\underset{\omega}{\sim\!\!\sim}\boxed{\mathcal{D}_{\alpha}^{\beta\gamma}}\;\ell}_{=0}
\end{aligned}
\tag{5.46}
$$

where we adopt the convention that ℓ, being internal, has to be integrated out. Note that the second term appears twice due to the symmetry $\mathcal{D}_{\alpha}^{\beta\gamma}=\mathcal{D}_{\alpha}^{\gamma\beta}$, but that the latter vanishes because $\int\frac{\mathrm{d}\ell}{2\pi}\,\mathrm{F}\,(\ell)=0$, by Eq. (5.35). The absence of closed loops in the linear response is a consequence of the Ito-discretisation, as we have noted after Eq. (5.35).

Similarly, we have

$$
\begin{aligned}
&\delta(\omega)\int_{-\infty}^{\infty}\left(\prod_{k=1}^{3}\frac{\mathrm{d}\ell_k}{2\pi}\right)\,\delta\left(\sum_{k=1}^{3}\ell_k\right)\mathcal{D}_{\alpha\beta}^{\gamma}\left(\delta_{J_{\alpha}^{\star}(\ell_1)}\delta_{J_{\beta}^{\star}(\ell_2)}\delta_{J_{\gamma}(\ell_3)}\delta_{J_i(\omega)}Z_0[\boldsymbol{J},\boldsymbol{J}^{\star}]\right)\\
&=\frac{2}{2!}\,i\;\underset{\omega}{\longrightarrow}\boxed{\mathcal{D}_{\alpha\beta}^{\gamma}}\;\ell\;+\frac{1}{2!}\,i\;\underset{\omega}{\sim\!\!\sim}\boxed{\mathcal{D}_{\alpha\beta}^{\gamma}}\;\ell\\
&=0,
\end{aligned}
\tag{5.47}
$$

and

$$
\begin{aligned}
&\delta(\omega)\int_{-\infty}^{\infty}\left(\frac{\mathrm{d}\ell}{2\pi}\right)\,\delta\,(\ell)\,\mathcal{D}_{\alpha,1}\left(\delta_{J_{\alpha}^{\star}(\ell)}\delta_{J_i(\omega)}Z_0[\boldsymbol{J},\boldsymbol{J}^{\star}]\right)\\
&=-\Omega^{-1/2}\,\mathcal{J}_{\,i\alpha}^{\,-1}\mathcal{D}_{\alpha,1}=i\;\underset{\omega}{\longrightarrow\!\!\circ}\;\mathcal{D}_{\alpha,1}
\end{aligned}
\tag{5.48}
$$

where we have introduced an extra vertex $\circ$ for $\mathcal{D}_{\alpha,1}$ which attaches only one external line. Note that the last term in Eq. (5.43) is zero by Wick's theorem and Eq. (5.44). Combining Eq. (5.43) with Eqs. (5.46-5.48), we find that, up to order $\Omega^{-1/2}$, $\langle\hat{q}_i\rangle$ is the sum of the following two diagrams:

$$
\langle\hat{q}_i(\omega)\rangle=\Omega^{-1/2}\left(\frac{1}{2!}\,i\;\underset{\omega}{\longrightarrow}\boxed{\mathcal{D}_{\alpha}^{\beta\gamma}}\;\ell\;+\;i\;\underset{\omega}{\longrightarrow\!\!\circ}\;\mathcal{D}_{\alpha,1}\right)+O(\Omega^{-1}).
\tag{5.49}
$$

These diagrams are known as tadpoles, and lead to the corrections to the mean concentrations predicted by the REs. Note that the above sum of diagrams differs from a pure loop expansion by the second diagram, the reason being the explicit dependence of

the propensity functions on the system size Ω. In the following, we denote these extra vertices, more specifically those with $s \neq 0$ in Eq. (5.23), by $\circ$. Noting, moreover, that the closed loop above corresponds to $\Sigma = \int \frac{\mathrm{d}\ell}{2\pi} \Delta(\ell)$, we can write

$$\langle \hat{q}_i \rangle = -\Omega^{-1/2} \mathcal{J}^{-1}_{i\alpha} \left(\frac{1}{2!} \mathcal{D}^{\beta\gamma}_{\alpha} \Sigma_{\beta\gamma} + \mathcal{D}_{\alpha,1} \right) \equiv \Omega^{-1/2} [\epsilon_i]_1. \tag{5.50}$$

We may now conclude that the average concentration is given by

$$\left\langle \frac{n_i}{\Omega} \right\rangle = [X]_i - \frac{1}{\Omega} \mathcal{J}^{-1}_{i\alpha} \left(\frac{1}{2!} \mathcal{D}^{\beta\gamma}_{\alpha} \Sigma_{\beta\gamma} + \mathcal{D}_{\alpha,1} \right) + O(\Omega^{-2}), \tag{5.51}$$

to order Ω^{-1}. This is exactly the same result as obtained using the moment equations in Chapter 3, Eqs. (3.15) and (3.20), when steady state conditions are assumed. As we have seen above, the direct computation of these corrections may be quite involved. In the next section, we summarize a set of rules, commonly known as Feynman rules, which greatly simplify the required calculations to a combinatorial task, and which hence eliminate the need to invoke Wick's theorem directly.

5.2.3 The Feynman rules for the correlation functions

The above observations can be summarized by the following set of rules.

Result 5.4 (Feynman rules for the SSE)**.** *The SSE of the m-point cumulant correlation is given by the sum of diagrams constructed following 12 algorithmic rules:*

(i) To calculate the m-point cumulant correlation function, draw m lines (called external lines).

(ii) Select a number of symbols either from $\mathcal{D}^{j_1\cdots j_\beta}_{i_1\ldots i_\alpha,0}$ or $\mathcal{D}^{j_1\cdots j_\beta}_{i_1\ldots i_\alpha,s>0}$. Denote the former by $\bullet$, and the latter by $\circ$. A symbol with $n = (\alpha+\beta)$ indices is represented by an n-vertex (a node in which exactly n lines meet).

(iii) Leave one end of each external line free and attach the other end to a vertex index. Draw lines between the remaining vertex indices such that the diagram is connected.

(iv) For each external line account with a factor of $\Omega^{-1/2}$, for each vertex $\mathcal{D}^{j_1\cdots j_\beta}_{i_1\ldots i_\alpha,0}$ account with a factor of $\Omega^{-(n-2)/2}$, and for each vertex $\mathcal{D}^{j_1\cdots j_\beta}_{i_1\ldots i_\alpha,s>0}$ account with a factor of $\Omega^{-s-(n-2)/2}$. The order in the SSE to which the diagram contributes is the product of these factors.

(v) Repeat steps (i)-(iv) and draw all possible diagrams up to the desired order in the SSE.

(vi) To each line that connects two upper vertex indices, assign a propagator ~~~~~. To each line that connects an upper and a lower vertex index, assign a propagator ⟶. Note that there are no lines connecting two lower vertex indices.

(vii) *Assign* 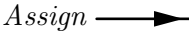 *to external lines attached to an lower vertex index, and otherwise*  .

(viii) *Assign a frequency to each line, and conserve frequency at each vertex. Conserve also total frequency over the entire diagram.*

(ix) *The value of each diagram is given by the product of the factors associated with all lines and vertices. To each line* 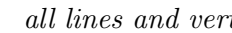 *with frequency* ω*, assign the factor* $\Delta(\omega)$*. To each line* 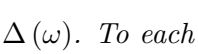 *with frequency* ω*, assign the factor* $\mathrm{F}(\omega)$.

(x) *A diagram with* L *internal loops will have* L *internal frequencies that are not fixed by the requirement for frequency conservation. Integrate over all frequencies, with measure* $\mathrm{d}\ell_i/(2\pi)$.

(xi) *Sum over all internal indices, accounting for the symmetry properties of the given diagram. The corresponding symmetry factor equals the number of ways in which the vertices in a diagram can be connected, divided by the symmetry of the vertex factors. Because every vertex factor* $\mathcal{D}^{j_1\ldots j_\beta}_{i_1\ldots i_\alpha,s}$ *is invariant against permutation of all upper or lower indices, the latter is given by* $\alpha!\beta!$.

(xii) *In conclusion, the* m*-point cumulant correlation function equals the sum over all connected diagrams with* m *external lines.*

Note that by rule (xi) our summation convention given after Eq. (5.22) is implied: multi-indices $i_1\ldots i_\alpha$ and $j_1\ldots j_\beta$ of the vertices $\mathcal{D}^{j_1\ldots j_\beta}_{i_1\ldots i_\alpha,s}$ are to be summed from 1 to N_S in the resulting equations.

5.3 Corrections to the linear noise approximation of the power spectra

We now demonstrate the diagrammatic technique by evaluating the power spectrum to order Ω^{-2}, i.e. including the next term beyond the LNA. The calculation of the requisite corrections is greatly facilitated by the set of Feynman rules presented in the previous section. The power spectrum is obtained as the sum of all diagrams with two external lines that include products of vertices of order Ω^{-2}. It is clear from Eqs. (5.22) and (5.40) that, to this order, we only need to consider diagrams with at most two vertices.

Since the SSE involves non-zero corrections to the mean concentrations, as derived in Section 5.2.2, it is important to ensure that the expressions for the power spectrum of fluctuations are indeed centred around the corrected mean concentrations. Note that the generating functionals for the centred concentration fluctuations $(\hat{\boldsymbol{Q}} - \langle\hat{\boldsymbol{Q}}\rangle)$ and the deviations from the REs $\hat{\boldsymbol{q}}$, Eq. (5.39), are related by the exponential factor $\mathrm{e}^{\Omega^{1/2}\int \mathrm{d}t'\boldsymbol{J}(t')\langle\boldsymbol{q}(t')\rangle}$. It hence follows that all cumulants beyond the first one agree and generate the same series of connected diagrams which is used in the following.

In order to simplify the construction of these diagrams, we divide them into three basic topologies shown in Figs. 5.1(a) and (b) which are denoted as tadpoles, Figs. 5.1(c)

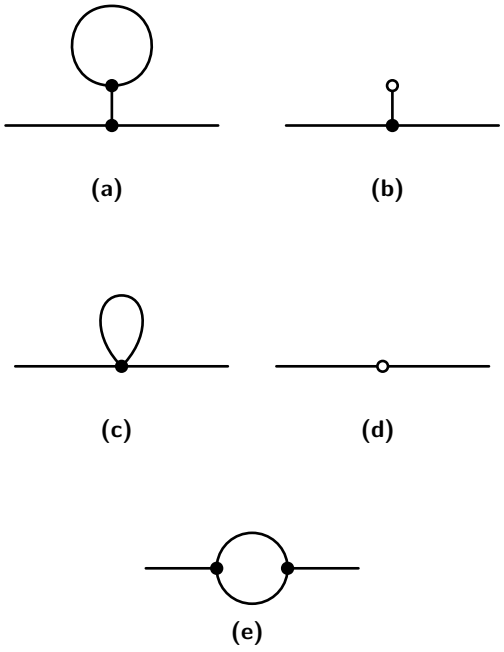

Figure 5.1:
Construction of two-point diagrams. Distinct topologies of two-point diagrams contributing to the intrinsic noise power spectrum to order Ω^{-2}. Since each external line contributes a factor of $\Omega^{-1/2}$ we only need to consider diagrams comprising a single vertex of order Ω^{-1} or combinations of two vertices which each contribute a factor of $\Omega^{-1/2}$. Note that the SSE involves diagrams (b) and (d) that differ from a pure loop expansion.

and (d) which we denote as snails (but which are also referred to as tadpoles in the literature), and Fig. 5.1(e) which are denoted as loop diagrams, respectively. We have already encountered tadpoles in Section 5.2.2. Denoting the contribution from tadpole diagrams by $\mathcal{T}$, the contribution from snail diagrams by $\mathcal{S}$, and the contribution from loop diagrams by $\mathcal{L}$, we can express the spectral matrix $\mathcal{S}$ as

$$\mathcal{S}(\omega) = \frac{1}{\Omega}\Delta(\omega) + \frac{1}{\Omega^2}\mathcal{T}(\omega) + \frac{1}{\Omega^2}\mathcal{S}(\omega) + \frac{1}{\Omega^2}\mathcal{L}(\omega) + O(\Omega^{-3}). \tag{5.52}$$

These terms determine the power spectrum to order Ω^{-2}. We now outline the explicit evaluation of these diagrams.

5.3.1 Tadpole diagrams

In Fig. 5.2, we list all possible tadpole diagrams to order Ω^{-2}. These contain one subdiagram which has already been evaluated in Section 5.2.2. The sum of the diagrams in (a) and (b) is then given by

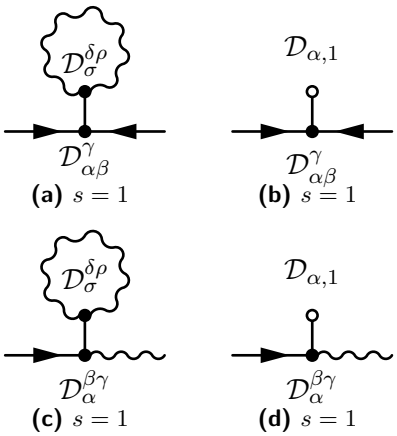

Figure 5.2:
Tadpole diagrams. All tadpole diagrams contributing to order Ω^{-2} to the intrinsic noise power spectrum. Note that none of these have internal symmetries; hence, the symmetry factor is $s = 1$ throughout.

$$\mathcal{T}_1(\omega) = \frac{1}{2!}$$
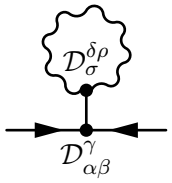

$$+ \frac{1}{2!}$$
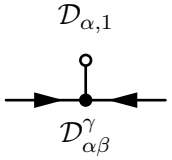

$$+ \text{h.c.}$$
$$= \left(\frac{1}{2!}\right) F_{i\alpha}(\omega)\mathcal{D}^{\gamma}_{\alpha\beta}[\epsilon_\gamma]_1 F^{\dagger}_{\beta j}(\omega) + \text{h.c.} \tag{5.53}$$

Note that by conserving the frequency, the argument of the line on left is ω while the one to the right is $-\omega$. In consequence, the latter line is accounted for by the factor $\mathrm{F}^{\dagger}(\omega)$ which we will from now on indicate by an arrow pointing left. Note also that by including also the Hermitian conjugate (h.c.) of the above diagram, we have accounted for the contribution from an equivalent time-reversed diagram. Note also that $[\epsilon_\gamma]_1$ is defined by Eq. (5.50). Analogously, for the diagrams in Figs. 5.2(c) and (d), we find

$$\mathcal{T}_2(\omega) = \frac{1}{2!}$$
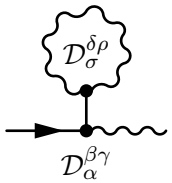

$$+ \frac{1}{2!}$$
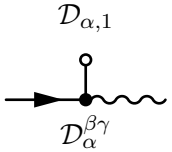

$$+ \text{h.c.}$$
$$= \left(\frac{1}{2!}\right) F_{i\alpha}(\omega)\mathcal{D}^{\beta\gamma}_{\alpha}[\epsilon_\gamma]_1 \Delta_{\beta j}(\omega) + \text{h.c.} \tag{5.54}$$

Finally, we denote the sum over the diagrams shown in Fig. 5.2 by

$$\mathcal{T}(\omega) = \mathcal{T}_1(\omega) + \mathcal{T}_2(\omega). \tag{5.55}$$

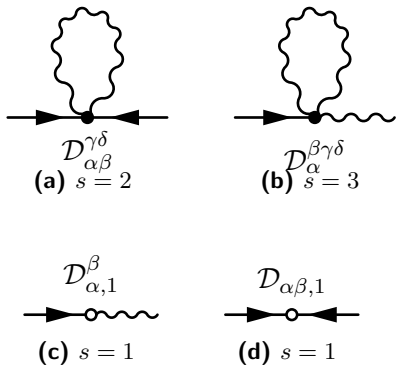

(a) $s = 2$ **(b)** $s = 3$ **(c)** $s = 1$ **(d)** $s = 1$

Figure 5.3:
Snail diagrams: All snail diagrams contributing to order Ω^{-2} to the intrinsic noise power spectrum. The symmetry factors (s) follow by considering the ways in which the right external line can be attached to the corresponding vertex.

5.3.2 Snail diagrams

The next contribution is given by topology in Fig. 5.1(c) which contains only a single 4-vertex where two upper indices are contracted in a loop. We have already found that such a loop equals the covariance matrix Σ. The resulting diagrams are given in Figs. 5.3(a) and (b), implying

$$\mathcal{S}_1(\omega) = \left(\frac{2}{2!2!}\right) F_{i\alpha}(\omega)\mathcal{D}^{\gamma\delta}_{\alpha\beta}\Sigma_{\gamma\delta}F^{\dagger}_{\beta j}(\omega) + \text{h.c.}, \tag{5.56}$$

$$\mathcal{S}_2(\omega) = \left(\frac{3}{3!}\right) F_{i\alpha}(\omega)\mathcal{D}^{\beta\gamma\delta}_{\alpha}\Sigma_{\gamma\delta}\Delta^{\dagger}_{\beta j}(\omega) + \text{h.c.} \tag{5.57}$$

Note that the diagram in Fig. 5.3(b) is non-zero only when one considers reactions with non-elementary propensity functions, e.g. trimolecular reactions or those of Michaelis-Menten type [125].

We progress to the topology shown in Fig. 5.1(d), which is resolved by a matrix multiplication. The two possible diagrams are generated from 2-vertices, as shown in Figs. 5.3 (c) and (d). The result is

$$\mathcal{S}_3(\omega) = F_{i\alpha}(\omega)\mathcal{D}^{\beta}_{\alpha,1}\Delta^{\dagger}_{\beta j}(\omega) + \text{h.c.}, \tag{5.58}$$

$$\mathcal{S}_4(\omega) = \frac{1}{2!}F_{i\alpha}(\omega)\mathcal{D}_{\alpha\beta,1}F^{\dagger}_{\beta j}(\omega) + \text{h.c.} \tag{5.59}$$

We denote the sum over all these diagrams by

$$\mathcal{S}(\omega) = \sum_{n=1}^{4}\mathcal{S}_n(\omega), \tag{5.60}$$

which concludes the evaluation of the diagrams shown in Fig. 5.3.

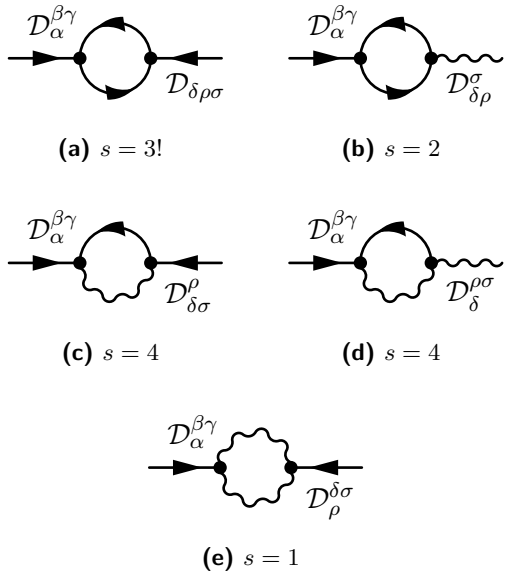

(a) $s = 3!$ **(b)** $s = 2$ **(c)** $s = 4$ **(d)** $s = 4$ **(e)** $s = 1$

Figure 5.4:
Loop diagrams. All diagrams that contribute to order Ω^{-2} to the intrinsic noise power spectrum, and that contain a frequency loop integral. The symmetry factors (s) follow by considering the ways in the right external line can be attached to the corresponding vertex, times the permutations of all internal lines. Note that in (e), we have only accounted for half of these permutations, since the diagram is self-adjoint.

5.3.3 Loop diagrams

The evaluation of all diagrams considered thus far has been possible by matrix multiplication. However, to evaluate the diagrams in the topology in Fig. 5.1(d), namely those which contain a loop formed by connecting two 3-vertices, one has to calculate the integrals occurring therein explicitly. The relevant diagrams are listed in Fig. 5.4, all of which consist of a line F connected to the 3-vertex $\mathcal{D}_\alpha^{\beta\gamma}$, and are hence non-zero only for networks involving bimolecular reactions. We can then write the overall contribution from each diagram in the general form

$$\mathcal{L}_n(\omega) = \frac{1}{2} F_{i\alpha}(\omega) \mathcal{D}_\alpha^{\beta\gamma} \left[\mathbf{V}^{\,j}_{(n)}(\omega) \right]_{\beta\gamma} + \text{h.c.}, \tag{5.61}$$

where we have defined the vertex functions $\mathbf{V}^{\,j}_{(n)}(\omega)$, which are effectively 3-tensors. As we shall see, the latter consist of a 3-vertex with the frequency loop integrated out.

Evaluation of vertex functions

Let us study in detail the vertex function $\mathbf{V}^{\,j}_{(1)}(\omega)$ that is defined by the right hand side of the first diagram shown in Fig. 5.4(e). The latter is simply the diagram with

the vertex $\mathcal{D}_{\alpha}^{\beta\gamma}$ removed, and can be written as

$$\Big[\,\mathbf{V}^{\,j}_{(1)}(\omega)\Big]_{\beta\gamma} \equiv \frac{3\times 2}{3!}\;\mathcal{D}_{\rho\delta\sigma}$$

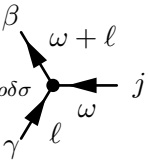

$$= \int_{-\infty}^{\infty} \frac{\mathrm{d}\ell}{2\pi} F_{\beta\rho}(\omega+\ell)\left(\mathcal{D}_{\rho\delta\sigma}F^{\dagger}_{\sigma j}(\omega)\right)F^{\dagger}_{\delta\gamma}(\ell), \tag{5.62}$$

where the symmetry factor has been obtained via the considerations given in the caption of Fig. 5.4. We now evaluate the integral by inserting the Fourier transform of $\mathrm{F}\,(\omega)$, Eq. (5.35), into the above equation to show that its solution can be obtained by solving a linear matrix equation. We start by fixing the external index j and writing down the 3-vertex matrix with the frequency loop integrated out:

$$\begin{aligned}\mathbf{V}^{\,j}_{(1)}(\omega) &= \int_{-\infty}^{\infty}\frac{\mathrm{d}\ell}{2\pi}\,\mathrm{F}\,(\omega+\ell)\,\mathrm{M}^{\,j}_{(1)}(\omega)\,\mathrm{F}^{\,\dagger}(\ell)\\ &= \int_{0}^{\infty}\mathrm{d}\tau \mathrm{e}^{(\,\mathcal{J}\,-i\omega)\tau}\,\mathrm{M}^{\,j}_{(1)}(\omega)\mathrm{e}^{\mathcal{J}^{\,T}\tau},\end{aligned} \tag{5.63}$$

where we have set $[\,\mathrm{M}^{\,j}_{(1)}]_{\rho\delta} = \mathcal{D}_{\rho\delta\sigma}F^{\dagger}_{\sigma j}(\omega)$. Note that the range of integration is positive since $\mathrm{F}\,(\tau)$ contains the Heaviside function. The value of this integral is given by the following result:

Result 5.5. *For $\mathcal{J}$ being asymptotically stable, the Fourier integral*

$$\mathbf{V}\,(\omega) = \int_{0}^{\infty}\mathrm{d}\tau \mathrm{e}^{(\,\mathcal{J}\,-i\omega)\tau}\,\mathrm{M}\,(\omega)\mathrm{e}^{\mathcal{J}^{\,T}\tau}, \tag{5.64}$$

which determines the vertex matrices, satisfies Sylvester's matrix equation

$$\mathfrak{S}(\omega)\,\mathbf{V}\,(\omega) + \,\mathrm{M}\,(\omega) = 0, \tag{5.65}$$

where $\mathfrak{S}$ represents the linear operator

$$\mathfrak{S}(\bullet) \equiv (\,\mathcal{J}\,-i\omega)(\bullet) + (\bullet)\,\mathcal{J}^{\,T}. \tag{5.66}$$

Derivation. Applying the linear operator $\mathfrak{S}(\omega)(\bullet) = (\,\mathcal{J}\,-i\omega)(\bullet)+(\bullet)\,\mathcal{J}^{\,T}$ to the above equation, we find

$$\begin{aligned}\mathfrak{S}(\omega)\,\mathbf{V}\,(\omega) &= \int_{0}^{\infty}\mathrm{d}\tau\left(\frac{\mathrm{d}}{\mathrm{d}\tau}\mathrm{e}^{(\,\mathcal{J}\,-i\omega)\tau}\right)\mathrm{M}\,\mathrm{e}^{\mathcal{J}^{\,T}\tau} + \int_{0}^{\infty}\mathrm{d}\tau\mathrm{e}^{(\,\mathcal{J}\,-i\omega)\tau}\,\mathrm{M}\,\left(\frac{\mathrm{d}}{\mathrm{d}\tau}\mathrm{e}^{\mathcal{J}^{\,T}\tau}\right)\\ &= \int_{0}^{\infty}\mathrm{d}\tau\frac{\mathrm{d}}{\mathrm{d}\tau}\left(\mathrm{e}^{(\,\mathcal{J}\,-i\omega)\tau}\,\mathrm{M}\,\mathrm{e}^{\mathcal{J}^{\,T}\tau}\right).\end{aligned} \tag{5.67}$$

Assuming that $\mathcal{J}$ is asymptotically stable ensures the absence of boundary terms, and we then obtain Eq. (5.65). □

Hence by the use of the above result, we find that $\mathbf{V}^{\,j}_{(1)}$ satisfies Sylvester's matrix equation

$$\mathfrak{S}\,\mathbf{V}^{\,j}_{(1)} + \mathrm{M}^{\,j}_{(1)}(\omega) = 0. \tag{5.68}$$

We will illustrate the evaluation of these terms for two more vertex functions. First we consider the vertex

$$\Big[\,\mathbf{V}^{\,j}_{(3)}(\omega)\Big]_{\beta\gamma} \equiv \frac{2\times 2}{2!}$$

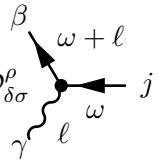

$$= 2\int_{-\infty}^{\infty}\frac{\mathrm{d}\ell}{2\pi}F_{\beta\delta}(\omega+\ell)\left(\mathcal{D}^{\rho}_{\delta\sigma}\,F^{\dagger}_{\sigma j}(\omega)\right)\Delta_{\rho\gamma}(\ell), \tag{5.69}$$

and setting $[\,\mathrm{M}^{\,j}_{(3)}]_{\delta\rho} = 2\,\mathcal{D}^{\rho}_{\delta\sigma}\,F^{\dagger}_{\sigma j}(\omega)$, we find

$$\begin{aligned}\mathbf{V}^{\,j}_{(3)}(\omega) &= \int_{-\infty}^{\infty}\frac{\mathrm{d}\ell}{2\pi}\,\mathrm{F}\,(\omega+\ell)\,\mathrm{M}^{\,j}_{(3)}(\omega)\,\Delta\,(\ell)\\ &= \int_{-\infty}^{\infty}\mathrm{d}\tau e^{-i\omega\tau}\,\mathrm{F}\,(\tau)\,\mathrm{M}^{\,j}_{(3)}(\omega)\,\Delta^{\,T}(\tau)\\ &= \int_{0}^{\infty}\mathrm{d}\tau e^{(\,\mathcal{J}\,-i\omega)\tau}\,\mathrm{M}^{\,j}_{(3)}(\omega)\,\Sigma\,e^{\,\mathcal{J}^{\,T}\tau},\end{aligned} \tag{5.70}$$

and thus,

$$\mathfrak{S}(\omega)\,\mathbf{V}^{\,j}_{(3)}(\omega) + \mathrm{M}^{\,j}_{(3)}(\omega)\,\Sigma\, = 0. \tag{5.71}$$

Next, consider the vertex

$$\Big[\,\mathbf{V}^{\,j}_{(*)}(\omega)\Big]_{\beta\gamma} \equiv \frac{1}{2!}$$

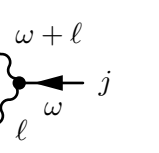

$$= \frac{1}{2}\int_{-\infty}^{\infty}\frac{\mathrm{d}\ell}{2\pi}\Delta_{\beta\rho}(\omega+\ell)\left(\mathcal{D}^{\rho\delta}_{\sigma}F^{\dagger}_{\sigma j}(\omega)\right)\Delta_{\delta\gamma}(\ell). \tag{5.72}$$

This can be written as the sum of two contributions. Letting $[\,\mathrm{M}^{\,j}_{(5)}]_{\delta\rho} = \frac{1}{2}\mathcal{D}^{\rho\delta}_{\sigma}F^{\dagger}_{\sigma j}(\omega)$, we have

$$\begin{aligned}\mathbf{V}^{\,j}_{(*)}(\omega) &= \int_{-\infty}^{\infty}\frac{\mathrm{d}\ell}{2\pi}\,\Delta\,(\omega+\ell)\,\mathrm{M}^{\,j}_{(5)}(\omega)\,\Delta\,(\ell)\\ &= \int_{-\infty}^{\infty}\mathrm{d}\tau e^{-i\omega\tau}\,\Delta\,(\tau)\,\mathrm{M}^{\,j}_{(5)}(\omega)\,\Delta^{\,T}(\tau)\\ &= \int_{0}^{\infty}\mathrm{d}\tau e^{(\,\mathcal{J}\,-i\omega)\tau}\,\Sigma\,\mathrm{M}^{\,j}_{(5)}(\omega)\,\Sigma\,e^{\,\mathcal{J}^{\,T}\tau}\\ &\quad + \Sigma\,\left(\int_{0}^{\infty}\mathrm{d}\tau e^{(\,\mathcal{J}\,-i\omega)^{\dagger}\tau}\,\mathrm{M}^{\,j}_{(5)}(\omega)e^{\,\mathcal{J}\,\tau}\right)\,\Sigma\end{aligned}$$

$$\equiv \mathbf{V}^{\,j}_{(5)}(\omega) + \Sigma\, \mathbf{V}^{\,j}_{(6)}(\omega)\, \Sigma\,, \tag{5.73}$$

and thus, the quantities $\mathbf{V}^{\,j}_{(5)}$ and $\mathbf{V}^{\,j}_{(6)}$ satisfy

$$\begin{aligned} &\mathfrak{S}(\omega)\, \mathbf{V}^{\,j}_{(5)}(\omega) + \Sigma\, \mathrm{M}^{j}_{(5)}(\omega)\, \Sigma = 0, \\ &\mathbf{V}^{\,j}_{(6)}(\omega)\mathfrak{S}^{\dagger}(\omega) + \mathrm{M}^{j}_{(5)}(\omega) = 0, \end{aligned} \tag{5.74}$$

where we have defined the adjoint of $\mathfrak{S}$ through

$$(\bullet)\mathfrak{S}^{\dagger} \equiv (\,\mathcal{J} + i\omega)(\bullet) + (\bullet)\,\mathcal{J}^{\,T}. \tag{5.75}$$

Sum of loop diagrams

The vertex functions corresponding to the diagrams shown in Figs. 5.4(b) through (d) can be evaluated in an analogous fashion, and are given by

$$\begin{aligned} \left[\mathfrak{S}\, \mathbf{V}^{\,j}_{(1)}\right]_{\beta\gamma} &= -\mathcal{D}_{\beta\gamma\sigma} F^{\dagger}_{\sigma j}(\omega), \\ \left[\mathfrak{S}\, \mathbf{V}^{\,j}_{(2)}\right]_{\beta\gamma} &= -\mathcal{D}^{\delta}_{\beta\gamma} \Delta_{\delta j}(\omega), \\ \left[\mathfrak{S}\, \mathbf{V}^{\,j}_{(3)}\right]_{\beta\gamma} &= -2\, \mathcal{D}^{\gamma}_{\beta\sigma} F^{\dagger}_{\sigma j}(\omega), \\ \left[\mathfrak{S}\, \mathbf{V}^{\,j}_{(4)}\right]_{\beta\gamma} &= -2\, \Sigma_{\beta\rho} \mathcal{D}^{\rho\delta}_{\gamma} \Delta_{\delta j}(\omega), \end{aligned} \tag{5.76}$$

respectively, which includes the result of the previous section. The evaluation of the remaining vertex functions shown in Fig. 5.4(e), however, results in two sets of equations

$$\begin{aligned} \left[\mathfrak{S}\, \mathbf{V}^{\,j}_{(5)}\right]_{\beta\gamma} &= -\frac{1}{2} \Sigma_{\beta\rho} \mathcal{D}^{\rho\delta}_{\sigma} F^{\dagger}_{\sigma j}(\omega) \Sigma_{\delta\gamma}, \\ \left[\mathfrak{S}^{\dagger}\, \mathbf{V}^{\,j}_{(6)}\right]_{\beta\gamma} &= -\frac{1}{2} \mathcal{D}^{\beta\gamma}_{\sigma} F^{\dagger}_{\sigma j}(\omega), \end{aligned} \tag{5.77}$$

that also involve the adjoint of $\mathfrak{S}$ defined by Eq. (5.75), as derived explicitly in the previous section. The sum of the five diagrams in Fig. 5.4 is then given by

$$\mathcal{L}(\omega) = \sum_{n=1}^{5} \mathcal{L}_n(\omega) = \frac{1}{2} F_{i\alpha}(\omega) \mathcal{D}^{\beta\gamma}_{\alpha} \left[\, \mathbf{V}^{\,j}(\omega)\right]_{\beta\gamma} + \text{h.c.}, \tag{5.78}$$

where $\mathbf{V}^{\,j}(\omega) = \sum_{n=1}^{6} \mathbf{V}^{\,j}_{(n)}(\omega)$. In the following, we present explicit solutions to these equations for multi-species reaction networks.

5.3.4 Explicit solution for general multi-species reaction networks

General expressions for the higher order corrections can be obtained via the diagonalisation of the Jacobian $\mathcal{J}$ of the REs, which satisfies

$$\mathrm{U}\ \mathcal{J}\ \mathrm{U}^{-1} = \mathrm{diag}(\lambda_1, ..., \lambda_{N_S}). \tag{5.79}$$

Here, the matrix on the right hand side is diagonal, with $\lambda_1, ..., \lambda_{N_S}$ being the eigenvalues of $\mathcal{J}$. The spectral matrix $\mathcal{S}$ can then be transformed as

$$\tilde{\mathcal{S}}(\omega) = \mathrm{U}\,\mathcal{S}(\omega)\,\mathrm{U}^T = \frac{1}{\Omega}\tilde{\Delta}(\omega) + \frac{1}{\Omega^2}\tilde{\mathcal{T}}(\omega) + \frac{1}{\Omega^2}\tilde{\mathrm{S}}(\omega) + \frac{1}{\Omega^2}\tilde{\mathcal{L}}(\omega) + O(\Omega^{-3}). \tag{5.80}$$

Applying the LNA, we find the transformed power spectral matrix

$$\tilde{\Delta}_{ij}(\omega) = \frac{\tilde{D}_{ij}}{(\lambda_i - i\omega)(\lambda_j + i\omega)}, \tag{5.81}$$

where $\tilde{\mathrm{D}} = \mathrm{U}\ \mathrm{D}\ \mathrm{U}^T$ is the diffusion matrix of the eigenmodes. The covariance of these eigenmodes $\tilde{\Sigma} = \mathrm{U}\ \Sigma\ \mathrm{U}^T$ is then

$$\tilde{\Sigma}_{ij} = -\frac{\tilde{D}_{ij}}{\lambda_i + \lambda_j}. \tag{5.82}$$

The general transformation rules for the system size coefficients, Eq. (5.23), are given by

$$\tilde{\mathcal{D}}^{j_1...j_m}_{i_1 i_2 ... i_n, s} = (U_{i_1\alpha_1} U_{i_2\alpha_2} ... U_{i_n\alpha_n})(U^{-1}_{\beta_1 j_1} U^{-1}_{\beta_2 j_2} ... U^{-1}_{\beta_m j_m})\mathcal{D}^{\beta_1...\beta_m}_{\alpha_1...\alpha_n, s}, \tag{5.83}$$

where again the summation convention stated after Eq. (5.22) is implied. In order to evaluate these, we transform $\tilde{\mathfrak{S}} = \mathrm{U}\,\mathfrak{S}\,\mathrm{U}^T$ such that for any $\tilde{\mathrm{V}} = \mathrm{U}\ \mathrm{V}\ \mathrm{U}^T$, we have $[\tilde{\mathrm{S}}\ \tilde{\mathrm{V}}]_{ij} = (\lambda_i + \lambda_j - i\omega)[\tilde{\mathrm{V}}]_{ij}$, and, hence,

$$[\tilde{\mathrm{V}}]_{ij} = \frac{1}{\lambda_i + \lambda_j - i\omega}[\tilde{\mathrm{M}}]_{ij}. \tag{5.84}$$

Using Eqs. (5.53) through (5.56) and (5.58), we find the tadpole contributions

$$\begin{aligned}\tilde{\mathcal{T}}_{ij}(\omega) =& \frac{1}{2}\frac{\delta_{i\alpha}\delta_{j\beta}}{(\lambda_i - i\omega)(\lambda_j + i\omega)}\left[\tilde{\mathcal{D}}^{\gamma}_{\alpha\beta} + \tilde{\mathcal{D}}^{\mu\gamma}_{\alpha}\frac{\delta_{\mu\nu}\tilde{D}_{\nu\beta}}{\lambda_\nu - i\omega}\right][\tilde{\epsilon}_\gamma]_1 \\ &+ (\omega \to -\omega, i \leftrightarrow j),\end{aligned} \tag{5.85}$$

and the snail contributions

$$\begin{aligned}\tilde{\mathrm{S}}_{ij}(\omega) =& \frac{1}{2}\frac{\delta_{i\alpha}\delta_{j\beta}}{(\lambda_i - i\omega)(\lambda_j + i\omega)}\left[\tilde{\mathcal{D}}_{\alpha\beta,1} + \tilde{\mathcal{D}}^{\gamma\delta}_{\alpha\beta}\tilde{\Sigma}_{\gamma\delta} + (2\tilde{\mathcal{D}}^{\mu}_{\alpha,1} + \tilde{\mathcal{D}}^{\mu\gamma\delta}_{\alpha}\tilde{\Sigma}_{\gamma\delta})\frac{\delta_{\mu\nu}\tilde{D}_{\nu\beta}}{\lambda_\nu - i\omega}\right] \\ &+ (\omega \to -\omega, i \leftrightarrow j).\end{aligned} \tag{5.86}$$

Note that $(\omega \to -\omega, i \leftrightarrow j)$ stands for the same expression but with ω replaced by $-\omega$ and i and j interchanged. Further, solving Eq. (5.76) and (5.77) using Eq. (5.84) and substituting the result in Eq. (5.78), we deduce the sum of loop diagrams

$$\begin{aligned}\tilde{\mathcal{L}}_{ij}(\omega) = &-\frac{1}{2}\frac{\delta_{i\alpha}\delta_{j\beta}}{(\lambda_i - i\omega)(\lambda_j + i\omega)}\frac{\tilde{\mathcal{D}}^{\theta\zeta}_{\alpha}\delta_{\mu\theta}\delta_{\gamma\zeta}}{\lambda_\mu + \lambda_\gamma - i\omega}\times \\ &\left[(\tilde{\mathcal{D}}^{\delta}_{\mu\gamma} + 2\tilde{\Sigma}_{\mu\rho}\tilde{\mathcal{D}}^{\rho\delta}_{\gamma})\delta_{\delta l}\frac{\tilde{\mathcal{D}}_{l\beta}}{\lambda_l - i\omega} + 2\tilde{\mathcal{D}}^{\gamma}_{\mu\beta} + \tilde{\mathcal{D}}_{\mu\gamma\beta} + \tilde{\Sigma}_{\mu\rho}\tilde{\mathcal{D}}^{\rho\delta}_{\beta}\tilde{\Sigma}_{\delta\gamma}\right] \\ &+ (\omega \to -\omega, i \leftrightarrow j),\end{aligned} \tag{5.87}$$

where we have used the symmetry of the last summand in the angled brackets. Note the overall minus sign in Eq. (5.87) which is missing in Ref. [4]. Note also that these equations are to be summed over all Greek indices, according to our summation convention.

From the analytical form of these correction terms, we recover the well-known fact that they vanish for reaction networks with at most unimolecular reactions; see for instance [51]. Note that the propensity functions are at most linear in the concentrations and independent of the system size Ω in that case. The former observation shows that all vertices with multiple upper indices are identically zero, while the latter implies that $\tilde{\mathcal{D}}_{\alpha\beta,1}$ and $\tilde{\mathcal{D}}^{\mu}_{\alpha,1}$ vanish and, hence, that the corrections given by Eqs. (5.86) and (5.87) are absent. It also follows from Eq. (5.50) that (5.85) vanishes, as the mean concentrations predicted by the CME agree to this order with the prediction from the REs. These correction terms hence stem from the nonlinearity in the law of mass action, and thus must increase with the size of the rate constants in the bimolecular reactions.

It can also be deduced from Eqs. (5.85) through (5.87) that the nonlinear corrections to the power spectrum involve denominators $(\lambda_i - i\omega)(\lambda_j + i\omega)$ and, hence, that they contribute to the amplitude of the power spectrum at the frequencies of the linear relaxation modes. Further, Eq. (5.87) involves the denominator $\lambda_\mu + \lambda_\gamma - i\omega$ which stems from nonlinear relaxation modes that are not described by the linear response. An analysis of this phenomenon is left to Section 5.5.

5.4 Applications

5.4.1 Dimerisation

As a first example, we consider bursty expression of a protein and dimerisation. A more simple reaction system describing synthesis in bursts of size m than in Section 4.4 can be formulated as

$$\varnothing \xrightarrow{k_{\text{in}}} mX, \quad 2X \xrightarrow{1} \varnothing. \tag{5.88}$$

The expansion coefficients can be calculated from the stoichiometric matrix $\mathrm{S} = (m, -2)$ and the propensities, which are given by the series

$$\boldsymbol{w}(n,\Omega) = \Omega\left(\boldsymbol{f}^{(0)}\left(\frac{n}{\Omega}\right) + \frac{1}{\Omega}\boldsymbol{f}^{(1)}\left(\frac{n}{\Omega}\right)\right), \tag{5.89}$$

with $\boldsymbol{f}^{(0)}([X]) = (k_{\mathrm{in}}, [X]^2)^T$ and $\boldsymbol{f}^{(1)}([X]) = (0, -[X])^T$, from which one deduces $\lambda_1 = \mathcal{J} = -4[X]$ and $D = \mathcal{D}_{11} = 2(2+m)[X]^2$. The concentration predicted by the RE, Eq. (5.16), is obtained as $[X] = (mk_{\mathrm{in}}/2)^{1/2}$. Hence, the power spectrum and variance, as found from the LNA, reads

$$\Delta(\omega) = \frac{2(2+m)[X]^2}{16[X]^2 + \omega^2}, \quad \Sigma = \frac{2+m}{4}[X]. \tag{5.90}$$

Further, using $\mathcal{D}_1^{11} = -4$ and $\mathcal{D}_{1,1}^0 = -4[X]$ the mean concentration is calculated from Eq. (5.51) as

$$\left\langle \frac{n}{\Omega} \right\rangle = [X] + \frac{1}{\Omega}\frac{2-m}{8} + O(\Omega^{-2}). \tag{5.91}$$

The higher order correction to the intrinsic noise power spectrum can now be derived by substituting the coefficients $\mathcal{D}_1^{111} = 0$, $\mathcal{D}_{11}^1 = 4(2+m)[X]$, $\mathcal{D}_{11}^{11} = 4(2+m)$ $\mathcal{D}_{1,1}^1 = 2$, and $\mathcal{D}_{111}^0 = 2\left(m^2-4\right)[X]^2$ into Eqs. (5.90), (5.85) and (5.86), and Eq. (5.87) by making use of Eq. (5.90). The result is

$$\mathcal{S}(\omega) = \frac{1}{\Omega}\Delta(\omega) + \Omega^2\left[\frac{64(2+m)[X]^3\left(2(2+m)[X]^2 - (m-1)\omega^2\right)}{\left(16[X]^2+\omega^2\right)^2\left(64[X]^2+\omega^2\right)}\right]. \tag{5.92}$$

Finally, the Fourier transform of the above expression yields the autocorrelation function

$$\begin{aligned}
&\left\langle \left(\frac{n(t+\tau)}{\Omega} - \left\langle\frac{n}{\Omega}\right\rangle\right)\left(\frac{n(t)}{\Omega} - \left\langle\frac{n}{\Omega}\right\rangle\right)\right\rangle \\
&\qquad = \int \frac{\mathrm{d}\omega}{2\pi}\mathrm{e}^{i\omega\tau}\mathcal{S}(\omega) \\
&\qquad = \mathrm{e}^{-4[X]\tau}\left(\frac{\Sigma}{\Omega} + \frac{1}{\Omega^2}\frac{(2+m)}{96}(14 - 13m + 12(3m-2)\tau[X])\right) \\
&\qquad\quad + \frac{1}{\Omega^2}\frac{(2+m)}{96}\mathrm{e}^{-8[X]\tau}(11m-10) + O(\Omega^{-3}).
\end{aligned} \tag{5.93}$$

The first term includes a Ω^{-2} correction to the amplitude of the linear response, while the second represents additional relaxation terms that decay twice as fast; see also the discussion concluding Section 5.3.4.

In order to verify the validity of our analysis, we calculate the Ω^{-2} correction to the LNA variance using the method given in Section 3.1.1. Using Eq. (3.21) together with

the equations for the moment expansion coefficients, Eqs. (3.15) through (3.17), yields

$$\left\langle \left(\frac{n(t)}{\Omega} - \left\langle \frac{n}{\Omega} \right\rangle \right)^2 \right\rangle = \frac{1}{\Omega}\Sigma + \frac{1}{\Omega^2}\frac{(2+m)(2-m)}{48} + O(\Omega^{-3}), \tag{5.94}$$

which agrees with Eq. (5.93) for $\tau = 0$. The particular case of $m = 2$, which obeys detailed balance with a Poissonian steady state, has been considered by Chaturvedi and Gardiner [128] (with $\kappa_2 = 2$ in their notation). They obtained the autocorrelation function

$$\frac{1}{\Omega}\mathrm{e}^{-4[X]\tau}\Sigma + \frac{1}{\Omega^2}\frac{\mathrm{e}^{-8\tau[X]}\left(1+\mathrm{e}^{4\tau[X]}(4\tau[X]-1)\right)}{2} + O(\Omega^{-3}), \tag{5.95}$$

which agrees with Eq. (5.93) in this case. It is interesting to observe that, despite the detailed balance of the reactions, the nonlinearity in the law of mass action manifests itself in the non-trivial dependence of the Ω^{-2} terms.

5.4.2 Noise-induced oscillations in the Brusselator reaction

The Brusselator describes a commonly studied set of autocatalytic oscillatory reactions [140], which involve two species interacting via

$$\varnothing \underset{k_1}{\overset{k_0}{\rightleftharpoons}} X, \quad X \xrightarrow{b} Y, \quad 2X + Y \xrightarrow{a} 3X. \tag{5.96}$$

The form of the propensities $\boldsymbol{w}(\boldsymbol{n}, \Omega) = (\Omega k_0, k_1 n_X, b n_X, a n_Y\, n_X(n_X-1)\Omega^{-2})$ implies the following expansion

$$\boldsymbol{w}(\boldsymbol{n}, \Omega) = \Omega\left(\boldsymbol{f}^{(0)}\left(\frac{\boldsymbol{n}}{\Omega}\right) + \frac{1}{\Omega}\boldsymbol{f}^{(1)}\left(\frac{\boldsymbol{n}}{\Omega}\right)\right), \tag{5.97}$$

where $\boldsymbol{f}^{(0)}([\boldsymbol{X}]) = (k_0, k_1[X], b[X], a[Y][X]^2)$ and $\boldsymbol{f}^{(1)}([\boldsymbol{X}]) = (0, 0, 0, -a[Y][X])$. This expansion, together with the stoichiometry

$$\mathrm{S} = \begin{pmatrix} 1 & 1 & -1 & 1 \\ 0 & 0 & 1 & -1 \end{pmatrix}, \tag{5.98}$$

determines the system size coefficients, Eq. (5.23). Specifically, the solution of the REs, Eq. (5.16), is given by $[X] = \frac{k_0}{k_1}$ and $[Y] = \frac{bk_1}{ak_0}$. The Jacobian of these equations then reads

$$\mathcal{J} = \begin{pmatrix} b - k_1 & a[X]^2 \\ -b & -a[X]^2 \end{pmatrix}. \tag{5.99}$$

Using Eq. (5.51), the mean concentrations are obtained as

$$\left\langle \frac{n_X}{\Omega} \right\rangle = [X] + O(\Omega^{-2}),$$

$$\left\langle \frac{n_Y}{\Omega} \right\rangle = [Y] + \frac{1}{\Omega} \frac{2b\left(2a[X]^2 - b\right)}{a[X]^2\left(a[X]^2 + k_1 - b\right)} + O(\Omega^{-2}), \tag{5.100}$$

which are accurate to order Ω^{-1}. Hence, to this order, the prediction from the CME agrees with the one from the REs for species X, but not for species Y. The leading order corrections to the power spectrum can be derived either algebraically or by making use of the eigenvalue representation, as follows. The eigenvalues of the Jacobian in Eq. (5.99) are given by

$$\lambda_{1,2} = -\frac{1}{2}\left(a[X]^2 + k_1 - b\right) \pm \frac{1}{2}\sqrt{\left(a[X]^2 + k_1 - b\right)^2 - 4ak_0[X]}, \tag{5.101}$$

while the corresponding eigenvectors are $U_{i1} = b$, and $U_{i2} = (\lambda_i + k_1 - b)$, for $i = 1, 2$. In particular, we see that the deterministic system undergoes a Hopf bifurcation when the real part of the above eigenvalues becomes positive. Since, strictly speaking, the SSE only applies to stable fixed points, we require $b < a[X]^2 + k_1$. The resulting analytical expressions for the power spectrum are, however, rather involved. Hence, we restrict our analysis to the study of species X in the case where $k_0 = 1 = k_1$.

On the basis of the LNA, we obtain

$$\Delta_X(\omega) = \frac{2\left(a^2 + (b+1)\omega^2\right)}{a^2 + \omega^2\left((a-b)^2 + 1 - 2b\right) + \omega^4}. \tag{5.102}$$

The intrinsic noise power spectrum, including corrections of order $O(\Omega^{-2})$, is then obtained via the procedure derived in Section 4 and reads

$$\mathcal{S}_X(\omega) = \frac{1}{\Omega}\Delta_X(\omega) + \frac{1}{\Omega^2}\frac{\sum_{i=1}^{5} a_i \omega^{2i}}{A(\omega)} + O(\Omega^{-3}), \tag{5.103}$$

where the denominator is given by

$$\begin{aligned} A(\omega) =& (a - b + 1)\left((a - b + 1)^2 + \omega^2\right) \times \\ & \left(a^2 + \omega^2\left((a-b)^2 - 2b + 1\right) + \omega^4\right)^2 \times \\ & \left(16a^2 + 4\omega^2\left((a-b)^2 - 2b + 1\right) + \omega^4\right). \end{aligned} \tag{5.104}$$

Here, the coefficients a_i are defined as

$$\begin{aligned} a_1 =& 32a^4 b\left(-3(11a+9)b^3 + ((58a+75)a+42)b^2\right. \\ & \left. -(((49a+96)a+72)a+19)b + 4((a+3)(4a+3)a+3)a + 8b^4\right), \\ a_2 =& 8a^2 b\left(16a^6 + 36a^5(3-2b) + 4a^4((34b-69)b+17)\right. \\ & +a^3((2(121-72b)b-359)b+40) + a^2(3b(b((32b-37)b+131)-12)-172) \\ & +2a(b(((10(3-2b)b-133)b+88)b+63)-18) \\ & \left.+(b-1)^2(((8b-7)b+82)b+1)b\right), \end{aligned}$$

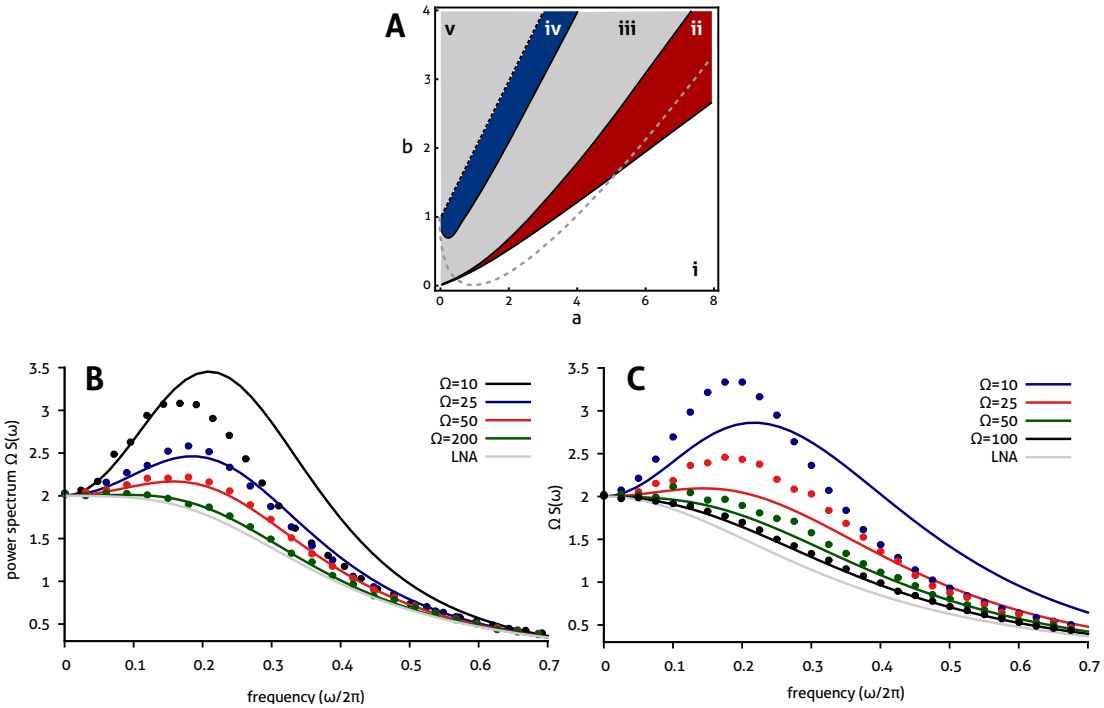

Figure 5.5:

Noise-induced oscillations in the Brusselator reaction. (A) Comparison of the parametric dependence of noise-induced oscillations for species X with the prediction from the LNA and with that obtained by including higher order corrections in the SSE, for $\Omega = 20$. In region (i, white area), both theories predict that no oscillations will occur; in (ii, red), the higher order expansion predicts noise-induced oscillations which are missed by the LNA. Note that these oscillations appear both for deterministically stable nodes and foci (separated by a dashed grey line). In regions (iii, grey) and (iv, blue), both theories predict noise-induced oscillations. Region (iv, blue) includes the appearance of secondary harmonics that are not captured by the LNA close to the deterministic Hopf bifurcation (dashed black line). The deterministically oscillatory regime in (v, grey) is not described by either theory. (B) The intrinsic noise power spectrum in the case of a deterministic focus ($k_0 = 1 = k_1$, $a = 4.5$, $b = 2$) is shown for decreasing values of Ω. For large Ω, the monotonous dependence on frequency is captured by the LNA (dashed grey line). A decrease in volume reveals noise-induced oscillations that are well described by the Ω^{-2} corrections (blue and red lines), but not by the LNA. These predictions are verified by stochastic simulation (dotted). Reducing the volume to $\Omega = 10$, we observe that our theory only qualitatively accounts for the frequency dependence. (C) A similar dependence is observed in the parameter regime corresponding to a deterministic node ($k_0 = 1 = k_1$, $a = 7.5$, $b = 3$). However, for small volumes, the higher order expansion only yields a qualitative description for the power spectrum of the noise-induced oscillations. (Note that in (B) and (C), the spectrum has been multiplied by Ω such that the prediction from the LNA is the same for all system sizes.)

$$
\begin{aligned}
a_3 =& 8b\left(12a^7 + a^6(8-40b) + a^5\left(32b^2-58b+3\right)\right.\\
&+a^4\left(37b^3+128b^2+b-55\right) + a^3(63-2b((b(44b+59)-52)b+24))\\
&+a^2\left(b\left(b\left(\left(70b^2+34b-189\right)b+228\right)-159\right)-52\right)\\
&\left.-4a(b-1)^2(((7b-4)(b+2)b+3)b+3)+5(b-1)^4(b+1)^2b\right),\\
a_4 =& 8b\left(-a^5+3a^4(b-1)+a^3(14-b(4b+5))+a^2(b(b(7b+59)-75)-17)\right.\\
&\left.+a(((42-b(9b+35))b+21)b+17)+4\left(b^2-1\right)^2 b\right),\\
a_5 =& -8b\left(a^3+a^2(7b+1)-a(7(b+1)b+5)+(b+1)^2b\right).
\end{aligned}
\tag{5.105}
$$

The above explicit expression for the power spectrum can be used to quantify the periodicity of typical trajectories of the underlying stochastic process, which is of importance in the study of single-cell oscillations [91]. Specifically, if the deterministic stability is given by a stable fixed point, a peak in the intrinsic noise power spectrum indicates a noise-induced oscillation. The parametric dependence of these oscillations is analysed in Fig. 5.5 using Eq. (5.103) for a system size of $\Omega = 20$. We find that the LNA predicts the fluctuations to decay monotonically with increasing frequency in parameter regions (i) and (ii), while it postulates noise-induced oscillations in parameter regions (iii) and (iv). By contrast, taking into account higher order corrections as given by the second term in Eq. (5.103), we infer that the dynamics is also oscillatory in region (ii), which is at odds with the prediction from the LNA. In Figs. 5.5B and C, we verify this dependence in two parameter regimes, one in which the eigenvalues of the Jacobian, as given in Eq. (5.101), are complex, and another in which these eigenvalues are purely real, corresponding to stable node oscillations [141]. There, we also show the dependence of the oscillations on the system size Ω. Finally, we note that in parameter regions (iv) close to the Hopf bifurcation, our theory predicts multiple spectral peaks that cannot be described by the LNA. A simplified treatment accounting for these effects is developed in the following.

5.5 Near-critical power spectra and noise-induced oscillations

We here deduce an approximate expression for the intrinsic noise power spectrum when the corresponding deterministic system is close to a Hopf bifurcation point. In what follows we assume that the eigenvalue spectrum of the Jacobian $\mathcal{J}$ is composed of a pair of conjugate eigenvalues $\lambda_1 = -\gamma + i\omega_0$, $\lambda_2 = -\gamma - i\omega_0$ and $N_S - 2$ real negative eigenvalues λ_i where $i = 3, ..., N_S$. The deterministic dynamics then corresponds to a focus which becomes unstable as we approach the Hopf bifurcation point $\gamma \to 0$.

We first summarize the qualitative characteristics that can be deduced from the LNA. By Eqs. (5.80) and Eq. (5.81) the LNA power spectrum of the s^{th} species is given by

$$
\mathcal{S}_s^{\mathrm{LNA}}(\omega) = \frac{1}{\Omega}\sum_{ij} U_{si}^{-1}\frac{\tilde{D}_{ij}}{(\lambda_i - i\omega)(\lambda_j + i\omega)}U_{js}^{-T}. \tag{5.106}
$$

The dominant terms in the above sum are those proportional to $G = \tilde{D}_{12} = \tilde{D}_{21}$ because of the dependence of the denominator as $\gamma \to 0$. In particular, one deduces that the power spectrum has a Lorentzian peak at $\omega \approx \omega_0$ whenever

$$\frac{\gamma}{\omega_0} \ll 1. \tag{5.107}$$

The phenomenon of noise-induced oscillations is therefore particularly conspicuous when the deterministic dynamics is close to a critical point giving rise to a limit cycle through a Hopf bifurcation [142, 143]. In this case the total power is concentrated in the peak and can be approximated by the peak height ($\sim \frac{G}{\Omega\gamma^2}$), multiplied by its spectral width at half maximum ($\sim 2\gamma$) and is of the order

$$\frac{1}{\Omega}\frac{G}{2\gamma}, \tag{5.108}$$

which is precisely the variance of the first two dominant eigenmodes in Eq. (5.82) when condition (5.107) holds. Since the total power is equal to the variance of the noise-induced oscillation it follows that Eq. (5.108) needs to be sufficiently small for the LNA to hold. Similar criteria have been obtained using multiple scale analysis in Refs. [144] and [145].

5.5.1 Nonlinear theory of noise-induced oscillations

As we have argued above, close to the bifurcation point, the covariance of the first two eigenmodes diverges as

$$\tilde{\Sigma}_{12} = \tilde{\Sigma}_{21} \simeq \frac{G}{2\gamma}. \tag{5.109}$$

This relation allows to simplify the higher order corrections to the LNA tremendously. In the limit of large $\tilde{\Sigma}$ it follows that the dominant contribution to the power spectrum is given by the last term in Eq. (5.87) which corresponds to the last diagram in Fig. (5.4), and is given by

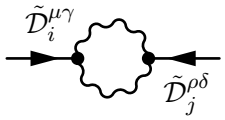

$$= -\frac{1}{2}\frac{\tilde{\mathcal{D}}_i^{\mu\gamma}\tilde{\Sigma}_{\mu\rho}}{(\lambda_i - i\omega)}\frac{1}{\lambda_\mu + \lambda_\gamma - i\omega}\frac{\tilde{\mathcal{D}}_j^{\rho\delta}\tilde{\Sigma}_{\delta\gamma}}{(\lambda_j + i\omega)} + (\omega \to -\omega, i \leftrightarrow j). \tag{5.110}$$

Using $\mathcal{S}(\omega) = \mathrm{U}^{-1}\tilde{\mathcal{S}}(\omega)\,\mathrm{U}^{-T}$, the power spectrum of the s^{th} species is reduced to

$$\mathcal{S}_s(\omega) = \frac{1}{\Omega}\sum_{ij} U_{si}^{-1}\frac{\tilde{D}_{ij}}{(\lambda_i - i\omega)(\lambda_j + i\omega)}U_{js}^{-T}$$

$$- \frac{1}{2\Omega^2} \sum_{\alpha\beta\mu\nu} \mathcal{M}_s^{\alpha\beta}(\omega)\tilde{\Sigma}_{\alpha\mu} \left(\frac{1}{\lambda_\alpha + \lambda_\beta - i\omega} + \frac{1}{\lambda_\mu + \lambda_\nu + i\omega} \right) \mathcal{M}_s^{\mu\nu}(-\omega)\tilde{\Sigma}_{\nu\beta}, \tag{5.111}$$

to order Ω^{-2} and γ^0 and we have here written out the summation explicitly. The first term is the LNA result and the coefficients of the second term denote the terms

$$\mathcal{M}_s^{\alpha\beta}(\omega) = \sum_{i=1}^{N_S} U_{si}^{-1} \frac{\tilde{\mathcal{D}}_i^{\alpha\beta}}{(\lambda_i - i\omega)} = \sum_{i,\mu,\nu=1}^{N_S} [(\mathcal{J} - i\omega)^{-1}]_{si} U_{\mu\alpha}^{-1} U_{\nu\beta}^{-1} \tilde{\mathcal{D}}_i^{\nu\mu}. \tag{5.112}$$

Since close to the bifurcation point, the covariance of the near-critical eigenmodes is dominated by its off-diagonal elements, Eq. (5.109), these also yield the dominant contributions to the sum in Eq. (5.111). Substituting now $\lambda_{1,2} = -\gamma \pm \omega_0$, the power spectrum reduces to

$$\begin{aligned} \mathcal{S}_s(\omega) \approx & \mathcal{S}_s^{\mathrm{LNA}}(\omega) \\ & + \frac{\Omega^{-2} G^2}{2\gamma} \left(\frac{|\mathcal{M}_s^{11}(\omega)|^2}{(\omega - 2\omega_0)^2 + (2\gamma)^2} + 2\,\frac{|\mathcal{M}_s^{12}(\omega)|^2}{\omega^2 + (2\gamma)^2} + \frac{|\mathcal{M}_s^{22}(\omega)|^2}{(\omega + 2\omega_0)^2 + (2\gamma)^2} \right) \\ & + O(\gamma^0) + O(\Omega^{-3}), \end{aligned} \tag{5.113}$$

which is the main result of this section. Note that we have also used $\mathcal{M}_s^{22}(\omega) = (\mathcal{M}_s^{11}(-\omega))^*$ and $\mathcal{M}_s^{12}(\omega) = (\mathcal{M}_s^{21}(-\omega))^*$ because the critical eigenvectors are complex conjugates. The first term in Eq. (5.113) is the prediction of the LNA and equals Eq. (5.106) which leads to a peak at $\omega \simeq \omega_0$. The second term in Eq. (5.113) leads to a peak at twice the LNA frequency $\omega \simeq 2\omega_0$ and the third term leads to a peak at zero frequency $\omega \simeq 0$ whenever we are close to the Hopf bifurcation point. These extra peaks are due to the combined influence of noise and nonlinearity on the chemical reactions. The fourth term is a non-resonant contribution that does not lead to a peak and hence can be omitted.

The conditions for the observability of the additional peaks at twice the frequency of the principal peak and at zero frequency require

$$|\mathcal{M}_s^{11}(2\omega_0)| \neq 0, \quad |\mathcal{M}_s^{12}(0)| \neq 0, \tag{5.114}$$

respectively. Using the definition in Eq. (5.112) it follows that the Hessian $\mathcal{D}_i^{\alpha\beta}$ of the corresponding deterministic system needs to be non-zero at the bifurcation point; however, this condition is not sufficient. Assuming that $|\mathcal{M}_s^{11}(2\omega_0)|$ is a continuous function of ω_0 then clearly the first condition in Eq. (5.114) is fulfilled for all values of $2\omega_0$ except the zeros of $\mathcal{M}_s^{11}$ which depend on the specific rate constants of the network under consideration. The second condition in Eq. (5.114) is independent of ω_0 and is not generally true for all biochemical processes of interest as we show in the following section.

The physical meaning of the peak at zero frequency is not as intuitive as the peaks at non-zero frequency and requires further explanation. Given that γ is very small (since we are close to the Hopf bifurcation) and assuming that $\mathcal{M}_s^{12}(0) \neq 0$, it follows that the spectrum associated with the second term in the bracket of Eq. (5.113) is approximately proportional to $|\mathcal{M}_s^{12}(0)|^2\omega^{-2}$ for $\omega_0 \gg \omega \gg \gamma$. A spectrum characterized by this scaling is associated with Brownian noise; to be more precise, given a Langevin equation $\frac{\partial}{\partial t}x(t) = \Gamma(t)$ where $\Gamma(t)$ is white noise, the power spectrum of the signal $x(t)$ is equal to $\langle\Gamma^2\rangle/\omega^2$. Thus it follows that the fluctuating signal whose spectrum is given by Eq. (5.113) can be interpreted as the sum of the three components: (i) a component which fluctuates about the mean with diffusion coefficient $\frac{\langle\Gamma^2\rangle}{2} = |\mathcal{M}_s^{12}(0)|^2G^2/(2\Omega^2\gamma)$; (ii) a noisy component with power concentrated at a frequency of ω_0; (iii) another oscillatory component as (ii) but with power concentrated at a frequency of $2\omega_0$. These components are respectively associated with the spectra given by the third term, the first term and the second term on the right hand side of Eq. (5.113). We next give a qualitative example demonstrating how our result can be applied to the interpretation of biological rhythms.

5.5.2 Noise-induced oscillations observed in individual fibroblast cells

Recently, Leise et al [146] reported experimental protein luminescence data from cultures of 80 highly rhythmic fibroblast cells. Fig. 5.6A compares two time traces of protein luminescence from single fibroblast cells against the averaged response of a culture of 20 cells (images reproduced from dataset S1 in Ref. [146]). While individual rhythms shown sustained circadian rhythms, the initially synchronized cell culture displays damped oscillations on average due to a gradual dephasing of individual cells.

It is still under debate what is the underlying single cell mechanism responsible for producing such oscillations. In the absence of noise, populations of synchronized self-sustained oscillators exhibit in-phase oscillations of constant amplitude while populations of damped oscillators show an in-phase decaying amplitude. In both cases, taking into account molecular fluctuations stemming from the stochastic nature of the underlying biochemical reactions leads to a population of cells with sustained (noisy) oscillations and with cell-to-cell variation in the phase. Hence, currently, experimental single cell data can be explained by both noisy self-sustained and damped oscillator models [90, 91]. While commonly only the principal component of the power spectrum is analysed, we here investigate if the experimental power spectrum can be fit by our theory including higher order resonances.

Single cell spectra were obtained from individual observations over a six week period and averaged over the cell population. This data (see dataset S1; also shown in Fig. 6b of Ref. [146]) shares the main features predicted by our theory, namely a peak at zero frequency, a dominant peak at the circadian frequency and a second harmonic. Our strategy is as follows: (i) we propose a biologically plausible network motif explaining

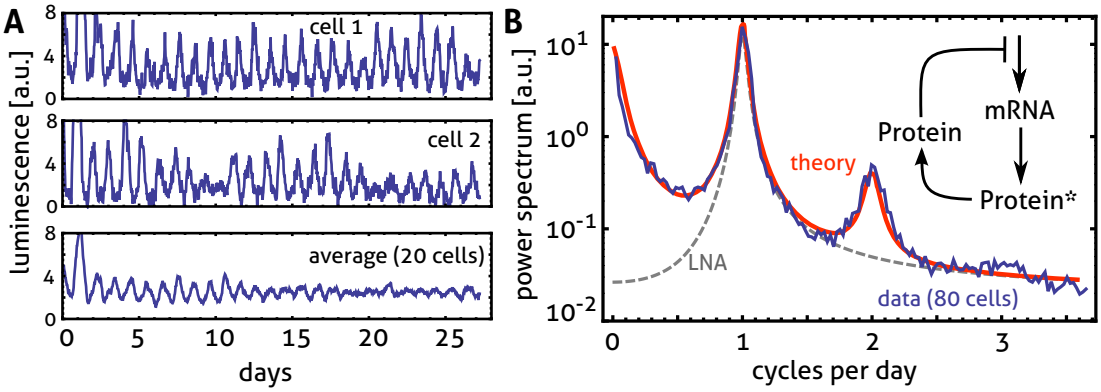

Figure 5.6:
Experimental power spectrum of circadian rhythm in fibroblast cells: comparison with LNA and nonlinear theory. (A) Single cell circadian oscillations in individual fibroblast cells over two weeks after medium change reproduced from experimental dataset S1 in Ref. [146]. Time courses of protein luminescence in two representative cells and the population average over the first 20 cells are shown. Individual show sustained oscillations while the average shows damped oscillations due to dephasing of individual cell rhythms. (B) The insets shows a biologically plausible motif for explaining the single cell dynamics observed in Leise et al. Fit of the experimental power spectrum (solid blue line) by the linear (LNA) theory (gray dashed line) and by the proposed nonlinear theory (red solid line) is shown. Note that the LNA captures well the principal peak while it misses the appearance of the peaks at zero and at a second harmonic frequency. The nonlinear theory is in excellent quantitative agreement with all features of the experimental data. The parameters for the theoretical curves are given in the main text.

the observed oscillatory single cell dynamics, (ii) we fit the principal peak of the experimental power spectrum using the LNA for this motif and (iii) we refine our fit by taking into account additional peaks in the spectrum using our main result, Eq. (5.113), applied to the motif.

The ability of biological systems to oscillate is often associated with the presence of a negative feedback loop in the underlying biochemical network [147]. Given the fact that any biochemical oscillator must be composed of at least three components [148] we propose a negative feedback motif involving mRNA (M) and two forms of a protein (P and P^*) as a candidate for explaining the experimental rhythmic fibroblast data (see inset in Fig. 5.6B for an illustration). The dynamics of this motif could be described deterministically by the following set of coupled REs:

$$\frac{\mathrm{d}[M]}{\mathrm{d}t} = \frac{k_0}{k_1 + [P]} - \alpha_1[M], \tag{5.115}$$

$$\frac{\mathrm{d}[P^*]}{\mathrm{d}t} = \beta_1[M] - \alpha_2[P^*], \tag{5.116}$$

$$\frac{\mathrm{d}[P]}{\mathrm{d}t} = \beta_2[P^*] - \frac{k_2[P]}{k_3 + [P]}, \tag{5.117}$$

where $[M]$, $[P^*]$ and $[P]$ are the concentrations of mRNA and the two protein species. The corresponding Jacobian is given by

$$\mathcal{J} = \begin{pmatrix} -\alpha_1 & 0 & -\chi \\ \beta_1 & -\alpha_2 & 0 \\ 0 & \beta_2 & -\alpha_3 \end{pmatrix}, \tag{5.118}$$

where $\alpha_{1,2,3}$, $\beta_{1,2}$ and χ are positive constants. Note that χ measures the strength of the negative feedback loop and is equal to $k_0/(k_1 + [P])^2$, whereas α_3 is a measure of the nonlinear protein degradation rate and is equal to $k_2k_3/(k_3 + [P])^2$. Indeed it can be shown that this is the generic form for the Jacobian of all negative feedback motifs with three components [149]. The only entries of the Jacobian which are functions of the protein concentration $[P]$ are $\mathcal{J}_{13}$ and $\mathcal{J}_{33}$. Hence the only non-zero Hessian elements are $\mathcal{D}_1^{33}$ and $\mathcal{D}_3^{33}$. The existence of non-zero Hessian elements is due to the nonlinear reaction mechanisms of the feedback repression and protein degradation. The Routh-Hurwitz theorem implies that the steady state is stable provided $(\alpha_1 + \alpha_2 + \alpha_3)(\alpha_1\alpha_2 + \alpha_2\alpha_3 + \alpha_3\alpha_1) > \alpha_1\alpha_2\alpha_3 + \beta_1\beta_2\chi$. If equality holds the system undergoes a Hopf bifurcation. Close to the bifurcation the system has a pair of complex conjugate eigenvalues with dominant imaginary part which can be approximated by $\omega_0 \approx \sqrt{\alpha_1\alpha_2 + \alpha_2\alpha_3 + \alpha_3\alpha_1}$; this determines the frequency of the principal peak of the power spectrum of the negative feedback loop close to the bifurcation.

We now use the functional form of the LNA power spectrum, given by the first term in Eq. (5.113) together with Eq. (5.118), to obtain a fit of the protein species P's spectrum to the principal peak of the experimental power spectrum. Since our proposed oscillator is composed of three components but the available experimental data provides measurements only for one of these components, we reduce the number of free parameters to fit the LNA by setting $\alpha_{1,2} = \beta_{1,2}$ and assuming the noise matrix D to be proportional to the unit matrix, i.e. a total of four free parameters since the Jacobian has three parameters and the diagonal noise matrix has one parameter. We then use a least squares nonlinear fitting procedure to obtain these four parameters, leading to $\alpha_{1,2} = \beta_{1,2} = 0.51$, $\alpha_3 = 0.82$, $\chi = 5.99$ and $\Omega^{-1}D_{11} = \Omega^{-1}D_{22} = \Omega^{-1}D_{33} = 0.01$. The result is shown as a grey dashed line in Fig. 5.6B. The solid blue line in Fig. 5.6 shows the power spectrum reproduced from the experimental dataset obtained by Leise et al [146].

We next refine our fit by using Eq. (5.113) in the previous section. For the computation we need the two parameters determining the critical eigenmodes of the Jacobian (γ and ω_0), the noise coefficient G/Ω, the matrix U of eigenvectors of the Jacobian and the Hessian. All of the latter except for the Hessian can be computed from the four free parameters previously determined by fitting the LNA spectrum since these completely

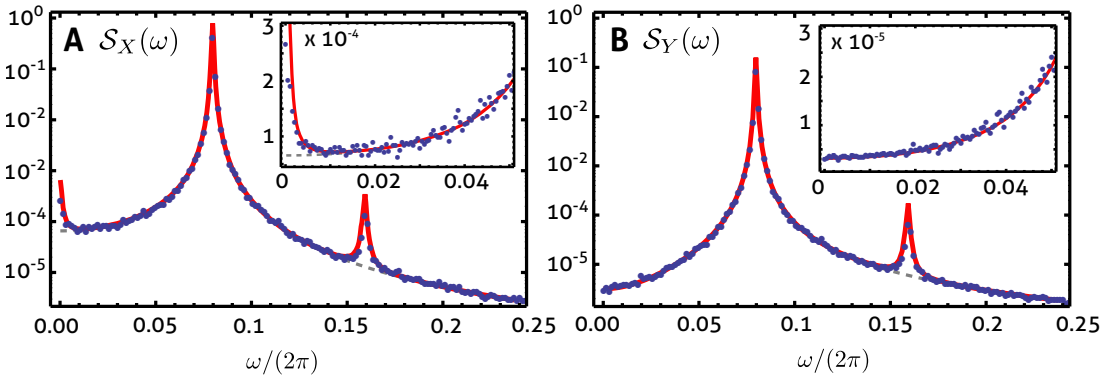

Figure 5.7:

Noise-induced oscillations in the mitosis control mechanism. We compare the predictions of our theory for the power spectra, Eqs. (5.125) (solid red line) to those obtained from stochastic simulations using the SSA (blue dots) for the inactive and active forms of protein, X and Y, as shown in (A) and (B), respectively. Note that our theory accurately predicts the peak at zero frequency in (A) (see also the inset for a magnified view) and the peaks at twice the fundamental frequency in (A) and (B) which are missed by the power spectra predicted by the LNA (grey dashed line). The parameters used are $k = 0.3953$, $b = 0.0946$ and $\Omega = 2.5 \times 10^5$ which yield $\gamma = 0.0025$ and $\omega_0 = 0.5$.

determine the Jacobian and the noise matrix. As before, we use a nonlinear fitting procedure to determine the two non-zero components of the Hessian matrix and find $\mathcal{D}_1^{33} = 16.20$ and $\mathcal{D}_3^{33} = 2.23$. The red line in Fig. 5.6B shows the corresponding result for the power spectrum given by Eq. (5.113). The agreement between the experimental data (blue line) and our theory is remarkable when considering that we required only two additional parameters to fit the two new features predicted by our theory, namely the peak at zero frequency and the second order harmonic. Subtracting a constant background of 0.001% of the central peak height from the experimental spectrum improved the agreement, presumably because this eliminates measurement noise which our theory does not describe.

5.5.3 Oscillator control of mitosis

In this section we investigate noise-induced oscillations in a theoretical model for the control of the mitotic phase of the cell cycle proposed by Tyson [150]

$$\varnothing \xrightarrow{k} X \xrightarrow{b} Y \xrightarrow{1} \varnothing, \quad 2Y + X \xrightarrow{1} 3Y, \tag{5.119}$$

where the species X and Y are the inactive and activate forms of a protein, respectively, and we assume mass action kinetics. In the following we give a detailed derivation how the power spectrum given by Eq. (5.113) is obtained for the model under consideration.

The analysis will be carried out in two steps; first we work out the power spectrum within the LNA and next we compute the novel higher-order corrections. The REs are

given by

$$\frac{\mathrm{d}}{\mathrm{d}t}[X] = k - b[X] - [Y]^2[X],$$
$$\frac{\mathrm{d}}{\mathrm{d}t}[Y] = b[X] + [Y]^2[X] - [Y], \tag{5.120}$$

with steady state solution $[X] = k/(k^2 + b)$ and $[Y] = k$. We make the following convenient definitions: $k = 2^{-1/2}\omega_0(1+\omega_0^2)^{1/2}$ and $b = \left(\theta^2 + \gamma - k^2\right)$ where $\theta^2 = (\sqrt{4\gamma(\gamma-1) + \left(1+2\omega_0^2\right)^2} - 1)/2$; it then follows that we can write the Jacobian at steady state as

$$\mathcal{J} = \begin{pmatrix} -\gamma - \theta^2 & \gamma - 1 - \theta^2 \\ \gamma + \theta^2 & -\gamma + \theta^2 \end{pmatrix}, \tag{5.121}$$

whose eigenvalues can be found analytically as in Ref. [150] and are given by

$$\lambda_{1,2} = -\gamma \pm i\sqrt{\gamma(1-\gamma) + \theta^2}. \tag{5.122}$$

We observe that the Hopf bifurcation is approached as $\gamma \to 0$ with $\omega_0 = \lim_{\gamma\to 0}\theta$ being the oscillation frequency.

Using $D_{11} = D_{22} = -2D_{12} = -2D_{21} = \omega_0\sqrt{2(1+\omega_0^2)}$ (in the limit $\gamma \to 0$) and the Jacobian given by Eq. (5.121), the LNA power spectra can be expressed as

$$\mathcal{S}_X^{\mathrm{LNA}}(\omega) = \frac{1}{\Omega}\frac{\omega_0\sqrt{2(1+\omega_0^2)}\left(1+\omega^2+\omega_0^2+\omega_0^4\right)}{(\gamma+\theta^2-\omega^2)^2 + (2\gamma\omega)^2}, \tag{5.123a}$$
$$\mathcal{S}_Y^{\mathrm{LNA}}(\omega) = \frac{1}{\Omega}\frac{\omega_0\sqrt{2(1+\omega_0^2)}\left(\omega^2+\omega_0^4\right)}{(\gamma+\theta^2-\omega^2)^2 + (2\gamma\omega)^2}. \tag{5.123b}$$

The latter have a resonance at $\omega \simeq \theta \simeq \omega_0$ in both variables due to the dependence of the denominator as $\gamma \to 0$. Next we calculate the corrections accounting for nonlinear effects close to the bifurcation.

Using the eigenvalues, Eq. (5.122), and the Jacobian, Eq. (5.121), one can compute the matrix of eigenvectors U. In the limit $\gamma \to 0$ we obtain

$$\mathrm{U} = \begin{pmatrix} \omega_0 & i+\omega_0 \\ \omega_0 & -i+\omega_0 \end{pmatrix}, \tag{5.124}$$

from which we obtain $G = \tilde{D}_{12} = \tilde{D}_{21} = \sqrt{2}\omega_0\left(1+\omega_0^2\right)^{3/2}$. Finally using the Hessian of Eq. (5.120), the coefficient G and the Jacobian $\mathcal{J}$ in Eq. (5.113), we find the corrections to the LNA spectrum of fluctuations

$$\mathcal{S}_X(\omega) = \mathcal{S}_X^{\mathrm{LNA}}(\omega) + \frac{\Omega^{-2}}{8\gamma}\frac{\left(1+\omega^2\right)(1+\omega_0)^3}{(\gamma+\theta^2-\omega^2)^2 + (2\gamma\omega)^2}\times$$

$$\left(\frac{1 + \left(\omega_0 + 2\omega_0^3\right)^2}{(\omega - 2\omega_0)^2 + (2\gamma)^2} + \frac{2 - 6\omega_0^2 + 8\omega_0^6}{\omega^2 + (2\gamma)^2} \right), \quad (5.125a)$$

$$\mathcal{S}_Y(\omega) = \mathcal{S}_Y^{\mathrm{LNA}}(\omega) + \frac{\Omega^{-2}}{8\gamma} \frac{\omega^2(1+\omega_0)^3}{(\gamma + \theta^2 - \omega^2)^2 + (2\gamma\omega)^2} \times \left(\frac{1 + \left(\omega_0 + 2\omega_0^3\right)^2}{(\omega - 2\omega_0)^2 + (2\gamma)^2} + \frac{2 - 6\omega_0^2 + 8\omega_0^6}{\omega^2 + (2\gamma)^2} \right). \quad (5.125b)$$

From the form of Eqs. (5.125) one can deduce that the theory predicts a second harmonic peak for both species but a peak at zero frequency only in the spectrum of species X, compare Fig. 5.7A and Fig. 5.7B. The excellent quantitative agreement between our theory and simulations verifies the accuracy of the proposed method.

6 Discussion

In this thesis we have developed systematic approximation methods for the CME. These methods have been formulated in terms asymptotic series solutions to the moments, correlation functions and probability distributions. The series obtained from the SSE can be truncated systematically to any desired order and have been given in closed form for the moments and probability distributions. A general diagrammatic method for the expansion of correlation functions and power spectra has been devised for biochemical networks in stationary conditions. While commonly the SSE is truncated after the LNA terms, we have shown that for low molecule number conditions, methods taking into account higher order terms in the SSE perform significantly better than the LNA.

In Chapter 3 we studied the expansion of the moments as an asymptotic series in the inverse system size. First, in Section 3.1, we derived a closed system of linear ODEs for the expansion coefficients (Result 3.1). Explicit expressions for the first few terms of this series have been given explicitly for reaction networks composed of an arbitrary number of species and reactions and their relation to previous results was discussed.

Next, in Section 3.2, we carried out a preliminary investigation of the convergence of the SSE. The first few moments of two generic reaction networks have been discussed. For the first example, an enzyme-catalysed reaction, we found that the moment expansion leads to a finite series and we showed that this result agrees exactly with the true moments. In a second example, a dimerisation reaction, an infinite series expansion was obtained and its asymptotic character was studied. We found that the absolute size of terms in the series of the first two moments decreases initially and then rapidly increases with increasing truncation order. The transition point of the divergence was determined analytically and a method for optimally truncating the SSE has been proposed. We expect this method to be particularly valuable to obtain biologically meaningful results when the validity of the SSE is under question. In Section 3.3, we applied this method to a model of gene expression with enzymatic degradation and demonstrated that the first few terms in the expansion of the moments describe the mean and variance of the CME distribution significantly better than the LNA. These results clearly highlight the necessity of taking into higher order terms in the SSE for the study of biochemical systems.

In Chapter 4 we investigated the question what asymptotic expansion of the probability distribution corresponds to the expansion of the moments. To that end, in Section 4.1 a continuous approximation to the time-dependent probability density has been employed extending van Kampen's LNA to higher orders in the SSE. This solu-

tion has been obtained from the PDE approximation of the CME for a single species using the technique of orthogonal polynomials (Result 4.2). We found, however, that the method does provide reliable results only for biochemical systems with large numbers of molecules and that the method can become inaccurate in low molecule number conditions.

We therefore extended the methodology taking into account the particularity of molecule counts. We proposed a new asymptotic expansion with discrete support, i.e. an asymptotic expansion of the discrete probability distribution. The latter has been obtained using the characteristic function approach in Section 4.2 and it was shown that it also provides a solution to the SSE of the CME but on the integer lattice (Result 4.5). We found that in low molecule number conditions, the prescribed discrete distribution approximations (incorporating higher order terms in the SSE) capture the underlying solution of the CME significantly better than the continuous approximation. In addition, in Section 4.3 we found that for networks with bimolecular reactions, renormalisation was required for achieving rapid convergence of the series (Result 4.6). This result highlights that the SSE is to be considered as an expansion about the mean and not about the RE solution. While the next to leading order correction terms to the LNA have been given explicitly, higher order terms had to be taken into account to accurately characterize the non-Gaussian distributions studied in our examples. We note that both, the continuous and discrete asymptotic expansions, cannot generally guarantee the positivity of the probability law. These undulations are particularly pronounced in the short-time behaviour of the expansion studied in Section 4.4, which our theory does not describe.

Previous means of obtaining approximate probability distributions for the CME have mainly focused on the inverse problem, i.e. reconstruction of the probability density from the moments [55, 59, 60]. These methods do not rely on the existence of a small parameter, and therefore require additional approximations such as moment closure. Specifically, they are based on the prior assumption that the first few moments contain all information about the probability distribution. Conversely, using the SSE, we have here obtained the probability distribution directly from the CME without the need to resort to moments. The inverse relation expressing the asymptotic expansion of the distributions in terms of the expansion of their moments has been given for completeness (Result 4.4). The present method enjoys the particular advantage over existing methods that the first few terms of the expansion can be written down explicitly as a function of the rate constants and for any number of reactions. We have demonstrated that the procedure leads to particularly simple expressions that approximate well the underlying non-Gaussian distributions of the CME.

In Chapter 5 we have presented a general diagrammatic approach for the systematic evaluation of multi-time correlation functions from the SSE. To that end, we have presented an alternative derivation of the SSE from the path-integral approach (Result 5.3). This result allowed us to formulate a set of Feynman rules for the calculation

of higher order terms in the SSE to be performed in an algorithmic fashion (Result 5.4). The proposed methodology permits the representation of correlation functions of stationary stochastic processes by a finite sum of diagrams that can be truncated at the desired order in the inverse system size. The technique therefore represents an effective bookkeeping device for the purposes of detailed calculation on the basis of the SSE.

We have explicitly demonstrated in Section 5.3 how to resolve the diagrammatic expansion by calculating expressions for the leading order correction to the LNA of the power spectra. Our results are applicable to general biochemical networks under stationary conditions and are therefore of immediate interest in applications. In particular, because the power spectrum is an important tool for quantifying rhythmicity in biological systems, both in theory [95–97] and in experiments [90, 92, 93]. In Section 5.4 we have illustrated the utility of this result through the analytical computation of the power spectra in a dimerization reaction and through a study of noise-induced oscillations in the Brusselator reaction. Specifically, we have demonstrated that our approach allows for the identification of noise-induced oscillations in parameter regimes that are not captured by the conventional LNA, including regimes in which a deterministic stability analysis predicts either stable foci or nodes. These oscillations are particularly pronounced close to a Hopf bifurcation. In this case, an effective theory proposed in Section 5.5 predicts that the spectra have three universal features: (i) a dominant peak at some frequency, (ii) a smaller peak at twice the frequency of the dominant peak and (iii) a peak at zero frequency. Of these, the LNA predicts only the first feature. Using recently acquired data of a circadian rhythm in fibroblast cells, we have demonstrated that the present approximation methods can closely resemble the outcomes of single-cell experiments.

Previously, the SSE has been used to assess the accuracy of different approximation schemes. Grima compared the accuracy of the asymptotic expansions of moment closure approximations using the leading order terms in the SSE [113]. It was found that moment closure procedures neglecting higher than second or third order cumulants are more accurate than the REs, but only the method neglecting higher than third order cumulants is more accurate than the LNA. The expansion of the moments given by Result 3.1 can be truncated to any desired order in the system size and hence could serve to establish also the validity of higher-order closure schemes. Similarly, our results may be used to obtain asymptotic error estimates for moments of high-order Kramers-Moyal expansions [1, 114]. Our results in Chapter 4 would allow to straightforwardly investigate error estimates for the corresponding distributions as well.

We highlight that the present analytical solution procedure of the CME has the potential to remove the necessity of stochastic simulations. While a numerical solution for the CME of a single species is rather straightforward [22], we expect the procedure to become computationally advantageous when generalized to the multivariate case, where numerical solution is usually prohibitive due to combinatorial explosion. This development could prove particularly valuable for parameter estimation of biochemi-

cal reactions in living cells. Though we have focused on the stochastic formulation of biochemical kinetics, master equations of Markov jump processes are common to many areas of research. The LNA of the master equation is routinely applied, for instance, in the theory of polymer assembly [151, 152], epidemics [153], game theory [154], economics [155], neural networks [156], quantum optics [157], and machine learning [158]. We expect that the approximation methods developed on the basis of higher order terms in the SSE may provide useful insights also in these fields.

Bibliography

[1] R. Grima, P. Thomas, and A. V. Straube. How accurate are the nonlinear chemical Fokker-Planck and chemical Langevin equations? *J Chem Phys*, **135**, 084103 (2011).

[2] P. Thomas, H. Matuschek, and R. Grima. Computation of biochemical pathway fluctuations beyond the linear noise approximation using iNA. In *Bioinformatics and Biomed (BIBM), 2012 IEEE Int Conf on*, pages 1–5. IEEE (2012).

[3] P. Thomas and R. Grima. Approximate probability distributions of the master equation. *Phys Rev E*, **92**, 012120 (2015).

[4] P. Thomas, et al. System size expansion of the master equation using Feynman rules and diagrams. *J Phys A: Math Theor*, **47**, 455007 (2014).

[5] P. Thomas, et al. Signatures of nonlinearity in single cell noise-induced oscillations. *J Theor Biol*, **335**, 222 (2013).

[6] A. Bar-Even, et al. Noise in protein expression scales with natural protein abundance. *Nat Genet*, **38**, 636 (2006).

[7] Y. Taniguchi, et al. Quantifying E. coli proteome and transcriptome with single-molecule sensitivity in single cells. *Science*, **329**, 533 (2010).

[8] I. L. Ross, C. M. Browne, and D. A. Hume. Transcription of individual genes in eukaryotic cells occurs randomly and infrequently. *Immunol Cell Biol*, **72**, 177 (1994).

[9] H. H. McAdams and A. Arkin. Stochastic mechanisms in gene expression. *Proc Natl Acad Sci*, **94**, 814 (1997).

[10] A. Arkin, J. Ross, and H. H. McAdams. Stochastic kinetic analysis of developmental pathway bifurcation in phage λ-infected Escherichia coli cells. *Genetics*, **149**, 1633 (1998).

[11] J. R. Newman et al. Single-cell proteomic analysis of S. cerevisiae reveals the architecture of biological noise. *Nature*, **441**, 840 (2006).

[12] Y. Ishihama, et al. Protein abundance profiling of the Escherichia coli cytosol. *BMC Genomics*, **9**, 102 (2008).

[13] D. T. Gillespie. A general method for numerically simulating the stochastic time evolution of coupled chemical reactions. *J Comput Phys*, **22**, 403 (1976).

[14] D. T. Gillespie. Exact stochastic simulation of coupled chemical reactions. *J Phys Chem*, **81**, 2340 (1977).

[15] D. Gillespie. Stochastic simulation of chemical kinetics. *Annu Rev Phys Chem*, **58**, 35 (2007).

[16] M. Delbrück. Statistical fluctuations in autocatalytic reactions. *J Chem Phys*, **8**, 120 (1940).

[17] D. A. McQuarrie. Kinetics of small systems. I. *J Chem Phys*, **38**, 433 (1963).

[18] D. A. McQuarrie, C. J. Jachimowski, and M. E. Russell. Kinetics of small systems. II. *J Chem Phys*, **40**, 2914 (1964).

[19] D. A. McQuarrie. Stochastic approach to chemical kinetics. *J Appl Prob*, **4**, 413 (1967).

[20] D. Gillespie. A rigorous derivation of the chemical master equation. *Phys A*, **188**, 404 (1992).

[21] W. Feller. *An Introduction to Probability Theory, Vol. 1.* Wiley, New York, NY, 3rd edition (1968).

[22] B. Munsky and M. Khammash. The finite state projection algorithm for the solution of the chemical master equation. *J Chem Phys*, **124**, 044104 (2006).

[23] V. Wolf, et al. Solving the chemical master equation using sliding windows. *BMC Syst Biol*, **4**, 42 (2010).

[24] P. Deuflhard, et al. Adaptive discrete Galerkin methods applied to the chemical master equation. *SIAM J Sci Comput*, **30**, 2990 (2008).

[25] S. Engblom. Galerkin spectral method applied to the chemical master equation. *Commun Comput Phys*, **5**, 871 (2009).

[26] L. Ferm and P. Lötstedt. Adaptive solution of the master equation in low dimensions. *Appl Numer Math*, **59**, 187 (2009).

[27] T. Jahnke and W. Huisinga. Solving the chemical master equation for monomolecular reaction systems analytically. *J Math Biol*, **54**, 1 (2007).

[28] S. Smith and V. Shahrezaei. General transient solution of the one-step master equation in one dimension. *Phys Rev E*, **91**, 062119 (2015).

[29] I. J. Laurenzi. An analytical solution of the stochastic master equation for reversible bimolecular reaction kinetics. *J Chem Phys*, **113**, 3315 (2000).

[30] I. Darvey and P. Staff. Stochastic Approach to First-Order Chemical Reaction Kinetics . *J Chem Phys*, **44**, 990 (1965).

[31] C. Gardiner. *Handbook of Stochastic Methods.* Springer, Berlin (2007).

[32] R. M. Mazo. On the discrepancy between results of Nicolis and Saito concerning fluctuations in chemical reactions. *J Chem Phys*, **62**, 4244 (1975).

[33] P. Visco, R. J. Allen, and M. R. Evans. Exact solution of a model DNA-inversion genetic switch with orientational control. *Phys Rev Lett*, **101**, 118104 (2008).

[34] P. Érdi and G. Lente. *Stochastic Chemical Kinetics.* Springer, New York (2014).

[35] C. W. Gardiner and S. Chaturvedi. The Poisson representation. I. A new technique for chemical master equations. *J Stat Phys*, **17**, 429 (1977).

[36] S. Iyer-Biswas, F. Hayot, and C. Jayaprakash. Stochasticity of gene products from transcriptional pulsing. *Phys Rev E*, **79**, 031911 (2009).

[37] A. Walczak, A. Mugler, and C. Wiggins. Analytic Methods for Modeling Stochastic Regulatory Networks. In X. Liu and M. D. Betterton, editors, *Computational Modeling of Signaling Networks*, volume 880 of *Methods in Molecular Biology*, pages 273–322. Humana Press (2012).

[38] L. Peliti. Path integral approach to birth-death processes on a lattice. *J Phys (Paris)*, **46**, 1469 (1985).

[39] M. Droz and A. McKane. Equivalence between Poisson representation and Fock space formalism for birth-death processes. *J Phys A: Math Gen*, **27**, L467 (1994).

[40] A. Kamenev. *Field theory of non-equilibrium systems.* Cambridge University Press, Cambridge (2011).

[41] T. Brett and T. Galla. Stochastic processes with distributed delays: chemical Langevin equation and linear-noise approximation. *Phys Rev Lett*, **110**, 250601 (2013).

[42] U. Täuber. *Critical dynamics: a field theory approach to equilibrium and non-equilibrium scaling behavior.* Cambridge University Press, Cambridge (2014).

[43] H. Haken. Exact stationary solution of the master equation for systems far from thermal equilibrium in detailed balance. *Phys Lett A*, **46**, 443 (1974).

[44] N. G. van Kampen. The expansion of the master equation. *Adv Chem Phys*, **34**, 245 (1976).

[45] D. F. Anderson, G. Craciun, and T. G. Kurtz. Product-form stationary distributions for deficiency zero chemical reaction networks. *Bull Math Biol*, **72**, 1947 (2010).

[46] J. Peccoud and B. Ycart. Markovian modeling of gene-product synthesis. *Theor Popul Biol*, **48**, 222 (1995).

[47] R. Grima, D. R. Schmidt, and T. J. Newman. Steady-state fluctuations of a genetic feedback loop: An exact solution. *J Chem Phys*, **137**, 035104 (2012).

[48] M. Cook, et al. Programmability of Chemical Reaction Networks. In A. Condon, et al., editors, *Algorithmic Bioprocesses*, Natural Computing Series, pages 543–584. Springer, Berlin (2009).

[49] J. Goutsias and G. Jenkinson. Markovian dynamics on complex reaction networks. *Physics Reports*, **529**, 199 (2013).

[50] D. T. Gillespie. *Markov processes: an introduction for physical scientists.* Academic Press, San Diego CA (1991).

[51] P. Warren, S. Tănase-Nicola, and P. Ten Wolde. Exact results for noise power spectra in linear biochemical reaction networks. *J Chem Phys*, **125**, 144904 (2006).

[52] C. J. Jachimowski, D. A. McQuarrie, and M. E. Russell. A Stochastic Approach to Enzyme-Substrate Reactions*. *Biochemistry*, **3**, 1732 (1964).

[53] S. Engblom. Computing the moments of high dimensional solutions of the master equation. *Appl Math Comput*, **180**, 498 (2006).

[54] C. S. Gillespie. Moment-closure approximations for mass-action models. *IET Syst Biol*, **3**, 52 (2009).

[55] V. Sotiropoulos and Y. N. Kaznessis. Analytical derivation of moment equations in stochastic chemical kinetics. *Chem Eng Sci*, **66**, 268 (2011).

[56] J. Hasenauer, et al. Method of conditional moments (MCM) for the Chemical Master Equation. *J Math Biol*, **69**, 687 (2014).

[57] D. Schnoerr, G. Sanguinetti, and R. Grima. The complex chemical Langevin equation. *J Chem Phys*, **141**, 024103 (2014).

[58] A. Ale, P. Kirk, and M. P. H. Stumpf. A general moment expansion method for stochastic kinetic models. *J Chem Phys*, **138**, 174101 (2013).

[59] P. Smadbeck and Y. N. Kaznessis. A closure scheme for chemical master equations. *Proc Natl Acad Sci*, **110**, 14261 (2013).

[60] A. Andreychenko, L. Mikeev, and V. Wolf. Model Reconstruction for Moment-Based Stochastic Chemical Kinetics. *ACM Trans Model Comput Simul*, **25**, 12 (2015).

[61] J. Elf and M. Ehrenberg. Fast evaluation of fluctuations in biochemical networks with the linear noise approximation. *Genome Res*, **13**, 2475 (2003).

[62] J. Paulsson. Summing up the noise in gene networks. *Nature*, **427**, 415 (2004).

[63] F. Hayot and C. Jayaprakash. The linear noise approximation for molecular fluctuations within cells. *Phys Biol*, **1**, 205 (2004).

[64] Y. Tao, Y. Jia, and T. G. Dewey. Stochastic fluctuations in gene expression far from equilibrium: Ω expansion and linear noise approximation. *J Chem Phys*, **122**, 124108 (2005).

[65] J. Paulsson. Models of stochastic gene expression. *Phys Life Rev*, **2**, 157 (2005).

[66] M. Scott, B. Ingalls, and M. Kaern. Estimations of intrinsic and extrinsic noise in models of nonlinear genetic networks. *Chaos*, **16**, 026107 (2006).

[67] F. J. Bruggeman, N. Blüthgen, and H. V. Westerhoff. Noise management by molecular networks. *PLoS Comput Biol*, **5**, e1000506 (2009).

[68] P. Thomas, A. V. Straube, and R. Grima. The slow-scale linear noise approximation: an accurate, reduced stochastic description of biochemical networks under timescale separation conditions. *BMC Syst Biol*, **6**, 39 (2012).

[69] M. Komorowski, J. Miekisz, and M. P. Stumpf. Decomposing Noise in Biochemical Signaling Systems Highlights the Role of Protein Degradation . *Biophys J*, **104**, 1783 (2013).

[70] D. A. Oyarzún, J.-B. Lugagne, and G.-B. V. Stan. Noise propagation in synthetic gene circuits for metabolic control. *ACS Synth Biol*, **4**, 116 (2014).

[71] A. Ruttor and M. Opper. Efficient statistical inference for stochastic reaction processes. *Phys Rev Lett*, **103**, 230601 (2009).

[72] M. Komorowski, et al. Bayesian inference of biochemical kinetic parameters using the linear noise approximation. *BMC Bioinform*, **10**, 343 (2009).

[73] M. Komorowski, et al. Sensitivity, robustness, and identifiability in stochastic chemical kinetics models. *Proc Natl Acad Sci*, **108**, 8645 (2011).

[74] V. Stathopoulos and M. A. Girolami. Markov chain Monte Carlo inference for Markov jump processes via the linear noise approximation. *Phil Trans R Soc A*, **371**, 20110541 (2013).

[75] B. Finkenstädt, et al. Quantifying intrinsic and extrinsic noise in gene transcription using the linear noise approximation: An application to single cell data. *Ann Appl Stat*, **7**, 1960 (2013).

[76] N. G. Van Kampen. *Stochastic Processes in Physics and Chemistry*. Elsevier, Amsterdam, 3rd edition (1997).

[77] N. G. van Kampen. A power series expansion of the master equation. *Can J Phys*, **39**, 551 (1961).

[78] T. G. Kurtz. Solutions of ordinary differential equations as limits of pure jump Markov processes. *J Appl Prob*, **7**, 49 (1970).

[79] T. G. Kurtz. Limit theorems for sequences of jump Markov processes approximating ordinary differential processes. *J Appl Prob*, **8**, 344 (1971).

[80] S. N. Ethier and T. G. Kurtz. *Markov processes: characterization and convergence*. John Wiley & Sons, Hoboken NJ (2009).

[81] T. G. Kurtz. Strong approximation theorems for density dependent Markov chains. *Stoch Proc Appl*, **6**, 223 (1978).

[82] F. Tostevin and P. R. Ten Wolde. Mutual information between input and output trajectories of biochemical networks. *Phys Rev Lett*, **102**, 218101 (2009).

[83] J. Elf, et al. Mesoscopic kinetics and its applications in protein synthesis. In L. Alberghina and H. Westerhoff, editors, *Systems Biology*, volume 13 of *Topics in Current Genetics*, pages 95–18. Springer, Berlin (2005).

[84] R. Pawula. Approximation of the linear Boltzmann equation by the Fokker-Planck equation. *Phys Rev*, **162**, 186 (1967).

[85] R. Grima. Noise-induced breakdown of the Michaelis-Menten equation in steady-state conditions. *Phys Rev Lett*, **102**, 218103 (2009).

[86] R. Grima. An effective rate equation approach to reaction kinetics in small volumes: Theory and application to biochemical reactions in nonequilibrium steady-state conditions. *J Chem Phys*, **133**, 035101 (2010).

[87] R. Grima. Investigating the robustness of the classical enzyme kinetic equations in small intracellular compartments. *BMC Syst Biol*, **3**, 101 (2009).

[88] P. Thomas, A. Straube, and R. Grima. Stochastic theory of large-scale enzyme-reaction networks: Finite copy number corrections to rate equation models. *J Chem Phys*, **133**, 195101 (2010).

[89] C. Cianci, et al. Analytical study of non-Gaussian fluctuations in a stochastic scheme of autocatalytic reactions. *Eur Phys J Special Topics*, **212**, 5 (2012).

[90] D. K. Welsh, et al. Bioluminescence imaging of individual fibroblasts reveals persistent, independently phased circadian rhythms of clock gene expression. *Curr Biol*, **14**, 2289 (2004).

[91] P. O. Westermark, et al. Quantification of circadian rhythms in single cells. *PLoS Comput Biol*, **5**, e1000580 (2009).

[92] N. Geva-Zatorsky, et al. Fourier analysis and systems identification of the p53 feedback loop. *Proc Natl Acad Sci*, **107**, 13550 (2010).

[93] C. H. Ko, et al. Emergence of noise-induced oscillations in the central circadian pacemaker. *PLoS Biol*, **8**, e1000513 (2010).

[94] H. Gang, et al. Stochastic resonance without external periodic force. *Phys Rev Lett*, **71**, 807 (1993).

[95] Z. Hou and H. Xin. Internal noise stochastic resonance in a circadian clock system. *J Chem Phys*, **119**, 11508 (2003).

[96] K. Davis and M. R. Roussel. Optimal observability of sustained stochastic competitive inhibition oscillations at organellar volumes. *FEBS Journal*, **273**, 84 (2006).

[97] Q. Li and X. Lang. Internal noise-sustained circadian rhythms in a Drosophila model. *Biophys J*, **94**, 1983 (2008).

[98] D. T. Gillespie. A diffusional bimolecular propensity function. *J Chem Phys*, **131**, 164109 (2009).

[99] R. Aris, P. Gray, and S. K. Scott. Modelling cubic autocatalysis by successive bimolecular steps. *Chem Eng Sci*, **43**, 207 (1988).

[100] M. A. Gibson and J. Bruck. Efficient exact stochastic simulation of chemical systems with many species and many channels. *J Phys Chem A*, **104**, 1876 (2000).

[101] H. Risken. *The Fokker-Planck Equation*. Springer, Berlin (1996).

[102] L. Comtet. *Advanced Combinatorics: The art of finite and infinite expansions*. D. Reidel, Dordrecht (1974).

[103] P. Hanggi, et al. Bistable systems: Master equation versus Fokker-Planck modeling. *Phys Rev A*, **29**, 371 (1984).

[104] M. Dykman, et al. Large fluctuations and optimal paths in chemical kinetics. *J Chem Phys*, **100**, 5735 (1994).

[105] J. Keizer. *Statistical thermodynamics of nonequilibrium processes*. Springer, New York (1987).

[106] F. Di Patti, et al. System size expansion for systems with an absorbing state. *Phys Rev E*, **83**, 010102 (2011).

[107] P. A. P. Moran. *An introduction to probability theory*. Clarendon Press, Oxford (1968).

[108] L. Isserlis. On a formula for the product-moment coefficient of any order of a normal frequency distribution in any number of variables. *Biometrika*, **12**, 134 (1918).

[109] G.-C. Wick. The evaluation of the collision matrix. *Phys Rev*, **80**, 268 (1950).

[110] J. Zinn-Justin. *Phase Transitions and Renormalization Group*. Oxford University Press, Oxford (2007).

[111] P. Thomas, H. Matuschek, and R. Grima. Intrinsic Noise Analyzer: A Software Package for the Exploration of Stochastic Biochemical Kinetics Using the System Size Expansion. *PLoS One*, **7**, e38518 (2012).

[112] P. Thomas, H. Matuschek, and R. Grima. How reliable is the linear noise approximation of gene regulatory networks? *BMC Genomics*, **14**, S5 (2013).

[113] R. Grima. A study of the accuracy of moment-closure approximations for stochastic chemical kinetics. *J Chem Phys*, **136**, 154105 (2012).

[114] R. Grima. Construction and accuracy of partial differential equation approximations to the Chemical Master equation. *Phys Rev E*, **84**, 056109 (2011).

[115] C. Cianci, F. Di Patti, and D. Fanelli. Non-Gaussian fluctuations in stochastic models with absorbing barriers. *Europhys Lett*, **96**, 50011 (2011).

[116] J. Paulsson, O. G. Berg, and M. Ehrenberg. Stochastic focusing: fluctuation-enhanced sensitivity of intracellular regulation. *Proc Natl Acad Sci*, **97**, 7148 (2000).

[117] J. P. Boyd. The devil's invention: asymptotic, superasymptotic and hyperasymptotic series. *Acta Appl Math*, **56**, 1 (1999).

[118] C. M. Bender and S. A. Orszag. *Advanced mathematical methods for scientists and engineers. 1978*. McGraw-Hill, New York (1995).

[119] G. N. Watson. *A treatise on the theory of Bessel functions*. Cambridge University Press, Cambridge (1995).

[120] E. Ozbudak, et al. Regulation of noise in the expression of a single gene. *Nat Genet*, **31**, 69 (2002).

[121] V. Shahrezaei and P. S. Swain. Analytical distributions for stochastic gene expression. *Proc Natl Acad Sci*, **105**, 17256 (2008).

[122] P. Bokes, et al. Exact and approximate distributions of protein and mRNA levels in the low-copy regime of gene expression. *J Math Biol*, **64**, 829 (2012).

[123] M. Abramowitz and I. A. Stegun. *Handbook of mathematical functions: with formulas, graphs, and mathematical tables*. 55. Courier Corporation (1964).

[124] N. N. Lebedev. *Special functions and their applications*. Dover Publications, New York (1972).

[125] P. Thomas, A. V. Straube, and R. Grima. Communication: Limitations of the stochastic quasi-steady-state approximation in open biochemical reaction networks. *J Chem Phys*, **135**, 181103 (2011).

[126] K. R. Sanft, D. T. Gillespie, and L. R. Petzold. Legitimacy of the stochastic Michaelis-Menten approximation. *IET Syst Biol*, **5**, 58 (2011).

[127] F. Verhulst. *Methods and applications of singular perturbations: boundary layers and multiple timescale dynamics*. Springer, New York (2006).

[128] S. Chaturvedi and C. W. Gardiner. The Poisson representation. II Two-time correlation functions. *J Stat Phys*, **18**, 501 (1978).

[129] M. Scott. Non-linear corrections to the time-covariance function derived from a multi-state chemical master equation. *IET Syst Biol*, **6**, 116 (2012).

[130] M. Srednicki. *Quantum field theory*. Cambridge University Press, Cambridge (2007).

[131] R. P. Feynman. Space-time approach to non-relativistic quantum mechanics. *Reviews of Modern Physics*, **20**, 367 (1948).

[132] S. S. Schweber. The sources of Schwinger's Green's functions. *Proc Natl Acad Sci*, **102**, 7783 (2005).

[133] P. C. Martin, E. Siggia, and H. Rose. Statistical dynamics of classical systems. *Phys Rev A*, **8**, 423 (1973).

[134] A. Lefevre and G. Biroli. Dynamics of interacting particle systems: stochastic process and field theory. *J Stat Mech Theor Exp*, **2007**, P07024 (2007).

[135] A. Altland and B. D. Simons. *Condensed matter field theory*. Cambridge University Press, Cambridge (2010).

[136] H. Calisto and E. Tirapegui. Ω-Expansion of van Kampen through functional integrals. *J Stat Phys*, **71**, 683 (1993).

[137] D. F. Anderson and T. G. Kurtz. Continuous time Markov chain models for chemical reaction networks. In *Design and analysis of biomolecular circuits*, pages 3–42. Springer (2011).

[138] J. Zinn-Justin. *Quantum Field Theory and Critical Phenomena*. Clarendon Press, Oxford (2002).

[139] U. Täuber. Population oscillations in spatial stochastic Lotka–Volterra models: a field-theoretic perturbational analysis. *J Phys A: Math Theor*, **45**, 405002 (2012).

[140] I. Prigogine and R. Lefever. Symmetry Breaking Instabilities in Dissipative Systems. II. *J Chem Phys*, **48**, 1695 (1968).

[141] D. Toner and R. Grima. Molecular noise induces concentration oscillations in chemical systems with stable node steady states. *J Chem Phys*, **138**, 055101 (2013).

[142] O. V. Ushakov, et al. Coherence resonance near a Hopf bifurcation. *Phys Rev Lett*, **95**, 123903 (2005).

[143] A. J. McKane, et al. Amplified biochemical oscillations in cellular systems. *J Stat Phys*, **128**, 165 (2007).

[144] R. Kuske, L. F. Gordillo, and P. Greenwood. Sustained oscillations via coherence resonance in SIR. *J Theor Biol*, **245**, 459 (2007).

[145] P. H. Baxendale and P. E. Greenwood. Sustained oscillations for density dependent Markov processes. *J Math Biol*, **63**, 433 (2011).

[146] T. Leise, et al. Persistent Cell-Autonomous Circadian Oscillations in Fibroblasts Revealed by Six-Week Single-Cell Imaging of PER2::LUC Bioluminescence. *PLoS ONE*, **7**, e33334 (2012).

[147] B. Novák and J. J. Tyson. Design principles of biochemical oscillators. *Nat Rev Mol Cell Biol*, **9**, 981 (2008).

[148] T. Wilhelm and R. Heinrich. Smallest chemical reaction system with Hopf bifurcation. *J Math Chem*, **17**, 1 (1995).

[149] J. J. Tyson. Biochemical Oscillations. In C. Fall, et al., editors, *Computational Cell Biology*, volume 20 of *Interdisciplinary Applied Mathematics*, pages 230–260. Springer, New York (2002).

[150] J. J. Tyson and S. Kauffman. Control of mitosis by a continuous biochemical oscillation: synchronization; spatially inhomogeneous oscillations. *J Math Biol*, **1**, 289 (1975).

[151] A. Melbinger, L. Reese, and E. Frey. Microtubule length regulation by molecular motors. *Phys Rev Lett*, **108**, 258104 (2012).

[152] J. Szavits-Nossan, et al. Inherent variability in the kinetics of autocatalytic protein self-assembly. *Phys Rev Lett*, **113**, 098101 (2014).

[153] G. Rozhnova and A. Nunes. Fluctuations and oscillations in a simple epidemic model. *Phys Rev E*, **79**, 041922 (2009).

[154] A. J. Bladon, T. Galla, and A. J. McKane. Evolutionary dynamics, intrinsic noise, and cycles of cooperation. *Phys Rev E*, **81**, 066122 (2010).

[155] M. Aoki. *Modeling aggregate behavior and fluctuations in economics: stochastic views of interacting agents*. Cambridge University Press, Cambridge (2001).

[156] P. C. Bressloff. Stochastic neural field theory and the system-size expansion. *SIAM J Appl Math*, **70**, 1488 (2009).

[157] L. A. Lugiato, M. O. Scully, and H. Walther. Connection between microscopic and macroscopic maser theory. *Phys Rev A*, **36**, 740 (1987).

[158] T. Heskes. On Fokker-Planck approximations of on-line learning processes. *J Phys A: Math Gen*, **27**, 5145 (1994).

List of abbreviations

CME	Chemical Master Equation
EMRE	effective mesoscopic rate equation
Eq.	Equation
Fig.	Figure
h.c.	Hermitian conjugate
IOS	Inverse Omega Square Approximation
LNA	linear noise approximation
ODE	ordinary differential equation
PDE	partial differential equation
RE	rate equation
SSA	stochastic simulation algorithm
SSE	system size expansion
Tab.	Table